

AD-A070 819

NORTHROP RESEARCH AND TECHNOLOGY CENTER PALOS VERDES --ETC F/6 20/9
PLASMA SHEATH PROCESSES. (U)

APR 79 W H LONG

NRTC78-46R

F33615-77-C-2048

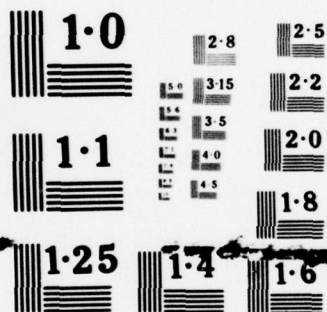
UNCLASSIFIED

AFAPL-TR-79-2038

NL

1 OF 2
AD
A070819





NATIONAL BUREAU OF STANDARDS
MICROCOPY RESOLUTION TEST CHART

LEVEL II

2

DA070819

AFAPL-TR-79-2038

PLASMA SHEATH PROCESSES

Northrop Corporation
Northrop Research and Technology Center
One Research Park
Palos Verdes Peninsula, California 90274

April 1979

TECHNICAL REPORT AFAPL-TR-79-2038

Final Report for Period 1 August 1977 - 31 October 1978

Approved for public release; distribution unlimited.

AIR FORCE AERO PROPULSION LABORATORY
AIR FORCE WRIGHT AERONAUTICAL LABORATORIES
AIR FORCE SYSTEMS COMMAND
WRIGHT-PATTERSON AIR FORCE BASE, OHIO 45433

DDC
RECEIVED
JUL 5 1979
RECEIVED
D

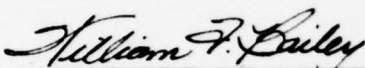
DDC FILE COPY

NOTICE

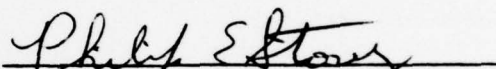
When Government drawings, specifications, or other data are used for any purpose other than in connection with a definitely related Government procurement operation, the United States Government thereby incurs no responsibility nor any obligation whatsoever; and the fact that the government may have formulated, furnished, or in any way supplied the said drawings, specifications, or other data, is not to be regarded by implication or otherwise as in any manner licensing the holder or any other person or corporation, or conveying any rights or permission to manufacture, use, or sell any patented invention that may in any way be related thereto.

This report has been reviewed by the Information Office (OI) and is releasable to the National Technical Information Service (NTIS). At NTIS, it will be available to the general public, including foreign nations.

This technical report has been reviewed and is approved for publication.

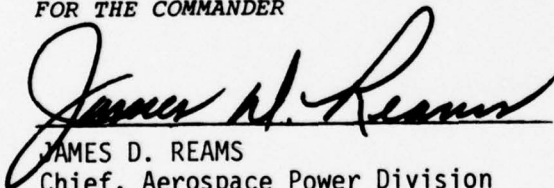


WILLIAM F. BAILEY, Major, USAF
Research Physicist



PHILIP E. STOVER
Chief, High Power Branch

FOR THE COMMANDER



JAMES D. REAMS
Chief, Aerospace Power Division

"If your address has changed, if you wish to be removed from our mailing list, or if the addressee is no longer employed by your organization please notify AFAPL/POD, W-PAFB, OH 45433 to help us maintain a current mailing list".

Copies of this report should not be returned unless return is required by security considerations, contractual obligations, or notice on a specific document.

UNCLASSIFIED

SECURITY CLASSIFICATION OF THIS PAGE (When Data Entered)

REPORT DOCUMENTATION PAGE		READ INSTRUCTIONS BEFORE COMPLETING FORM
1. REPORT NUMBER AFAPL-TR-79-2038	2. GOVT ACCESSION NO.	3. RECIPIENT'S CATALOG NUMBER
4. TITLE (and Subtitle) PLASMA SHEATH PROCESSES.	5. TYPE OF REPORT & PERIOD COVERED Final Technical Report 15 Aug 1977-31 Oct 1978	6. PERFORMING ORG. REPORT NUMBER NRTC 78-46R
7. AUTHOR(s) William H. Long, Jr.	8. CONTRACT OR GRANT NUMBER(s) F 33615-77-C-2048	
9. PERFORMING ORGANIZATION NAME AND ADDRESS Northrop Research and Technology Center One Research Park Palos Verdes Peninsula, California 90274	10. PROGRAM ELEMENT, PROJECT, TASK AREA & WORK UNIT NUMBERS FY1455-77-00034	
11. CONTROLLING OFFICE NAME AND ADDRESS Air Force Aero Propulsion Laboratory AFAPL/POD Wright-Patterson Air Force Base, Ohio 45433	12. REPORT DATE April 1979	
14. MONITORING AGENCY NAME & ADDRESS (if different from Controlling Office) 12 123p.	13. NUMBER OF PAGES 118	
	15. SECURITY CLASS. (of this report) Unclassified	
	15a. DECLASSIFICATION DOWNGRADING SCHEDULE ---	
16. DISTRIBUTION STATEMENT (of this Report) Approved for public release; distribution unlimited.	Accession For NTIS GRA&I <input checked="" type="checkbox"/> DDC TAB <input type="checkbox"/> Unannounced <input type="checkbox"/> Justification <input type="checkbox"/>	
17. DISTRIBUTION STATEMENT (of the abstract entered in Block 20, if different from Report)	By _____ Distribution/ Availability Codes	
18. SUPPLEMENTARY NOTES	Dist. A	Avail and/or special
19. KEY WORDS (Continue on reverse side if necessary and identify by block number) Plasma sheath, boundary layer, electric discharge, electron kinetics, electrodes.		
20. ABSTRACT (Continue on reverse side if necessary and identify by block number) A model of the plasma sheath in high pressure ionized gas flows is presented. Nonequilibrium electron energy distributions are determined from a numerical solution of the collisional Boltzmann equation in the presence of strong field and density gradients. Self-consistent coupling to the electric field, ion kinetics and gas dynamics is included. In subsonic flows, the sheath and the boundary layer can be treated independently. A stability analysis indicates two forms of thermal instability occur in the cathode sheath at high pressures.		

DD FORM 1 JAN 73 1473 EDITION OF 1 NOV 65 IS OBSOLETE

UNCLASSIFIED

SECURITY CLASSIFICATION OF THIS PAGE (When Data Entered)

407 696

HB

TABLE OF CONTENTS

	Page
1.0 OBJECTIVE	1
2.0 SUMMARY	2
3.0 INTRODUCTION	4
3.1 Literature Search	5
3.2 Evaluation of Appropriate Theories	6
4.0 MATHEMATICAL MODEL	10
4.1 Boltzmann Equation	10
4.2 Electric Field and Ion Kinetics	22
5.0 COMPUTER PROGRAMS	25
5.1 Program SHEATH	25
5.2 Program CATFAL	31
6.0 NUMERICAL RESULTS	39
6.1 Nonequilibrium Electron Kinetics	39
6.2 Cathode Fall and Negative Glow	57
7.0 SHEATH CHARACTERISTICS	69
7.1 Linear Field Approximation	69
7.2 Gas Heating in the Cathode Sheath	75
8.0 STABILITY ANALYSIS	92
8.1 Electrode Cooling and Thermal Stability	92
8.2 Field Tailoring and Auxiliary Ionization	96
9.0 CONCLUSIONS	99
10.0 REFERENCES	100
APPENDIX	106
GLOSSARY	114

LIST OF FIGURES

		Page
Figure 1	Storage Array for Collision Integral	27
Figure 2	Schematic Drawing of the Nozzle and Discharge Region	32
Figure 3	Relevant Quantities in the Boundary Layer Equations	34
Figure 4	Electron Current at the Anode	40
Figure 5	Current Density and Ionization Coefficient	42
Figure 6	Electron Kinetics in a Nonuniform Field	43
Figure 7	Cross Sections in Argon	46
Figure 8	Drift Velocity and Ionization Coefficient	47
Figure 9	Electron Current at the Anode	50
Figure 10	Electron Energy Distribution at the Anode	51
Figure 11	Electron Current and Number Density	52
Figure 12	Townsend Ionization Coefficient and Mean Energy	54
Figure 13	Self-Consistent Solution of the Cathode Fall	55
Figure 14	Ionization and Recombination Rate Constants	60
Figure 15	Townsend Coefficients and Mean Energy	62
Figure 16	Electron Energy Distribution in the Cathode Fall and Negative Glow: Ar	63
Figure 17	Electron Current and Number Density	64
Figure 18	Electron Energy Distribution in the Cathode Fall and Negative Glow: He	66
Figure 19	The Cathode Region in Helium	67
Figure 20	Voltage-Current Characteristic and Cathode Fall Distance in N_2	74
Figure 21	Electric Field in Cathode Sheath with Gas Heating	86
Figure 22	Temperature Variation in the Cathode Sheath	87
Figure 23	Temperature Rise in the Cathode Sheath	89
Figure 24	Temperature Distribution in the Cathode Sheath-Boundary Layer	91
Figure 25	Voltage-Current Characteristics with Gas Heating	97

1.0 OBJECTIVE

The research performed under this contract is directed toward an understanding of plasma processes in boundary and electrode regions. The aim is to develop a self-consistent theory combining electron and ion kinetics in the presence of strong field and density gradients with the boundary layer equations of gasdynamics. The present study has direct application to problems in high-pressure, flowing gas discharges and in MHD power generators.

In electric discharges, the development of arcs and nonuniform current distributions begins at the electrodes. The interaction between a thermal boundary layer and the space-charge sheath adjacent to electrodes and other solid boundaries is therefore critical to the determination of electric discharge stability and uniformity. If an understanding of the basic processes in these regions can be achieved, it may be possible to extend the useful operating range of discharge-pumped devices to higher power densities and longer pulses.

In an MHD generator, the internal voltage losses across the boundary layer and sheath limit the energy conversion efficiency. Current constrictions on the electrodes can cause surface deterioration. An understanding of the collisional sheath and boundary layer problems will lead to improved system designs.

2.0 SUMMARY

In the first quarter, a literature search was performed to identify relevant theories and to evaluate their applicability to the present study. The important processes which must be included in a self-consistent model of the plasma sheath were identified. The Boltzmann equation for electrons in a nonuniform field was derived in a form amenable to numerical solution.

In the second quarter, a computer program was developed to model the electron kinetics in a highly nonuniform electric field. Cases were run in several gases using a constant field for comparison with previous Monte Carlo solutions. The nonequilibrium character of the electron energy distribution was clearly demonstrated, thus pointing out the limitations of earlier sheath models. The equations for electric field and ion kinetics were formulated for use in a fully self-consistent solution of the cathode sheath.

In the third quarter, the evolution of electron energy distributions in the cathode fall and negative glow was examined by assuming a linearly falling electric field followed by a zero-field drift region. The results agree well with experimental distributions measured at the edge of the cathode fall. Recombination and attachment were included in the model but only had a significant effect in the negative glow. Analytic solutions to the Boltzmann equation were derived for a specific choice of cross sections in order to test some of the angular approximations used in the code.

In the fourth quarter, cathode sheath characteristics were derived using the linear field approximation. It was found that the usual scaling laws apply in terms of the reduced pressure at the cathode surface. Gas heating in the sheath was examined and the temperature distribution was calculated. For subsonic flows, the **principal** cooling mechanism is conduction to the cathode

surface. In this regime, the boundary layer problem can be separated from the sheath problem. A computer program for the solution of the boundary layer equations including gas heating was described.

In the last quarter, numerical calculations of the temperature distribution in the cathode sheath and boundary layer were presented. The temperature rise across the sheath was shown to increase linearly with pressure. An analysis was made of the thermal stability at the cathode surface. A critical current density was found at which the surface temperature and electric field increase until arcing occurs. This event can be forestalled by cooling the electrode and by the use of a buffer gas with high thermal conductivity. Auxiliary ionization and field tailoring, which are designed to eliminate ionization instabilities and maintain constant E/N in the positive column, affect the sheath only through the imposed local current density and do not significantly alter sheath characteristics.

3.0 INTRODUCTION

The problem as stated in Section 1.0 is to develop a self-consistent theory of plasma processes in boundary and electrode regions. The approach taken under this contract consists of two basic parts: First, a refinement of the existing theories of the sheath and cathode fall regions to include the effects of field and density gradients and the anisotropy of the electron velocity distribution; then, a coupling to the gas dynamic equations with transverse flow to study the growth of boundary layer thickness and the effect of convective cooling on sheath structure. The basic processes which must be included in this model are described below.

A plasma consists of electrons, ions, and neutral particles in the presence of electric and/or magnetic fields. If the gas is weakly ionized, and all collisions are binary encounters, the particles are completely described by distribution functions which satisfy a Boltzmann equation with the appropriate Lorentz force and collision term. In most practical cases, the distribution function for neutral particles is close to the equilibrium-Maxwellian form, so that moment equations can be used to describe the local gas properties in terms of an average density, flow velocity and temperature. For a sheath imbedded in a turbulent boundary layer, the effects of viscosity and thermal conductivity must be included along with a source term for gas heating.

Because of their mass, the ions can also be described by moment equations, with the inclusion of relevant production and loss processes, momentum and energy transfer to neutrals, and Joule heating. However, due to their greater mobility and resulting nonequilibrium behavior, the electrons must be dealt with in terms of the full space and velocity distribution function. Electrons play a dominant role in determining sheath structure. Consequently, their accurate description is considered an essential part of the present study. The electron velocity distribution must be obtained from a numerical solution of the collisional Boltzmann equation without the usual angular approximation. The treatment of electron and ion kinetics must be self-consistent with the

solution of Poisson's equation for the electric field. In the presence of an applied magnetic field, additional field equations are required along with a modified Lorentz force term.

3.1 Literature Search

A literature search was conducted covering the areas of nonequilibrium electron kinetics and collision-dominated sheaths. The list of references presented is meant to be more representative than exhaustive. Preference was given to the most recent papers and the latest work of a given author. Studies of the turbulent boundary layer which did not treat electric sheaths were not included. The considerable research on electric probe theory was also not considered immediately applicable. Only one paper was found¹ which analyzed the interaction between sheath and boundary layer. The results of that work will be incorporated into the present study.

The term "nonequilibrium electron kinetics" refers to either spatial or temporal nonequilibrium as occurs, for example, in the Townsend discharge and in streamer development, respectively. In either case, the electron energy distribution is not completely specified by the local electric field and gas density but must be considered in the full context of spatial or temporal growth. Studies of electron kinetics can be broken into two major groups, 1) those based on Monte Carlo simulation^{5, 10, 12, 13, 15, 17} and 2) those based on analysis of the Boltzmann equation.^{4, 6, 7, 11, 14, 16} They include several detailed comparisons of the two methods.^{4, 5, 8} Most of the calculations were based on a uniform electric field, except for one assuming a logarithmic⁹ and one a linear¹⁰ dependence. There were only two papers involving the self-consistent treatment of nonequilibrium electron kinetics with the field equations. One was a Monte Carlo simulation of the temporal development of electron avalanches or streamers.¹³ The other was a study of a low-pressure plasma diode using the Krook model to describe the collision term in the Boltzmann equation.¹⁴ These theories will be discussed in the following section.

The subject of collision-dominated sheaths was broadened to include other situations involving the interaction between a plasma and space-charge-induced fields. The papers in this category can be divided roughly into two groups, 1) analyses of steady-state sheaths^{18, 20, 24, 26-30} and 2) simulations of discharge initiation^{19, 22, 25} and glow-to-arc transitions.^{21, 23} Both problems involve the same system of equations and there is little difference in the general method of solution. Only the assumptions made and the processes included differentiate these studies. All treatments are based on the use of moment equations to describe the electrons and ions. Some consider gas heating effects²¹. Others include an external ionization source.^{20, 24, 27} Most models deal with only one spatial dimension (except References 18, 21, and 23, which consider two). The applicability of these approaches to the present study will be addressed in the following section.

3.2 Evaluation of Appropriate Theories

The theories identified in the literature search and listed in Section 3.4 will now be evaluated on the basis of their potential in meeting the requirements of the present study. The requirements are as follows:

- a) The system of equations must include as a minimum, the Poisson equation for the electric field, the collisional Boltzmann equation for electrons, the moment equations for ions and the boundary layer equations for the neutral gas. The kinetic equations for electrons and ions may be replaced by Monte Carlo simulation with an appropriate collision model.
- b) The theory must consider the proper boundary conditions at the wall-sheath interface and at the sheath-plasma interface. The sheath-plasma boundary conditions may be omitted if the calculations are continued to the opposite wall or electrode.

- c) The solution must be obtainable in two spatial dimensions with full, self-consistent coupling between all equations.
- d) The treatment of electron kinetics must utilize realistic cross sections, including angular dependence, a source term for external ionization and loss terms for attachment and recombination.
- e) The equations for ion kinetics must include the inertia term, charge exchange, and the same production-loss terms as for electrons.
- f) The boundary layer equations must consider gas heating in the sheath, as well as heat conduction to the wall.
- g) Since the computer code is to be used in a parametric mapping of sheath characteristics over quite a broad parameter space, it must be reasonably economical in the use of central processor memory and time.

First, a comparison will be made between Boltzmann and Monte Carlo techniques. Although the two approaches are mathematically equivalent, there are important economic and scientific differences. Economically, the Monte Carlo methods are very costly as far as computer time is concerned. No quantitative comparisons were found, but all authors who tried both, found the Monte Carlo simulation to be much more time consuming than a Boltzmann analysis. Scientifically, the Boltzmann approach gives a greater insight into the physics of a particular situation. Approximate solutions can be found analytically which illustrate the dependence on relevant parameters, and the sensitivity to changes in input data can be more easily determined. Also, exact analytic solutions in certain situations provide a benchmark for numerical results. The principal advantage of the Monte Carlo method is the ease with which it can be formulated into a computer code.

Recent solutions of the Boltzmann equation have dealt with the problem of electron swarm motion in a uniform electric field, when ionization and/or attachment are appreciable.^{4, 8} These studies treat the effect of electron density gradients by an expansion in higher-order spatial derivatives. (The present author has calculated the diffusion coefficients for these higher-order terms in argon at low values of E/N , where electron impact ionization is negligible.³⁶) Using this approach, the electron density in an avalanche or swarm can be described by an expanded continuity equation with position- and time- independent coefficients. A comparison with Monte Carlo results indicates excellent agreement.^{5, 8}

The technique described above is not immediately applicable to the sheath problem, because of the assumption of a uniform electric field. An extension of the method to include spatial gradients of the field does not appear practical. A more feasible approach, outlined by Allis,⁷ involves a direct solution of the Boltzmann equation without expansion. He derives an equation for the flux of electrons in the two-dimensional space (W, V), where W is the total electron energy and V is the electric potential. This approach neglects the specific angular dependence of the distribution function and hence prevents the use of differential cross sections. We propose to include a third independent variable defining the component of electron motion in the field direction and to solve the Boltzmann equation numerically. This method will be discussed in the following section.

A technique similar to the one proposed here has been used by Fournier, et al⁶ to analyze the cathode region of a glow discharge. His work has not been published in detail, so it is not clear what calculational methods were used or what assumptions were made. Preliminary results indicate that this method provides an accurate description of the electron kinetics in a sheath. Other approaches^{3, 9} which make simplifying assumptions in order to ease the numerical calculation are useful in understanding the physics of a situation and in arriving at analytic expressions for trans-

port and ionization coefficients but are not considered accurate enough or general enough for the present study.

An analysis which comes very close to meeting the requirements of our model for electron and ion kinetics was presented by Whipple, et al.¹⁴ They obtained a self-consistent solution of the Boltzmann equation for electrons and ions along with Poisson's equation, in a low-pressure plasma diode. The main shortcoming of this work was the use of an inverse fifth power law potential to describe collisions between charged particles and neutrals. The method of solution, however, involves a nested iteration scheme which should work equally well with the more accurate collision term required here.

The analyses of collision-dominated sheaths cover a variety of special situations, from MHD generators to gas discharges, from the cathode fall region to the positive column, both transient and steady state. The equations used to describe the plasma, however, differ little from one treatment to the next. The methods of solution depend on geometry and time scale, but qualitatively are very similar. The principal drawback in all cases is in the treatment of electron kinetics. The use of moment equations with equilibrium coefficients is more accurate in some situations than in others but always falls short of providing a complete model.

What all the studies have shown is that in treating sheaths and streamers, it is important to consider neutral density variations, space charge induced fields and nonequilibrium electron kinetics. However, these effects have never been brought together into a single, unified theory of the plasma sheath. The only significant addition to the model of the cathode fall since Ward's early work^{29, 30} has been the inclusion of an external source term.^{20, 24, 27} The recent renewal of interest in the problem^{2, 3, 6} should lead to significant contributions in the near future.

4.0 MATHEMATICAL MODEL

The equations describing electron and ion kinetics in an electric field are presented below. The Boltzmann collision term for electrons is derived in its full angular dependent form so as to be applicable in the case of strongly anisotropic distributions. Elastic and inelastic collisions are treated along with various electron production and loss processes. The continuity and momentum equations for positive and negative ions are modified to include a source term. The gas dynamic equations will be presented in Section 5.2.

4.1 The Boltzmann Equation

The distribution function, $f(\vec{c}, \vec{r}, t)$, provides a complete statistical description of the electrons in a weakly-ionized gas. The number of electrons in the volume element $(\vec{r}, \vec{r}+d\vec{r})$ with velocities in the range $(\vec{c}, \vec{c}+d\vec{c})$ at time t is given by $f(\vec{c}, \vec{r}, t) d\vec{c} d\vec{r} dt$. The equation which describes the evolution of this function in space and time is the collisional Boltzmann equation,

$$\frac{\partial f}{\partial t} + \vec{c} \cdot \nabla_{\vec{r}} f + \vec{a} \cdot \nabla_{\vec{c}} f = \left(\frac{\partial f}{\partial t} \right)_c \quad (1)$$

where \vec{a} is the acceleration due to electric and magnetic fields. In general,

$$\vec{a} = - \frac{e}{m} (\vec{E} + \vec{c} \times \vec{B}) \quad (2)$$

where e is the absolute value of the electronic charge. The term on the right in Equation (1) represents the change in f due to collisions and will be described in detail below.

If we consider for the moment, variations in one spatial dimension, with axis antiparallel to the applied electric field, then Equation (1) can be rewritten for $f(c, c_y, y)$ as

$$c_y \frac{\partial f}{\partial y} + \frac{e}{m} E(y) \frac{\partial f}{\partial c_y} = \left(\frac{\partial f}{\partial t} \right)_c \quad (3)$$

where $E(y)$ is the magnitude of the local electric field. By dividing both sides of Equation (3) by c_y and $eE(y)$ we have,

$$\frac{\partial f}{\partial \phi} + \frac{\partial f}{\partial \xi} = \frac{1}{ec_y E(y)} \left(\frac{\partial f}{\partial t} \right)_c \quad (4)$$

where $\phi = e \int_0^y E(y) dy$ is the electron potential energy and $\xi = \frac{1}{2} mc_y^2$ is the electron⁰ kinetic energy in the field direction. If we define the total kinetic energy as $\epsilon = \frac{1}{2} mc^2$, then f can be represented as the sum of two functions, $f_-(\epsilon, \xi, \phi)$ and $f_+(\epsilon, \xi, \phi)$, for the distribution of electrons moving with ($c_y < 0$) and against ($c_y > 0$) the electric field, respectively.

In the absence of collisions, f is constant along the lines $\xi - \phi = \text{const.}$ These are known as the characteristics and also correspond to electron trajectories in the two-dimensional space (ξ, ϕ) . When collisions are included, the term on the right in Equation (4) represents the change in f along the characteristics. As we shall see below, the collision term is a complicated function of f and the various cross sections. The present method of solution will be to estimate f , use this in evaluating the collision term, and then integrate Equation (4) along the characteristics. The distribution function thus obtained becomes the next estimate in an iterative procedure which continues until convergence is reached. This technique has been used in similar situations by the present author³¹ and others^{33, 34} with considerable success.

The boundary conditions for f_+ are given at $\phi = 0$ and those for f_- at $\phi = \phi_{\text{max}}$. The function $f_+(\epsilon, \xi, 0)$ may represent the distribution of electrons ejected from a cathode surface by ion impact, or it may equal zero for a nonemitting surface. The function $f_-(\epsilon, \xi, \phi_{\text{max}})$ is either the distribution of electrons at the head of the positive column ($\phi_{\text{max}} = V_c$), or at the anode ($f_- = 0$), or along an axis of symmetry ($f_- = f_+$). Along the locus of turning points, $\xi = 0$, the condition $f_+(\epsilon, 0, \phi) = f_-(\epsilon, 0, \phi)$ applies.

Boltzmann Collision Term

The collision term in the Boltzmann equation represents the rate at which electrons are scattered into or out of a given region of phase space as a result of collisions with ions, neutrals, or other electrons. For the present, we shall consider only collisions with neutral particles and recombination with positive ions. The neutral particle reactions include elastic, inelastic and superelastic scattering, ionization and attachment. The first three processes result in a change of phase space coordinates for a single electron, whereas the second two processes involve the creation or removal of an electron. Positive ion recombination also involves the loss of an electron. The collision term is then the sum of contributions from the various processes, i. e.

$$\left(\frac{\partial f}{\partial t}\right)_c = \left(\frac{\partial f}{\partial t}\right)_e + \left(\frac{\partial f}{\partial t}\right)_h + \left(\frac{\partial f}{\partial t}\right)_s + \left(\frac{\partial f}{\partial t}\right)_i + \left(\frac{\partial f}{\partial t}\right)_{a,r} \quad (5)$$

The individual terms will now be derived.

a) Elastic Collisions:

The number of electrons per unit volume with velocities in the range $(\vec{c}, \vec{c} + d\vec{c})$ which are scattered through an angle (γ, ψ) into the solid angle $d\omega$ by elastic collisions with molecules in the range $(\vec{C}, \vec{C} + d\vec{C})$ in a time interval dt is,

$$dn = f(\vec{c}) d\vec{c} F(\vec{C}) d\vec{C} g \sigma_e(\gamma, g) d\omega dt \quad (6)$$

where g is the magnitude of the relative velocity and $\sigma_e(\gamma, g)$ is the differential elastic cross section. The scattering is defined by a polar angle γ and azimuth angle ψ which give the rotation of the relative velocity in the center of mass coordinate system. The functions $f(\vec{c})$ and $F(\vec{C})$ are the velocity distributions of the electrons and molecules respectively. (The spatial dependence has been suppressed here since all collisions are considered point encounters involving no change in position.) The rate of change of the distribution function is found by dividing dn by $d\vec{c}$ and dt .

Consider now a background gas which is perfectly cold, i.e. $F(\vec{C}) = N\delta(\vec{C})$. This is an excellent approximation in describing collisions between electrons and heavy particles when the electron mean energy is much greater than the gas thermal energy. The relative velocity, g , is now equal to the initial electron velocity, c . After integrating Equation (6) over C we have,

$$\frac{dn}{d\vec{c} dt} = f(\vec{c}) N c \sigma_e(\gamma, c) d\omega \quad (7)$$

where

$$d\omega = \sin \gamma d\gamma d\psi$$

Each collision term can be divided into two parts, one being the rate at which electrons are scattered out of a given element in velocity space and the other being the rate at which they are scattered in. The rate of scattering out can be found from Equation (7) by integrating over all possible scattering angles. This gives,

$$\left(\frac{\partial f}{\partial t}\right)_{e, out} = f(\vec{c}) N c Q_e(c) \quad (8)$$

$$\text{where } Q_e(c) = \int \sigma_e(\gamma, c) d\omega$$

The number of electrons scattered into the interval $(\vec{c}, \vec{c} + d\vec{c})$ is just the sum of electrons scattered out of all other intervals $(\vec{c}_1, \vec{c}_1 + d\vec{c}_1)$ which have final velocities in $(\vec{c}, \vec{c} + d\vec{c})$. That is,

$$\left(\frac{\partial f}{\partial t}\right)_{e, in} = \int d\vec{c}_1 f(\vec{c}_1) N c_1 \int d\omega \sigma_e(\gamma, c_1) \delta(\vec{c}_2 - \vec{c}) \quad (9)$$

where \vec{c}_2 is the final velocity of an electron with initial velocity \vec{c}_1 . The delta function in Equation (9) is given in cylindrical coordinates by

$$\delta(\vec{c}_2 - \vec{c}) = \frac{\delta(c_2 - c) \delta(\theta_2 - \theta) \delta(\phi_2 - \phi)}{c_2^2 \sin \theta_2} \quad (10)$$

For an elastic encounter with a stationary target,

$$c_2 = c_1 \left[1 - \frac{2Mm}{(M+m)} (1 - \cos\gamma) \right]^{1/2} \quad (11)$$

$$\text{and } c_2 \cos \theta_2 = \frac{m}{M+m} c_1 \cos \theta_1 + \frac{M}{M+m} c_1 (\cos \theta_1 \cos \gamma + \sin \theta_1 \sin \gamma \cos \psi) \quad (12)$$

where m and M are the masses of the electron and the molecule respectively.

We now change the variable of integration in Equation (9) from c_1 to c_2 and expand all functions of c_1 in a Taylor series around c_2 , since $c_1 - c_2$ is of order m/M which is small. Thus,

$$dc_1 \sim \left[1 + \frac{m}{M} (1 - \cos \gamma) \right] dc_2 \quad (13)$$

$$\begin{aligned} \text{and } c_1^3 f(c_1, \theta_1) \sigma_e(\gamma, c_1) &\sim c_2^3 f(c_2, \theta_1) \sigma_e(\gamma, c_2) \\ &+ (c_1 - c_2) \frac{\partial}{\partial c} \left[c^3 f(c, \theta_1) \sigma_e(\gamma, c) \right]_{c=c_2} \end{aligned} \quad (14)$$

$$\text{with } c_1 - c_2 \sim c_2 \frac{m}{M} (1 - \cos \gamma) \quad (15)$$

Using these expressions in Equation (9) and integrating over c_2 and ϕ_2 , we have

$$\begin{aligned} \left(\frac{\partial f}{\partial t} \right)_{e, \text{in}} &\sim N \int \sin \theta_1 d\theta_1 f(c, \theta_1) c \int d\omega \sigma_e(\gamma, c) \frac{\delta(\theta_2 - \theta)}{\sin \theta_2} \\ &+ \frac{m}{M} \frac{N}{c^2} \frac{\partial}{\partial c} c^4 \int \sin \theta_1 d\theta_1 f(c, \theta_1) \int d\omega (1 - \cos \gamma) \sigma_e(\gamma, c) \frac{\delta(\theta_2 - \theta)}{\sin \theta_2} \end{aligned} \quad (16)$$

The second term on the right is a result of the small amount of energy transferred from the electron to the target in the form of recoil motion.

b) Inelastic Collisions:

Since the rate of scattering out is independent of the final electron velocity, we have, in direct analogy with the elastic case,

$$\left(\frac{\partial f}{\partial t} \right)_{h, \text{out}} = N f(c, \theta) c Q_h(c) \quad (17)$$

where $Q_h(c) = \int \sigma_h(\gamma, c) d\omega$ for each inelastic process. (There is an implied summation over h when more than one inelastic process exists.)

In an inelastic collision the final velocity is related to the initial velocity by,

$$\frac{1}{2} mc_2^2 = \frac{1}{2} mc_1^2 - \epsilon_h \quad (18)$$

where ϵ_h is the kinetic energy transferred to internal energy of the molecule. (Here recoil has been neglected for inelastic collisions. It can be included along with the recoil term for elastic scattering if necessary.)

From this relation it follows that $c_1 dc_1 = c_2 dc_2$. We can now replace σ_e with σ_h in Equation (9) and integrate over c_2 and ϕ_2 to obtain,

$$\left(\frac{\partial f}{\partial t} \right)_{h, in} = N \frac{c_+^2}{c} \int \sin \theta_1 d\theta_1 f(c_+, \theta_1) \int d\omega \sigma_h(\gamma, c_+) \frac{\delta(\theta_2 - \theta)}{\sin \theta_2} \quad (19)$$

The angles before and after the collision are related by,

$$c \cos \theta_2 = c_+ (\cos \theta_1 \cos \gamma + \sin \theta_1 \sin \gamma \cos \psi). \quad (20)$$

$$\text{where } \frac{1}{2} mc_+^2 = \frac{1}{2} mc^2 + \epsilon_h.$$

c) Superelastic Collisions:

The superelastic collision term is obtained from the corresponding inelastic collision term by changing ϵ_h to $-\epsilon_h$, σ_h to σ_s and N to N^* . The reverse cross section, σ_s , is related to the forward by detailed balance, i.e.

$$c_1 \sigma_s(\gamma, c_1) = c_2 \sigma_h(\gamma, c_2) \quad (21)$$

$$\text{where } \frac{1}{2} mc_2^2 = \frac{1}{2} mc_1^2 + \epsilon_h. \quad (22)$$

Using these expressions in Equations (17) and (19) we have,

$$\left(\frac{\partial f}{\partial t}\right)_{s, out} = N^* f(c, \theta) c_+ Q_h(c_+) \quad (23)$$

$$\text{and } \left(\frac{\partial f}{\partial t}\right)_{s, in} = N^* c_- \int \sin \theta_1 d\theta_1 f(c_- \theta_1) \int d\omega \sigma_h(\gamma, c) \frac{\delta(\theta_2 - \theta)}{\sin \theta_2} \quad (24)$$

$$\text{where } \frac{1}{2} mc_{\pm}^2 = \frac{1}{2} mc^2 \pm \epsilon_h.$$

d) Ionizing Collisions:

First, we define the probability per unit time that an electron with velocity c_1 making an ionizing collision produces an electron (scattered or ejected) with velocity in the range $(c_2, c_2 + dc_2)$ as,

$$Nc_1 Q_i(c_1, c_2) dc_2$$

Then, by conservation of energy, another electron is also produced with velocity c_3 given by,

$$\frac{1}{2} mc_3^2 = \frac{1}{2} mc_1^2 - \frac{1}{2} mc_2^2 - \epsilon_i \quad (25)$$

where ϵ_i is the ionization energy. (We have assumed for the present that the scattered and ejected electrons are produced isotropically.) The collision term for scattering out by ionizing collisions is then

$$\left(\frac{\partial f}{\partial t}\right)_{i, out} = Nf(c, \theta) c \int_0^{c_-/\sqrt{2}} Q_i(c, c_2) dc_2 \quad (26)$$

where as before, $\frac{1}{2} mc_{\pm}^2 = \frac{1}{2} mc^2 \pm \epsilon_i$. The upper limit of integration is the velocity at which the scattered and ejected electrons have equal energy. Above this value, we begin counting the same events over again.

The collision term for electrons scattered into the range $(c, c+dc)$ is, by analogy with the inelastic term,

$$\left(\frac{\partial f}{\partial t}\right)_{i, in} = \frac{N}{2} \int \sin \theta_1 d\theta_1 \int_{c_+}^{\infty} f(c_1, \theta_1) \frac{c_1^2}{c} Q_i(c_1, c) dc_1 \quad (27)$$

The integration is carried out over all velocities which can contribute to the population at c .

e) Attachment and Recombination:

These processes result in the loss of an electron, so the only effect on the distribution function is,

$$\left(\frac{\partial f}{\partial t}\right)_{a, r, out} = N f(c, \theta) c [Q_a(c) + Q_r(c)] \quad (28)$$

Now the Boltzmann collision term is equal to the sum of all contributions scattered in, minus the sum of those scattered out.

All of the terms representing electrons scattered into the interval $(\vec{c}, \vec{c} + d\vec{c})$ involve an integration over the scattering angle, γ , the angle before collision, θ_1 , and a delta function specifying the orientation after the collision θ_2 .

For example, the elastic term neglecting recoil is,

$$\frac{1}{c} \left(\frac{\partial f}{\partial t}\right)_{e, in} = N \int \sin \theta_1 d\theta_1 d\phi_1 f(c, \theta_1) \int d\omega \sigma_e(\gamma, c) \frac{\delta(\theta_2 - \theta) \delta(\phi_2 - \phi)}{\sin \theta_2} \quad (29)$$

The delta function can be eliminated by noting that $d\omega = \sin \theta_2 d\theta_2 d\phi_2$ and performing the integration over θ_2 and ϕ_2 . Thus,

$$\frac{1}{c} \left(\frac{\partial f}{\partial t}\right)_{e, in} = N \int \sin \theta_1 d\theta_1 d\phi_1 f(c, \theta_1) \sigma_e(\gamma, c) \quad (30)$$

where $\cos \gamma = \cos \theta_1 \cos \theta + \sin \theta_1 \sin \theta \cos(\phi_1 - \phi)$. A similar transfor-

mation can be made on the remaining scattered-in collision terms. Given a differential cross section, σ_e , the integral in Equation (30) can be thought of as an operator, K_e , acting on f . Then, if we define an operator, K , as the sum of operators for each collision process, we can write Equation (4) as

$$\frac{\partial f}{\partial \varphi} + \frac{\partial f}{\partial \xi} = \frac{1}{e E/N(\varphi)} \left(\frac{\epsilon}{\xi} \right)^{1/2} \{ K - Q(\epsilon) \} f \quad (31)$$

where $Q(\epsilon)$ is the total cross section for electrons with kinetic energy, $\epsilon = \xi + \eta$.

The operator, K , acts in the two-dimensional space (ξ, η) , i.e. the value of Kf on the plane $\varphi = \varphi_0$ is independent of the values of f for $\varphi \neq \varphi_0$. Thus K can be represented numerically as a four-dimensional matrix. Since the range in each dimension must be subdivided into at least 100 intervals, the storage of such a matrix is completely out of the question. The functions Kf and f , defined in terms of three independent variables, would require three-dimensional arrays for their storage, also highly impractical. However, the function f does not have to be saved from one iteration to the next in solving Equation (31). Only Kf must be stored, and this can be done by making a simplifying assumption. In most practical cases, the function Kf is nearly isotropic in velocity space. Therefore, we will expand the angular dependence of Kf in Legendre polynomials, e.g.

$$K_e f = \frac{1}{Nc} \left(\frac{\partial f}{\partial t} \right)_{e, in} = \sum_{l=0}^{\infty} A_l(c) P_l(\cos \theta) \quad (32)$$

$$\text{where} \quad A_l(c) = \frac{2l+1}{2} \int_{-1}^1 \frac{1}{Nc} \left(\frac{\partial f}{\partial t} \right)_{e, in} P_l(\cos \theta) d(\cos \theta) \quad (33)$$

It should be pointed out at the beginning that the expansion in Equation (32) is quite different from the usual expansion of f . In particular, if $\sigma_e(\gamma, c)$ can be represented as the sum of n Legendre polynomials, $P_l(\cos \gamma)$, then

the sum in Equation (32) will also have n nonzero terms, regardless of the angular dependence of f . As a special case, if $\sigma_e(c)$ is isotropic, then Kf is always independent of θ and can be represented by one term,

Now, using Equation (29) in (33), we have

$$A_l(c) = Nc \frac{2l+1}{2} \int \sin \theta_1 d\theta_1 f(c, \theta_1) \int d\omega \sigma_2(\gamma, c) P_l(\cos \theta_2) \quad (34)$$

The addition theorem for spherical harmonics gives

$$P_l(\cos \theta_2) = \sqrt{\frac{4\pi}{2l+1}} \sum_{m=-l}^l P_l(\cos \theta_1) Y_l^m(\gamma, \psi) \quad (35)$$

which, after integrating over the angle ψ , becomes

$$\int_0^{2\pi} P_l(\cos \theta_2) d\psi = 2\pi P_l(\cos \theta_1) P_l(\cos \gamma) \quad (36)$$

When this is inserted into Equation (34), the integrals can be separated and Equation (32) becomes,

$$\left(\frac{\partial f}{\partial t} \right)_{e, in} = Nc \sum_{l=0}^{\infty} \frac{1}{2l+1} f_l(c) Q_l(c) P_l(\cos \theta) \quad (37)$$

where $Q_l(c) = 4\pi \sigma_l(c) = 4\pi \frac{2l+1}{2} \int d(\cos \gamma) \sigma(\gamma, c) P_l(\cos \gamma)$

and $f_l(c) = \frac{2l+1}{2} \int d(\cos \theta) f(c, \theta) P_l(\cos \theta)$

In evaluating the integrals for the recoil term, there is an additional factor of $(1-\cos \gamma)$ to be considered. The integration over scattering angle,

$$\int d(\cos \gamma) (1-\cos \gamma) \sigma_e(\gamma, c) P_l(\cos \gamma)$$

can be carried out by employing the recursion relation,

$$xP_\ell(x) = \frac{\ell+1}{2\ell+1} P_{\ell+1}(x) + \frac{\ell}{2\ell+1} P_{\ell-1}(x) \quad (38)$$

to obtain

$$\frac{2}{2\ell+1} \left[\sigma_\ell(c) - \frac{\ell+1}{2\ell+3} \sigma_{\ell+1}(c) - \frac{\ell}{2\ell-1} \sigma_{\ell-1}(c) \right]$$

The complete Boltzmann collision term can now be written,

$$\begin{aligned} \left(\frac{\partial f}{\partial t} \right)_c = & Nc \sum_{\ell=0}^{\infty} \frac{1}{2\ell+1} f_\ell(c) Q_\ell^e(c) P_\ell(\cos\theta) \\ & + \frac{m}{M} \frac{N}{c^2} \frac{\partial}{\partial c} \left\{ c^4 \sum_{\ell=0}^{\infty} \frac{1}{2\ell+1} f_\ell(c) \left[Q_\ell^e(c) - \frac{\ell+1}{2\ell+3} Q_{\ell+1}^e(c) \right. \right. \\ & \left. \left. - \frac{\ell}{2\ell-1} Q_{\ell-1}^e(c) \right] P_\ell(\cos\theta) \right\} \\ & + N \sum_{\ell=0}^{\infty} \frac{1}{2\ell+1} \sum_h \frac{c_+^2}{c} f_\ell(c_+) Q_\ell^h(c_+) P_\ell(\cos\theta) \\ & + N \sum_{\ell=0}^{\infty} \frac{1}{2\ell+1} \int_{c_+}^{\infty} \frac{c_1^2}{c} f_\ell(c_1) Q_\ell^i(c_1, c) dc_1 P_\ell(\cos\theta) \\ & - Ncf(c, \theta) \left[Q_o^e + \sum_h Q_o^h + \int_0^{c-\sqrt{2}} Q_o^i(c, c_2) dc_2 + Q_o^a + \frac{n_+}{N} Q_o^r \right] \quad (39) \end{aligned}$$

It has been assumed that secondary electrons produced in ionizing collisions are emitted isotropically. The contributions from superelastic collisions have been omitted. Because of the very small ratio of electron mass to neutral mass, the recoil term can also be neglected for most electric discharge applications.

The Boltzmann equation, in terms of the electron energy, $\epsilon = \frac{mc^2}{2e}$, is then

$$\begin{aligned}
 \frac{\partial f}{\partial \varphi} + \frac{\partial f}{\partial \xi} = & \frac{1}{eE/N(\varphi)} \frac{1}{\cos \theta} \left[\sum_{l=0}^{\infty} \frac{1}{2l+1} \left\{ f_l(\epsilon, \varphi) Q_l^e(\epsilon) \right. \right. \\
 & + \sum_h \frac{\epsilon + \epsilon_h}{\epsilon} f_l(\epsilon + \epsilon_h, \varphi) Q_l^h(\epsilon + \epsilon_h) \\
 & + \left. \int_{\epsilon + \epsilon_i}^{\infty} \frac{\epsilon'}{\epsilon} f_l(\epsilon', \varphi) Q_l^i(\epsilon', \epsilon) d\epsilon' \right\} P_l(\cos \theta) \\
 & - f(\xi, \eta, \varphi) \left\{ Q_0^e(\epsilon) + \sum_h Q_0^h(\epsilon) + \int_0^{(\epsilon - \epsilon_i)/2} Q_0^i(\epsilon, \epsilon') d\epsilon \right. \\
 & \left. \left. + Q_0^a(\epsilon) + \frac{n_+}{N} Q_0^r(\epsilon) \right\} \right] \quad \text{where } \cos \theta = \pm \left(\frac{\xi}{\epsilon} \right)^{1/2} \quad (40)
 \end{aligned}$$

The integro-differential equation above can be solved for the distribution function $f(\xi, \eta, \varphi)$, or $f(\epsilon, \theta, \varphi)$, given a nonuniform $E/N(\varphi)$ and a known set of cross sections. The program which was developed to do this will be described in the following section.

4.2 Electric Field and Ion Kinetics

Poisson's equation for the scalar potential, ϕ , defined by $E = -\nabla \phi$, is

$$-\nabla^2 \phi = \frac{e}{\epsilon_0} (n_+ - n_- - n_e) \quad (41)$$

where n_+ , n_- , and n_e are the positive ion, negative ion, and electron number densities, respectively. For the present, only one type of positive ion and negative ion will be considered. The equations can easily be modified to include more than one.

The heavy ions are governed by the moment equations, which represent conservation of number, momentum and energy. The continuity equations are

$$\nabla \cdot (n_+ \vec{v}_+) = S + zn_e - r_i n_+ n_- - r_e n_+ n_e = S_+ \quad (42)$$

$$\nabla \cdot (n_- \vec{v}_-) = an_e - dn_- - r_i n_+ n_- = S_- \quad (43)$$

where \vec{v}_+ and \vec{v}_- are the positive and negative ion drift velocities. The terms on the right hand side represent production and loss due to external ionization, S , Townsend ionization, z , attachment, a , detachment, d , and ion-ion and electron-ion recombination, r_i and r_e , respectively. The coefficients involving electron impact are defined in terms of the electron energy distribution and the appropriate cross sections, i.e.

$$z = \alpha v_e = N \sqrt{\frac{2e}{m}} \int_0^\infty Q^i(\epsilon) f_o(\epsilon, \phi) \epsilon d\epsilon$$

$$a = N \sqrt{\frac{2e}{m}} \int_0^\infty Q^a(\epsilon) f_o(\epsilon, \phi) \epsilon d\epsilon$$

$$\text{and } r_e = \sqrt{\frac{2e}{m}} \int_0^\infty Q^r(\epsilon) f_o(\epsilon, \phi) \epsilon d\epsilon$$

Notice that these coefficients are functions of position, as well as of the boundary conditions which go into calculating $f_0(\epsilon, \varphi)$.

The mean velocities, \vec{v}_+ and \vec{v}_- , are determined by momentum conservation,

$$m_+ n_+ (\vec{v}_+ \cdot \vec{V}) \vec{v}_+ + \vec{V} \cdot \vec{p}_+ - e n_+ \vec{E} = -m_+ n_+ \nu_+ (\vec{v}_+ - \vec{V}) - m_+ \vec{v}_+ S_+ \quad (44)$$

$$m_- n_- (\vec{v}_- \cdot \vec{V}) \vec{v}_- + \vec{V} \cdot \vec{p}_- + e n_- \vec{E} = -m_- n_- \nu_- (\vec{v}_- - \vec{V}) - m_- \vec{v}_- S_- \quad (45)$$

where m_+ and m_- are the masses of positive and negative ions, respectively and ν_+ and ν_- are the total collision frequencies of these ions with neutrals. The mean neutral velocity is \vec{V} . An equation of state relates the ion pressure, p_\pm , to the mean thermal velocity, c_\pm , and the temperature, T_\pm . Thus

$$p_\pm = \frac{1}{3} m_\pm n_\pm c_\pm^2 = n_\pm k T_\pm \quad (46)$$

The series of moment equations for heavy ions is terminated by assuming their thermal motion to be in equilibrium at the local gas temperature, T . This approximation is fairly good because of the nearly equal masses of ions and neutrals and the fact that at high pressures the sheath is collision dominated.

Let us consider now a plasma consisting of positive ions and electrons in a one-dimensional geometry. Then using Equation (42) in (44) without gas flow,

$$\frac{\partial}{\partial y} n_+ (m_+ v_+^2 + kT_+) = m_+ n_+ \nu_+ v_+ - e E n_+ \quad (47)$$

If diffusion is negligible compared to inertia ($n_+ \sim \text{const}$) and the drift energy is large compared to thermal energy ($m_+ v_+^2 \gg kT_+$), then

$$\frac{\partial v_+}{\partial y} = \frac{\nu_+}{2} - \frac{eE}{2m_+ v_+} \quad (48)$$

or in terms of the potential, φ ,

$$\frac{\partial v_+}{\partial \varphi} = \frac{v_+}{2E} - \frac{e}{2m_+} \frac{1}{v_+} \quad (49)$$

The collision frequency for momentum transfer is given by

$$\nu_+ = NQv_+ \quad (50)$$

where Q is dominated by charge exchange and can be considered independent of velocity.¹³

Given $E(\varphi)$, Equation (29) is integrated to obtain $v_+(\varphi)$. Then the positive ion number density is determined from

$$n_+ = \frac{j_+}{ev_+} = \frac{j - j_e}{ev_+} \quad (51)$$

where j is given and $j_e(\varphi)$ is obtained from the solution of Boltzmann's equation for electrons. Finally, Equation (41) is written in terms of φ ,

$$\frac{\partial}{\partial \varphi} \left(\frac{E^2}{2} \right) = \frac{e}{\epsilon_0} [n_e(\varphi) - n_+(\varphi)] \quad (52)$$

and integrated to yield a new $E^{(1)}(\varphi)$. This is used in Equation (29) and the procedure is repeated until convergence is reached. The Boltzmann equation for electrons must be solved for each new field, $E^{(i)}$.

5.0 COMPUTER PROGRAMS

Two computer programs are described briefly in this section. The first was developed entirely under the present contract to solve the two-dimensional Boltzmann equation for electrons which is then coupled self-consistently with the ion kinetics, gas dynamics, and field equations. The second is a program for solving the boundary layer equations along a flat plate which was modified in a previous contract to include a heat addition term defined by the electric discharge.

5.1 Program SHEATH

The approach used to solve the Boltzmann equation involves a numerical integration along the characteristics, $\xi - \phi = \text{const}$, combined with an iteration scheme for evaluating the collision integral, Kf . Initially it is assumed that there is no contribution from scattered-in electrons, i.e. $Kf = 0$, and Equation (40) is integrated in both the forward and backward directions for each value of η . This gives a first approximation to the distribution function $f^{(1)}$ from which a new $Kf^{(1)}$ is calculated, and the procedure is repeated until convergence is reached.

The operations required to generate successive approximations to the collision integral are performed as the integration proceeds, so that the function f does not have to be stored between iterations. Only Kf has to be retained. By performing the integrations in a specific order, the same array can be used to store the old and the new values of Kf . If Kf is represented by the first two terms in a Legendre expansion, then two two-dimensional arrays are needed. These arrays are trapezoidal in shape, since $f(\xi, \eta, \phi) = 0$ for $\xi > \phi + \xi_0$, where ξ_0 is the maximum value of longitudinal energy for electrons leaving the cathode.

The storage arrays for Kf are arranged in core as in Figure 1 to minimize central memory requirements. The dimensions were chosen to give 1 eV resolution for a 200 V cathode fall. The energy distribution of electrons

emitted from a cathode by positive ion impact has a cutoff at $\epsilon_i - 2\phi_w$, where ϵ_i is the ionization potential of the gas and ϕ_w is the work function of the cathode material. This cutoff is usually less than 20 eV, so that 20 mesh points at the cathode are again sufficient for 1 eV resolution. The area of the array in Figure 1 is 48,240₁₀ (136,160g) words. Obviously, the storage of f (or of Kf without angular expansion), which would require at least ten times this much core, is impractical.

Boundary conditions are specified at the cathode and at the anode. At the cathode, the energy and angular distribution of emitted electrons are given. At the anode, the distribution of backscattered and ejected secondary electrons is given in terms of the incident primary flux. At the turning points, the forward and backward fluxes are equal.

The algorithm used for the numerical integration of Equation (40) is the following,

$$f_{i+1} = \left[C_{i+1} + C_i + \left(\frac{2}{\Delta\xi} - \frac{Q_{i+1}}{E/N_{i+1}} \right) f_i \right] \left(\frac{2}{\Delta\xi} + \frac{Q_i}{E/N_i} \right) \quad (53)$$

where $C = \frac{1}{eE/N} \left(\frac{\epsilon}{\xi} \right)^{1/2} Kf$ and $\Delta\xi$ is the energy step. The scheme is second order and absolutely stable. The relative error at each step is,

$$\epsilon = \frac{C''}{2} \left(\frac{\Delta\xi}{2} \right)^2 + \frac{2}{3} \left(\frac{\Delta\xi}{2} \frac{Q}{E/N} \right)^3 \quad (54)$$

The error is small as long as

$$\Delta\xi \leq 0.5 E/NQ$$

This condition is easily satisfied near the cathode surface, where $E/NQ \sim \epsilon_i$, and ϵ_i is typically 20 eV. It can also be satisfied in the positive column, where $E/NQ \sim 1$ eV. However, in the negative glow, the field becomes very small and may even reverse directions. Under these conditions,

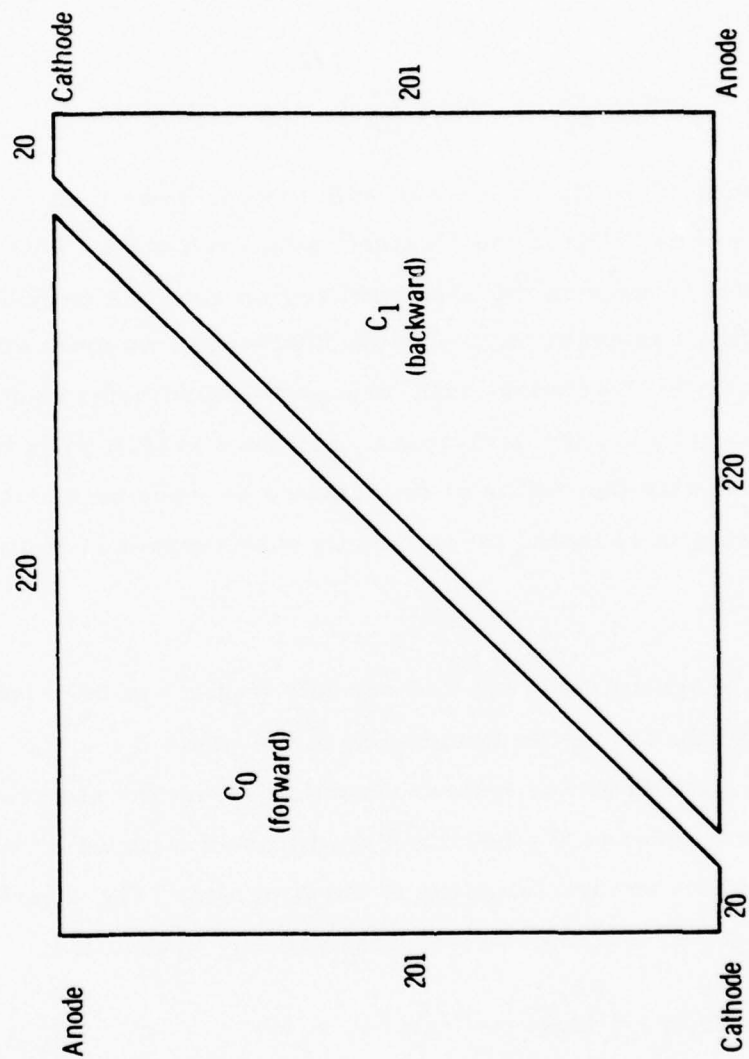


Figure 1 Storage Array for Collision Integral

the algorithm of Equation (53) cannot be used and in fact the choice of variables in Equation (40) is no longer appropriate, since position becomes a multivalued function of the potential.

In the region where $E/NQ \ll 1$ eV, the Boltzmann equation can better be expressed as,

$$\frac{\partial f}{\partial y} + eE(y) \frac{\partial f}{\partial \xi} = N(y) \left(\frac{\epsilon}{\xi} \right)^{1/2} \left\{ K - Q(\epsilon) \right\} f \quad (55)$$

Now a fixed position step, Δy , is chosen with the condition that, $\Delta y \leq 0.283/NQ$, where $1/NQ$ is the electron mean free path. This choice of variables cannot be used in the high field region near the cathode. Therefore, to fully define f in every region of the discharge, we must start with coordinates (ξ, η, φ) in the cathode fall, change to coordinates (ξ, η, y) in the negative glow and Faraday dark space, and back to (ξ, η, φ) in the positive column. Basically the choice of coordinates depends on whether the distribution function is changing more rapidly with respect to position or potential.

With the present program, only the cathode fall region has been examined. The code is currently set up for integration in the plane $\eta = 0$, i.e. electrons are restricted to moving either with or directly against the electric field. This simplification reduces the running time by about a factor of ten and allows rapid checkout and modification of the program. The distribution function is normalized in a one-dimensional velocity space, i.e.

$$\int_0^{\infty} \left[f_+(\epsilon, \varphi) + f_-(\epsilon, \varphi) \right] \epsilon^{-1/2} d\epsilon = n_e(\varphi) \quad (56)$$

where f_+ is the distribution of electrons moving toward the anode and f_- is the distribution moving toward the cathode. These functions satisfy Equation(31) with one of the following pairs of collision terms.

(a) Forward scattering:

$$\begin{aligned}
 Kf_+ &= \sum_h Q^h(\epsilon + \epsilon_h) f_+(\epsilon + \epsilon_h, \varphi) \\
 &+ 2 \int_{\epsilon + \epsilon_i}^{\infty} \frac{Q^i(\epsilon')}{\epsilon' - \epsilon_i} f_+(\epsilon', \varphi) d\epsilon' \\
 Q(\epsilon) &= \sum_h Q^h(\epsilon) + Q^i(\epsilon)
 \end{aligned} \tag{57}$$

(b) Isotropic scattering:

$$\begin{aligned}
 Kf_{\pm} &= \frac{Q^e(\epsilon)}{2} [f_+(\epsilon, \varphi) + f_-(\epsilon, \varphi)] + \frac{1}{2} \sum_h Q_h(\epsilon + \epsilon_h) [f_+(\epsilon + \epsilon_h, \varphi) + f_-(\epsilon + \epsilon_h, \varphi)] \\
 &+ \int_{\epsilon + \epsilon_i}^{\infty} \frac{Q^i(\epsilon')}{\epsilon' - \epsilon_i} [f_+(\epsilon', \varphi) + f_-(\epsilon', \varphi)] d\epsilon' \\
 Q(\epsilon) &= Q^e(\epsilon) + \sum_h Q^h(\epsilon) + Q^i(\epsilon)
 \end{aligned} \tag{58}$$

(c) Anisotropic scattering:

$$\begin{aligned}
 Kf_{\pm} &= Q_+^e(\epsilon) f_{\pm}(\epsilon, \varphi) + Q_-^e(\epsilon) f_{\mp}(\epsilon, \varphi) \\
 &+ \sum_h [Q_+^h(\epsilon + \epsilon_h) f_{\pm}(\epsilon + \epsilon_h, \varphi) + Q_-^h(\epsilon + \epsilon_h) f_{\mp}(\epsilon + \epsilon_h, \varphi)] \\
 &+ \int_{\epsilon + \epsilon_i}^{\infty} \frac{2}{\epsilon' - \epsilon_i} [Q_+^i(\epsilon') f_{\pm}(\epsilon', \varphi) + Q_-^i(\epsilon') f_{\mp}(\epsilon', \varphi)] d\epsilon' \\
 Q(\epsilon) &= Q_+^e(\epsilon) + Q_-^e(\epsilon) + \sum_h [Q_+^h(\epsilon) + Q_-^h(\epsilon)] + Q_+^i(\epsilon) + Q_-^i(\epsilon)
 \end{aligned} \tag{59}$$

The cross sections for attachment and recombination are small at high energies and are therefore not included in the analysis of the cathode fall region. They will be important, however, in the negative glow, Faraday dark space, and positive column. The secondaries produced by ionizing collisions are assumed to be evenly distributed in energy from zero to $\epsilon - \epsilon_i$. This is a good approximation near threshold. However, at higher energies the distribution is peaked near zero and $\epsilon - \epsilon_i$, with a minimum at $(\epsilon - \epsilon_i)/2$. Previous workers have found that the actual distribution of secondaries makes little difference to the overall results. This aspect may be investigated with the present code in the future.

The input parameters required by the program are (1) the electric field strength at the cathode, (2) the reduced gas pressure (this is the actual pressure reduced to standard temperature, i.e. $p_0 = p(273.16^\circ\text{K}/T)$, and (3) the voltage difference between cathode and anode. The function $E/N(\varphi)$ is then generated internally for either a constant or linear dependence on y . The cross sections are read in next, following a standardized format used previously by the author in an equilibrium Boltzmann code. (The specific input deck structure will be provided in the user's manual.) And finally, the energy distribution of electrons leaving the cathode is given.

The output data supplied by the program may be varied to suit the users' needs. Presently, the listing is set up as follows: The input parameters and cross sections are printed first. Then, in order to monitor the convergence, the electron current, j_e , as a function of potential, and the energy distribution, f_A , at the anode are listed after each iteration. The criterion for convergence is that the electron current at the anode change by no more than one percent. When this is reached, the following quantities are printed as functions of φ : the electron mean energy, $\bar{\epsilon}$, the distance from the cathode, y , the electron number density, n_e , the electron drift velocity, v_e , Townsend's first ionization coefficient, defined as $\alpha = \frac{1}{j_e} \frac{\partial j_e}{\partial y}$, and E/N . Even though the entire distribution function $f(\xi, \eta, \varphi)$ is never known

at any given time in the calculation, it can be printed out if desired. All the important information, however, can be extracted by listing $f(\xi, \eta, \varphi_0)$ at specific locations, φ_0 , and by listing various moment integrals, such as drift velocity, mean energy, diffusion coefficient, etc., as functions of position.

5.2 Program CATFAL

CATFAL is a computer program for calculating laminar and turbulent boundary layer development in compressible flow including the effects of cathode fall. The program is an extension of a program written at Princeton University and was developed under contract with Air Force Weapons Laboratory to analyze a high power CO CW gas laser. The laser configuration is illustrated in Figure 2. Gas flows through a two-dimensional supersonic nozzle at Mach 3.5 to 4.0. A high voltage (2-5 kV) is applied perpendicular to the flow and a discharge established in the region where the optical power is to be extracted. The electrical discharge is stabilized by means of an electron beam whose electrons have an energy of approximately 150 keV. In such a laser, a large potential gradient exists in the proximity of the cathode which is usually referred to as the "cathode fall region".

In this region, due to the large potential drop, strong electric fields are established. This results in a substantial amount of power in the form of heat being dissipated in the boundary layer next to the cathode. Such action produces a disturbance which propagates into the flow region. Because of the stringent requirements of flow homogeneity in CO CW lasers, the CATFAL computer program was written to estimate the magnitude of the flow disturbance. The code predicts the effect of cathode fall on the growth rate of the boundary layer. The analytical model for CATFAL was developed by Claudio Parazzoli, formerly of Northrop. Experiments were performed to verify the numerical predictions of CATFAL and those results are published in Reference 1.

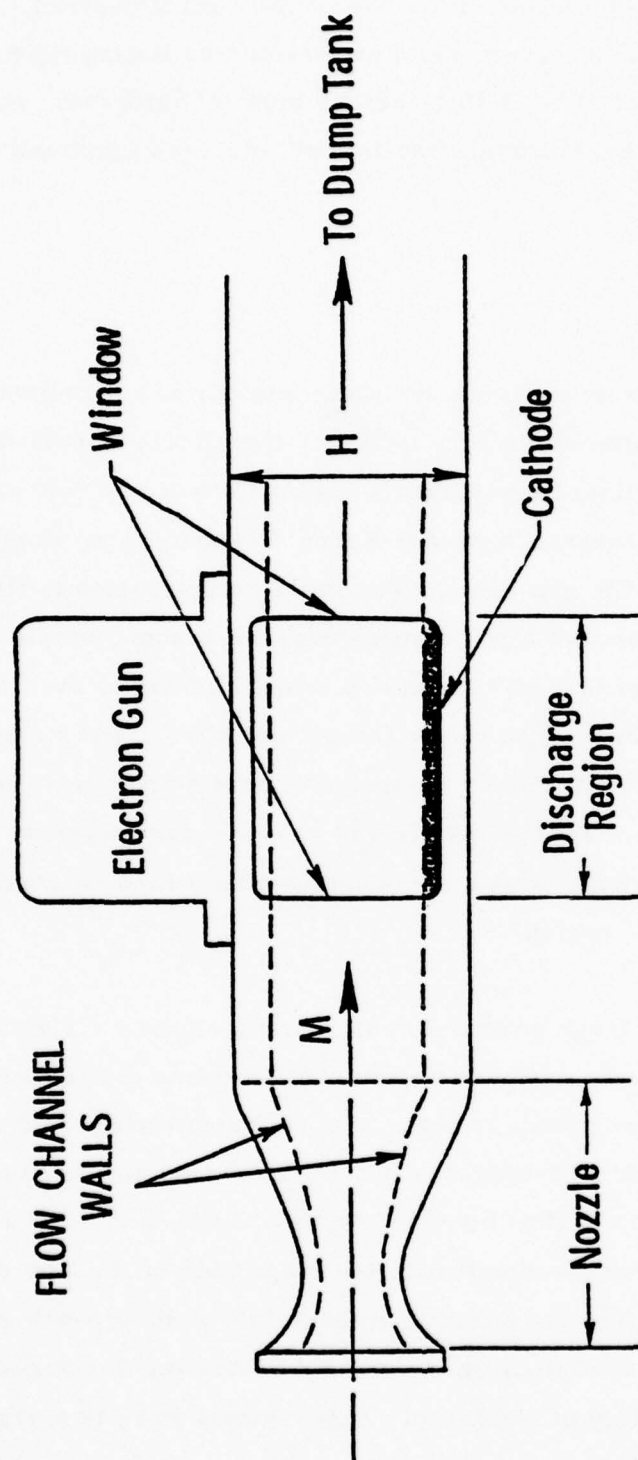


Figure 2 Schematic Drawing of the Nozzle and Discharge Region

5.2.1 Analytical Model

In this section we shall briefly describe the boundary layer equations for a turbulent compressible flow on a flat plate and we shall put them in a form manageable for numerical calculations.

Boundary Layer Equations

The equations governing the flow of a compressible, two-dimensional boundary layer are:

Continuity Equation

$$\frac{\partial \rho u}{\partial x} + \frac{\partial \rho v}{\partial y} = 0 \quad (60)$$

Momentum Equation

$$\rho u \frac{\partial u}{\partial x} + \rho v \frac{\partial u}{\partial y} = \rho_e u \frac{dU}{dx} + \frac{\partial \tau}{\partial y} \quad (61)$$

Energy Equation

$$\rho u \frac{\partial h^0}{\partial x} + \rho v \frac{\partial h^0}{\partial y} = \frac{\partial}{\partial y} (q + u\tau) + \dot{Q} \quad (62)$$

Figure 3 illustrates the relevant quantities in Equations (60) through (62).

Equations (60) to (62) apply both to laminar and turbulent boundary layer provided that the definitions for τ and q are taken to be

$$\tau/\rho = \nu \frac{\partial u}{\partial y} - \overline{u'v'}$$

$$q/\rho = \nu_g \frac{\partial h}{\partial y} - \overline{v'h'}$$

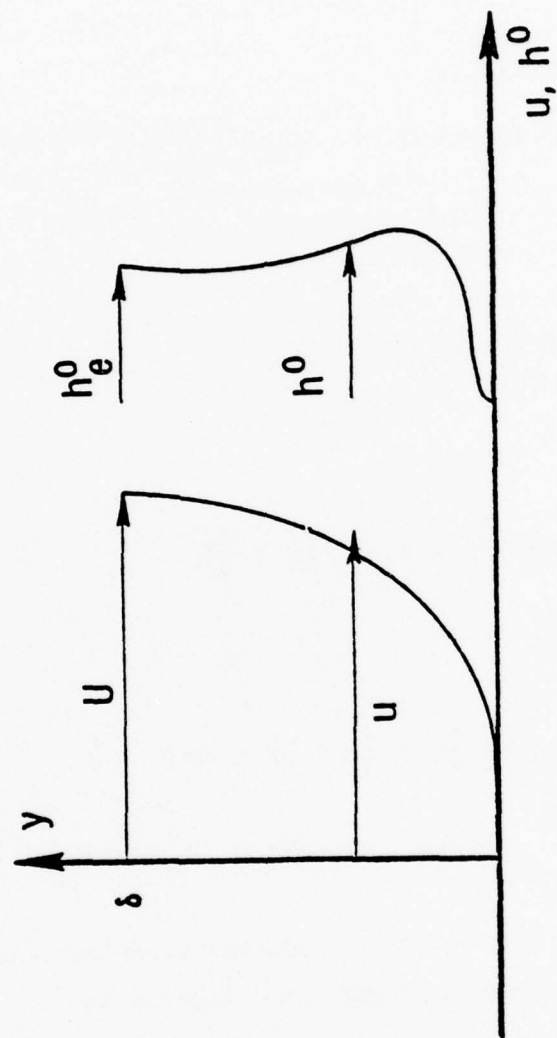


Figure 3 Relevant Quantities in the Boundary Layer Equations

where $-\overline{u'v'}$ is the kinematic Reynold's stress; $-\overline{v'h'}$ is the kinematic turbulent heat flux; $\nu = \frac{\mu}{\rho}$ is the molecular kinematic viscosity, and $\nu_g = \frac{k}{\rho c_p}$ is the molecular kinematic conductivity.

Then we define an effective viscosity and an effective conductivity as:

$$\tau/\rho = \nu_e \frac{\partial u}{\partial y}$$

$$\frac{q}{\rho} = \nu_{eg} \frac{\partial h}{\partial y}$$

Finally, the following quantities are introduced for convenience in the calculation:

$$f'(x, \eta) = \frac{\rho_e U(x) - \rho u(x, y)}{\rho_e U(x)} \quad (63)$$

$$g'(x, \eta) = \frac{h_e^0 - h^0(x, y)}{h_e^0 - h_r} \quad (64)$$

$$d(x, \eta) = \frac{\epsilon(x)}{(x, y)} \quad (65)$$

$$\eta = \frac{y}{\delta^*(x)} \quad (66)$$

where δ^* is the boundary layer displacement thickness given as:

$$\delta^* = \int_0^\infty [\rho_e U(x) - \rho u(x, y)] / \rho_e U(x) dy \quad (67)$$

When written in terms of the new variables defined in Equations (64) to (66), Equations (60) to (62) become:

Momentum Equation

$$\begin{aligned}
 & - \left\{ \frac{\gamma}{d} [d(1-f')] \right\}' + \left[(\eta-f) Q - \frac{\rho_w v_w}{\rho_e U} - \delta^* f_x \right] d f'' + \\
 & + \left\{ \left[Q(\eta-f) - \frac{\rho_w v_w}{\rho_e U} - \delta^* f_x \right] d' - (2-f') (dP + d_x \delta^*) \right\} f' - \\
 & - \left[(\eta-f) Q - \frac{\rho_w v_w}{\rho_e U} - \delta^* f_x \right] d' + P(d-1) + d_x \delta^* = \\
 & = (1-f') \delta^* d f'_x
 \end{aligned} \tag{68}$$

Energy Equation

$$\begin{aligned}
 & \left[\frac{\gamma g}{d} \left\{ g'' - \frac{1}{H} \frac{\frac{\gamma_e - 1}{2} M_e^2}{1 + \frac{\gamma_e - 1}{2} M_e^2} \left(\frac{v_e}{v_{eg}} - 1 \right) [d^2 (1-f')^2] \right\}' \right]' + \\
 & + g'' \left[Q(\eta-f) - \delta^* f_x - \frac{\rho_w v_w}{\rho_e U} \right] = (1-f') \delta^* g'_x + \\
 & + \frac{\delta^* \dot{Q}}{\rho_e U (h_e^0 - h_r)}
 \end{aligned} \tag{69}$$

$$d = \left[\frac{1}{\frac{\gamma_e - 1}{2} M_e^2} \frac{(1-g'H) \left(1 + \frac{\gamma_e - 1}{2} M_e^2 \right) - 1 - \frac{\gamma_e - 1}{\gamma_e} I(d)}{(1-f')^2} \right]^{\frac{1}{2}} \tag{70}$$

where $I(d)$ is:

$$I(d) = \int_1^d \frac{\gamma(x)}{\gamma(x) - 1} dx$$

with $x = \frac{\rho_e}{\rho}$ and γ is the variable specific heat ratio across the boundary layer. Equations (68) to (70) are similar to expressions II-14, II-15 and II-16 in Reference 1. The major differences are in Equations (69) and (70). Equation (69) contains the heat addition term in the R. H. S.

$\frac{\delta^* \dot{Q}}{\rho_e U (h_e^0 - h_r)}$ which is absent in Equation II-15 of Reference 1. Equation (70) accounts for a variable specific heat ratio across the boundary layer, and reduces to Equation II-16 of Reference 1 if we take $\gamma = \gamma_e$. In the derivation of Equation (70), the specific heat ratio of γ_e , in the free stream, has been taken to be constant.

References 1 and 47 give detailed discussions of the form of normalized effective viscosity $\nu_e = \frac{\nu_e}{U \delta^*}$, and effective heat conductivity $\nu_{eg} = \frac{\nu_{eg}}{U \delta^*}$.

5.2.2 Computer Code

The original gas dynamics program was written by H. J. Herring and G. L. Mellor at Princeton University.⁴⁷ The program performs a numerical integration of the equations of motion for a compressible two-dimensional boundary layer. Calculations may be carried out for both laminar and turbulent flow for arbitrary Reynolds number and freestream Mach number distribution. Planar or axisymmetric bodies with wall heating or cooling, wall suction or blowing and rough or smooth wall can be included.

Modifications were made to the program to include bulk heat addition due to the cathode fall of a glow discharge in the two-dimensional planar case. Boundary layer equations were modified to include a heat addition term.

The program can handle arbitrary gas mixtures of up to four components. Calculation of molecular viscosity and heat conductivity of gas mixtures as a function of temperature is included. Allowance of variable specific heats and ion and electron drift velocities in a gas mixture are computed as a function of E/N and tabulated for utilization in computing the power term. Poisson's equation and current continuity equations are then solved using iterative techniques and Runge-Kutta integration to satisfy certain boundary conditions.

The MAIN program was modified to compute viscosity and heat conductivity for an arbitrary gas mixture of up to four components. Subroutine VISC provides fourth order polynomial curve fits of viscosity, heat conductivity and Prandl number as a function of temperature. SHRSUB then computes the specific heat ratio for the gas mixture.

The MAIN program iterates to find velocity (FP) and enthalpy (GP) profiles within desired convergence criteria. Before each FP-GP iteration, subroutine POWER solves Poisson's equation and the current continuity equations using a fourth order Runge-Kutta approximation. An iterative procedure is used to satisfy the boundary conditions. Power dissipation in the vicinity of the cathode is computed and included in the boundary layer calculation.

The program, written entirely in FORTRAN, has been run on the CDC 175 and has a core requirement less than 160,000 words (octal). Typical running time with heat addition is normally 3-4 minutes. Output at each X position is written on file 9 and can be saved on tape or permanent file for subsequent restart if desired.

6.0 NUMERICAL RESULTS

The computer program, SHEATH, was developed in stages over a period of time and was checked at each stage by making comparisons with cases published in the literature. All of these runs were made assuming constant gas density and a known electric field variation. One self-consistent field solution is given at the end of Section 6.1. The difficulties encountered in extending the self-consistent solution into the negative glow are discussed in Section 6.2.

6.1 Nonequilibrium Electron Kinetics

The first runs were made in mercury for comparison with the Monte Carlo simulations of Parker, et al.¹⁵ The ionization cross section of Kieffer, et al.³⁷ was fitted to the functional form,

$$Q^i(\epsilon) = \frac{A}{\epsilon} \ln \left(\frac{\epsilon + \epsilon_i^2 / \epsilon}{2\epsilon_i} \right)$$

where $A = 5.25 \epsilon_i \sigma_{\max}$, $\epsilon_i = 10.4$ eV, and $\sigma_{\max} = 6.5 \text{Å}^2$. (At this point the subroutine for reading cross section data in numerical form had not been incorporated into the program.) Forward scattering was assumed with no backscatter from the anode. The electrons were allowed to fall 300 V at a constant E/p_0 of 4000 V/cm/Torr. The energy distribution of electron current striking the anode is shown in Figure 4.

A similar case was examined in Reference 15 with a gap separation of 1000 V. The two distributions compare very well below about 250 eV, indicating that the low energy electrons have reached an equilibrium with the field. A plot of f_A/ϵ indicates that the distribution is very nearly Maxwellian in this region, with a temperature of ~100 eV. The peak in the energy distribution above 300 eV represents those electrons which have suffered no ionizing collisions. The 5 eV width of this peak is a reflection of the energy distribution leaving the cathode. The gap below 300 V has a width of $\epsilon_i - W$, where W is the width of the primary peak. As pointed out

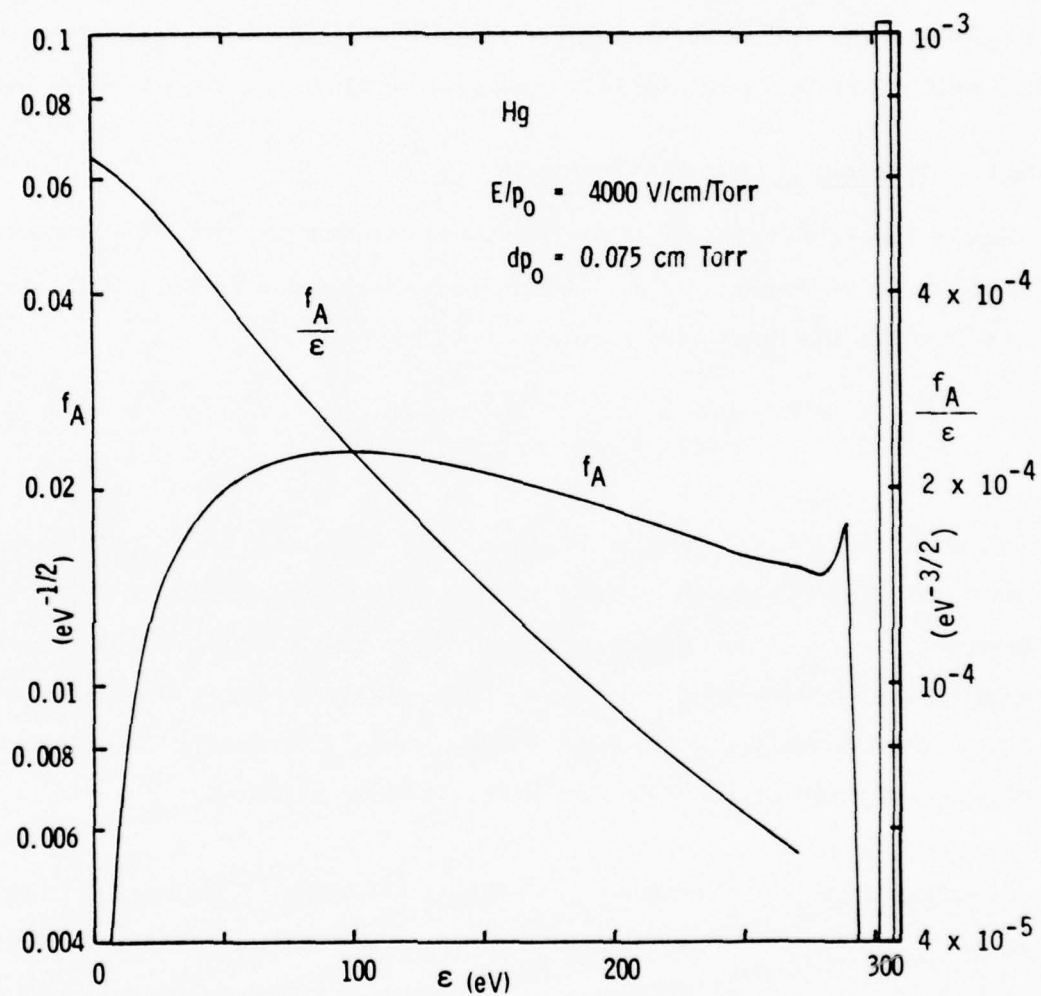


Figure 4 Electron Current at the Anode

earlier, $W = \epsilon_i - 2\phi_w$, so the width of the gap is just equal to twice the work function of the cathode material, ϕ_w .

The electron current density and first Townsend ionization coefficient are shown in Figure 5. There is no ionization until the electrons have first been accelerated to the ionization threshold. This occurs at $y = \epsilon_i/E = 0.0104$ cm. The Townsend coefficient rises rapidly above threshold and overshoots the eventual equilibrium value of $\alpha_0 \sim 4.0 \text{ cm}^{-1}$. (This is to be compared with the value obtained in Reference 15 of $\alpha_0 \sim 5.1 \text{ cm}^{-1}$ at the same E/N and pressure, but using a different ionization cross section.) The nonequilibrium behavior of α over most of the discharge gap is obvious from the figure. However, the multiplication factor, $M = j_e(d)/j_e(0) = 3.6$, is very close to the value $e^{\alpha_0 d} = 3.3$ which would obtain for constant $\alpha = \alpha_0$.

The foregoing example was meant to simulate conditions typical of dielectric breakdown in low pressure gases, where the electric field is uniform. In order to investigate the nonequilibrium behavior of electrons in the cathode region of a glow discharge, we examined the following problem. Let the electric field fall linearly from 1000 V/cm at the cathode to 50 V/cm at the midplane and remain constant from there to the anode. The reduced pressure is 0.25 Torr and the potential difference is again 300 V (270 V in the "cathode fall" and 30 V in the "negative glow"). The results are shown in Figure 6.

The behavior of α over the first 0.4 cm is very similar to that of Figure 5, even though in the present case the electric field has fallen to less than 300 V/cm. This is because most of the ionization in this region comes from the primary group, whose energy is $\epsilon = \phi$, independent of the local field. The Townsend ionization coefficient for a monoenergetic group of electrons is $\alpha(\epsilon) = NQ^i(\epsilon)$, which has a maximum value of 5.75 cm^{-1} at 60 eV. This maximum is never reached in practice, however, because secondaries are produced at low energies with lower ionization efficiencies than the primary group.

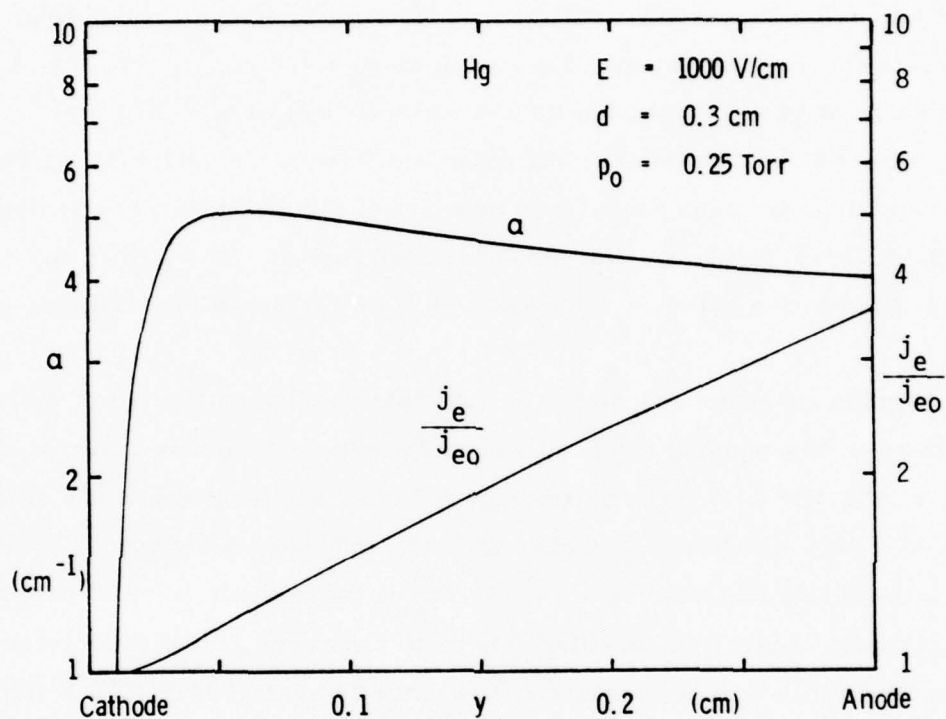


Figure 5 Current Density and Ionization Coefficient

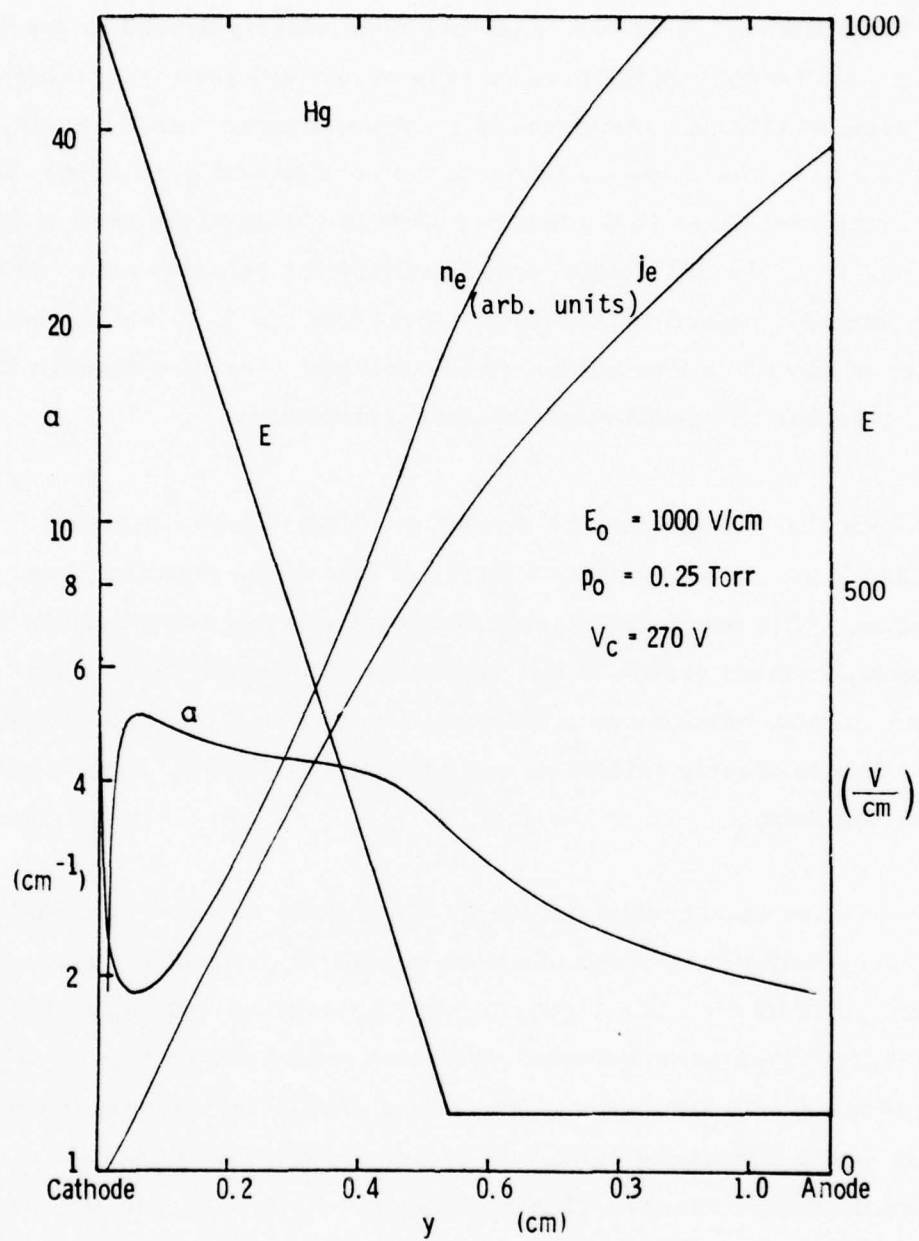


Figure 6 Electron Kinetics in a Nonuniform Field

The persistence of ionization after the electric field is reduced is another nonequilibrium feature evident in Figure 6. The rate at which α decays from one equilibrium value to a lower one must clearly depend on the degree of angular scattering. In the present case of forward scattering (which is actually no scattering at all) the persistence is most pronounced. As we shall see later, in the case of isotropic scattering the persistence is reduced. The situation with real gases in the negative glow is closer to the case of forward scattering, since the differential cross sections for energies above 20 eV are very strongly peaked in the forward direction. In fact, the beam-like character of electrons leaving the cathode fall and persisting through the negative glow has been well established experimentally.³⁸

The electron current and number density are also shown in Figure 6. Notice that j_e increases by about a factor of four in the negative glow or drift region. With previous theories of the cathode fall using equilibrium coefficients, current growth in this region would be negligible. Thus predicted current densities as a function of cathode fall potential would be low. This is clearly evident in a comparison of Ward's³⁰ results with experimental data.

As electrons are accelerated away from the cathode surface, the number density drops initially in order to maintain current continuity. Then as ionization picks up the density goes through a minimum and begins to rise exponentially. This same behavior was observed by Tran Ngoc, et al³⁹ in their Monte Carlo simulation. The initial drop is less severe if electrons are emitted from the cathode at higher energy, since they reach ionization threshold sooner. The electron density is rising faster than the current at $y = 0.4$ cm because the drift velocity is falling with the field.

The next set of runs was made in argon with isotropic scattering and one inelastic process in addition to ionization. The results are compared with

the Monte Carlo simulations of Sakai, et al.⁵ in a uniform field. The cross sections used here are shown in Figure 7. They are similar, though not identical to those employed in Reference 5. The inelastic cross section, which is meant to represent the sum of all electronic excitations, was taken from Schaper, et al.⁴⁰ For elastic scattering we used the momentum transfer cross section of Spencer, et al.⁴¹ and for ionization, the measurements of Rapp, et al.⁴²

The drift velocity and ionization coefficient for $E/N = 565 \text{ Td}$ ($1 \text{ Td} = 10^{-17} \text{ V cm}^2$) are shown in Figure 8 as a function of distance from the cathode. The most striking feature of these curves is the series of discontinuities in the drift velocity beginning near the cathode and diminishing in amplitude as y increases. Similar oscillations had been observed previously by Sakai, et al.¹² and were ascribed to the onset of inelastic thresholds. This behavior can now be more fully explained as follows.

Below the first inelastic threshold at 11.5 eV there are only primary electrons which have suffered no inelastic collisions. Due to elastic scattering however, these electrons are moving both with and against the electric field. Their drift velocity is towards the anode and increases as they are accelerated by the field.

Above the first inelastic threshold, there appears a group of electrons which have suffered one inelastic collision. They have an energy $\epsilon = \varphi - \epsilon_h$. Those electrons which are moving toward the cathode will be decelerated by the field until they reach zero velocity at the point $y = \epsilon_h / E$. Thus, immediately above the first inelastic threshold, there is a group of electrons with zero drift velocity superimposed on the primary group. This gives rise to the first discontinuity. The drift velocity then continues to increase as both groups of electrons are accelerated toward the anode.

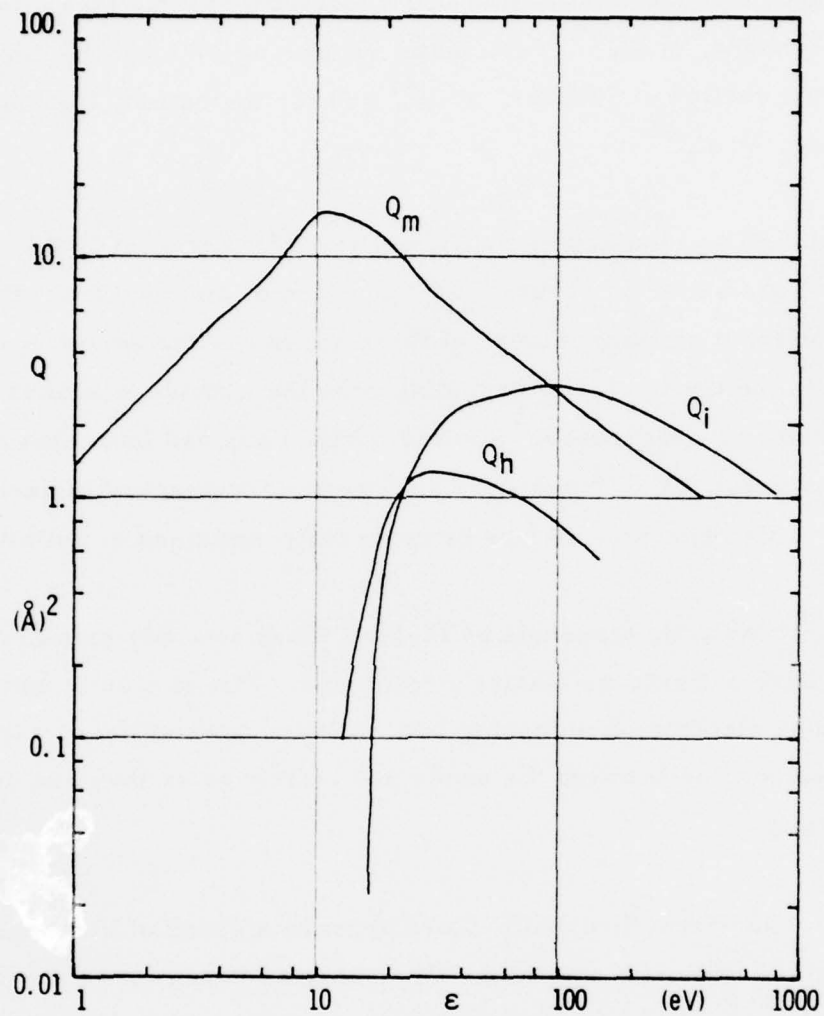


Figure 7 Cross Sections in Argon

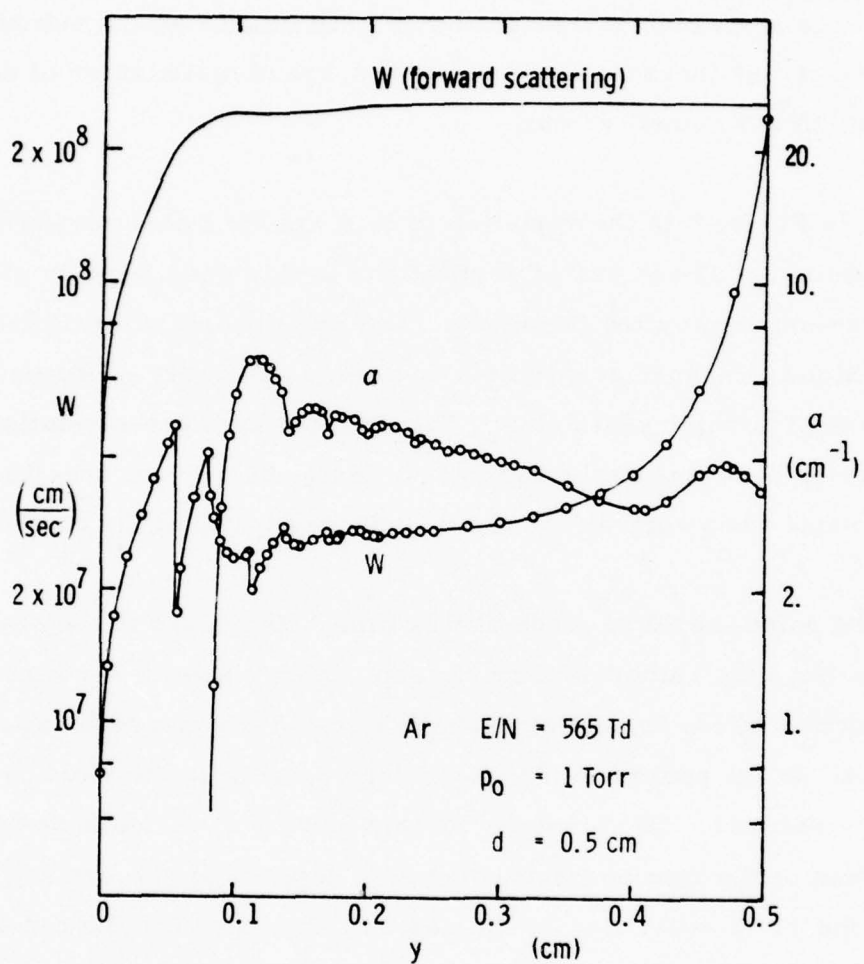


Figure 8 Drift Velocity and Ionization Coefficient

A similar drop in the drift velocity occurs at the ionization threshold of 16 eV, except that here the energy loss is not discrete but is distributed over a range of values. A series of discontinuities occurs at two, three, and four times the inelastic and ionization thresholds, caused by electrons which have undergone two, three, and four inelastic or ionizing collisions, and so on. The amplitude of the oscillations diminishes as the number of secondary electrons increases. These have a broad distribution of energies and the effect is smeared out.

Also shown in Figure 8 is the variation in drift velocity when forward scattering is assumed. There are no oscillations in this case because all the electrons are moving toward the anode. The equilibrium value of drift velocity, which is reached at about $y = 0.2$ cm, is an order of magnitude larger than for isotropic scattering. This implies an inverse relationship for the electron densities in the two cases, since the current densities are almost the same when normalized to the current density at the cathode.

An important point should be made at this time with regard to the emission of electrons from the cathode. Experiments which measure secondary electron ejection by ion impact are usually carried out in a high vacuum environment. In the presence of a gas at high pressure, the yield can be considerably reduced. The electron current density at the cathode is not only a function of the rate of ejection but also depends on the surface E/N and on the degree of scattering by the gas. In the cases considered above, electrons were ejected from the cathode at the rate of γ per unit area. The current density in the case of forward scattering was $e\gamma$, while for isotropic scattering it was only $0.3 e\gamma$ because 70% of the ejected electrons were backscattered in the gas and reabsorbed by the cathode.

The Townsend α coefficient in Figure 8 is zero below the ionization threshold then rises rapidly to a peak and undergoes a few oscillations analogous to

those in the drift velocity. The equilibrium value of 4.5 cm^{-1} at $y = 0.2 \text{ cm}$ compares well with the value obtained by Tagashira, et al.¹² of 4.3 cm^{-1} . The drift velocity at this point is $2.7 \times 10^7 \text{ cm/sec}$ compared to $3.2 \times 10^7 \text{ cm/sec}$ in Reference 4. The increase in drift velocity from $y = 0.2 \text{ cm}$ to 0.5 cm is a consequence of the boundary condition at the absorbing anode. The flux of electrons moving toward the cathode decreases from its equilibrium value to zero at the anode. At this point all electrons are moving in the forward direction so the drift velocity is the same as that with forward scattering.

The distribution of electron current striking the anode is shown in Figure 9. The most prominent feature of this plot is the series of equally spaced peaks below 100 V. These represent the groups of electrons which have undergone 0, 1, 2, ... inelastic energies leaving the cathode. In this case, a box of 0.5 eV width has been assumed. The series of plateaus represent electrons which have undergone one ionizing and 0, 1, 2, ... inelastic collisions. Electrons experiencing more than one ionizing collision and all secondary electrons make up the body of the distribution.

In Figure 10 the electron energy distribution is plotted on a linear scale for comparison with the Monte Carlo results of Sakai, et al.⁵ Although there is considerable statistical scatter in the Monte Carlo data, some areas of similarity and difference can be pointed out. The Monte Carlo results fall consistently below the present results at energies below 10 eV and consistently above 10 eV and 20 eV. The high energy tail of the distribution is in fairly good agreement. The differences may be due to the different cross sections used or they may reflect the approximations made in angular scattering.

The next run in argon was made with an electric field which varied linearly with position, falling from 600 V/cm/Torr at the cathode to 30 V/cm/Torr at the anode. Figure 11 shows the variation of electron current and number density with distance from the cathode. The anode is at 0.33 cm Torr and

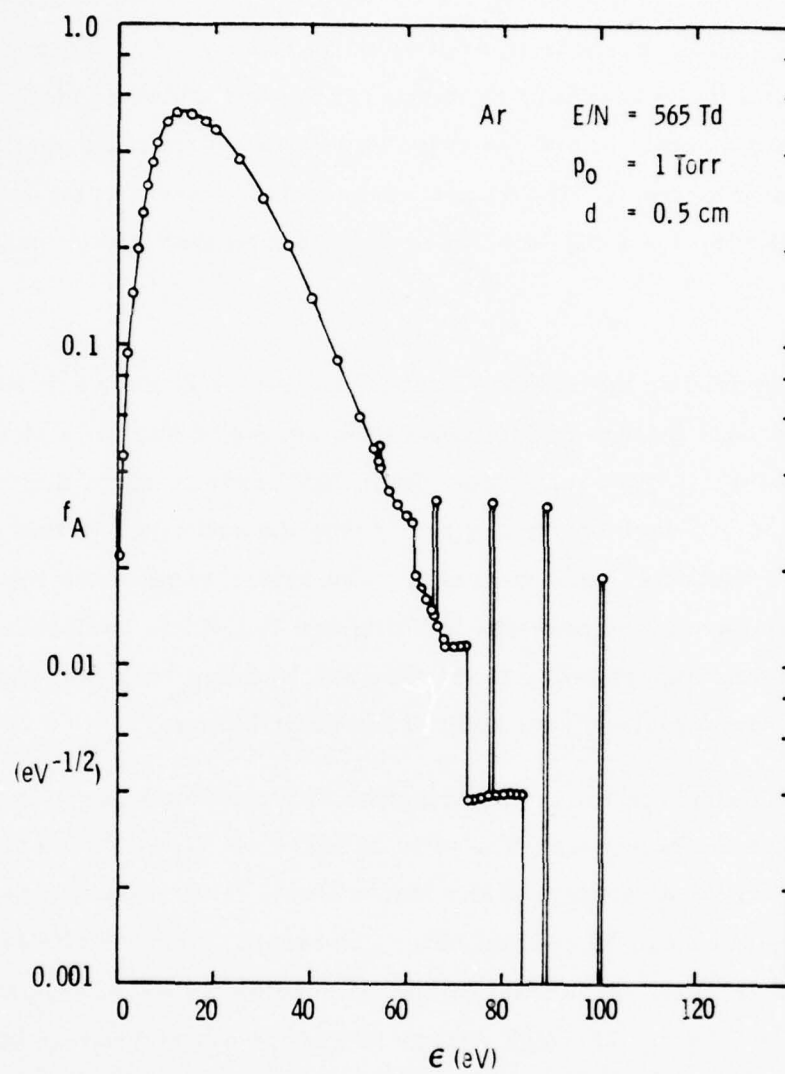


Figure 9 Electron Current at the Anode

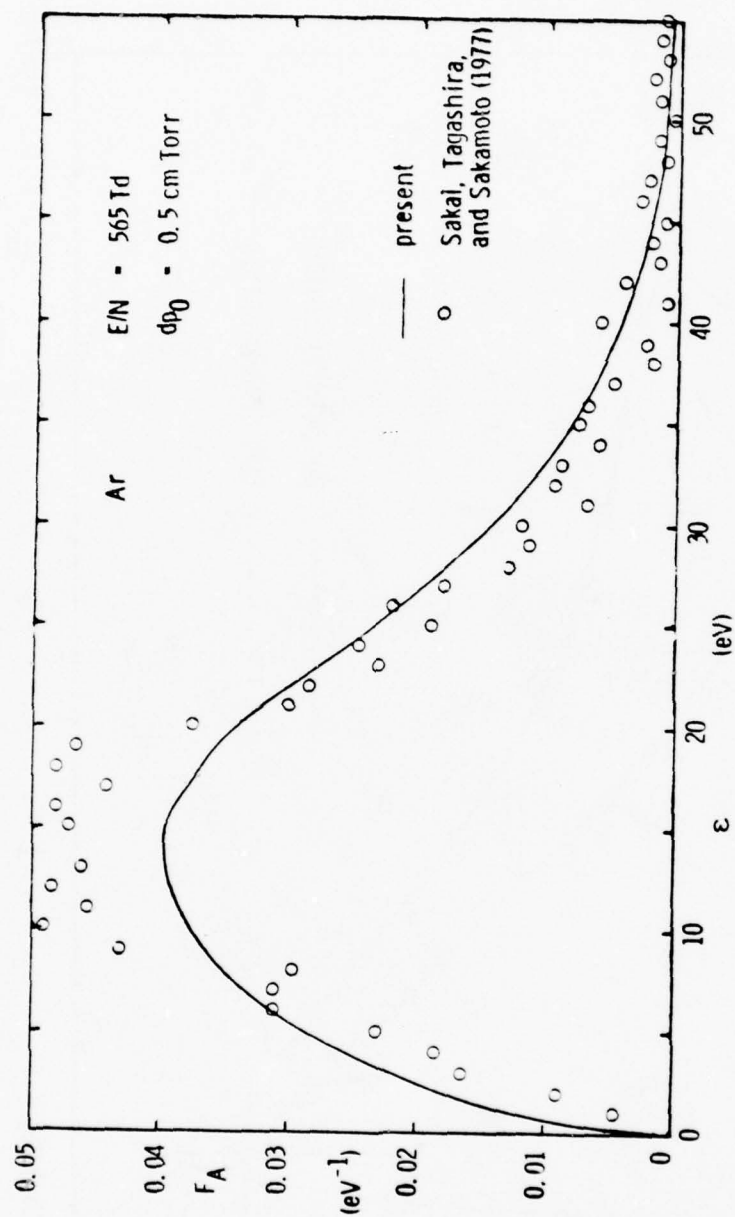


Figure 10 Electron Energy Distribution at the Anode

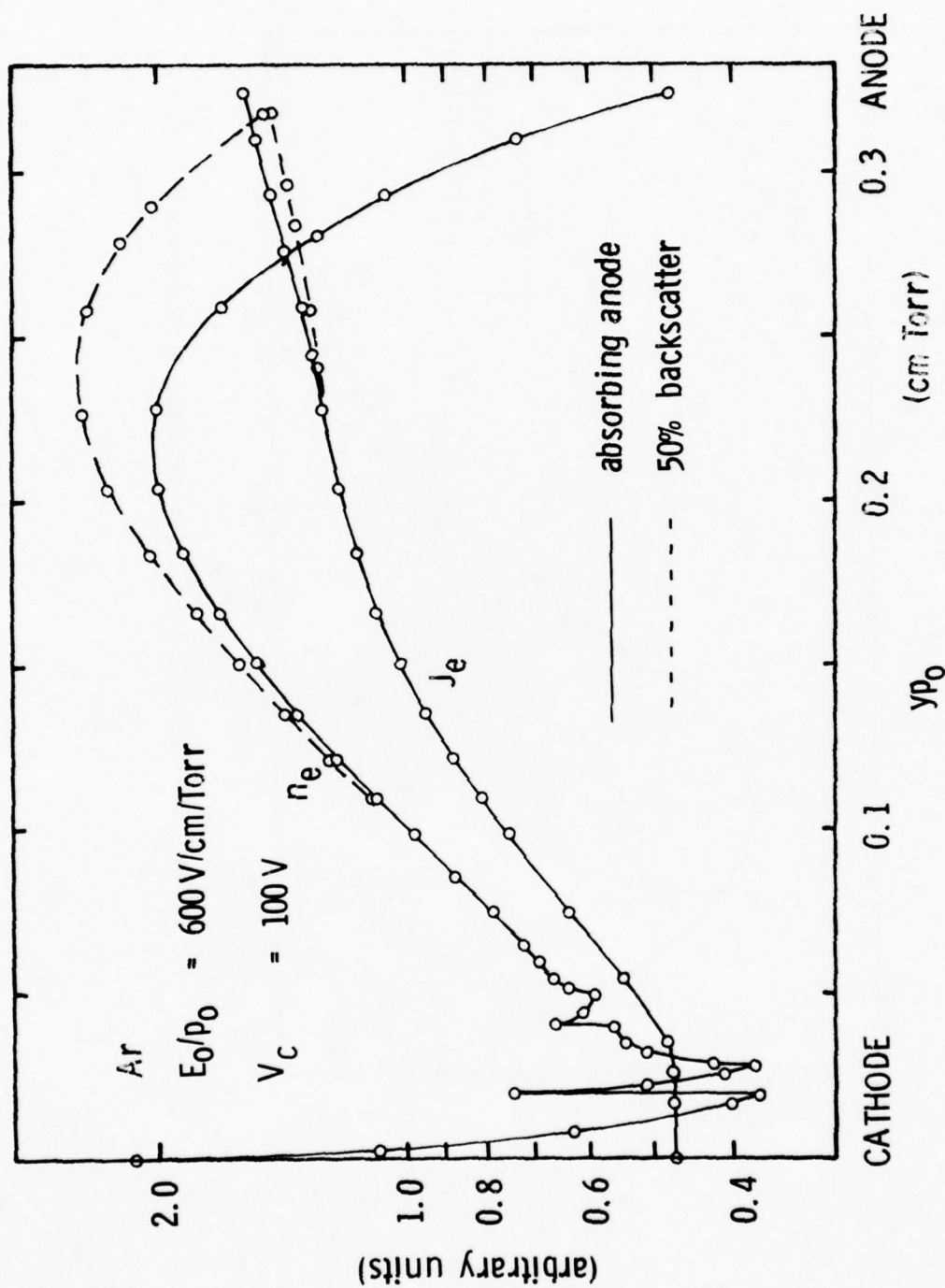


Figure 11 Electron Current and Number Density

was taken to be either perfectly absorbing or to reflect 50% of the incident electrons. The electron current is constant below the ionization threshold which occurs at 0.028 cm Torr. It then rises smoothly and begins to level off before rising again in front of the anode. The number density behaves just as the inverse of the drift velocity at low energies since $j_e = en_e W$. The falloff in approaching the anode indicates a rising drift velocity. Notice that with 50% backscatter, the effect of the anode on the electron distribution is reduced.

The Townsend ionization coefficient for this case is shown in Figure 12. The form is quite different from what would be obtained by assuming an equilibrium energy distribution at the local E/N . The ionization in the latter case would be greatest at the cathode and fall off as shown by the dotted line. The actual ionization is zero near the cathode due to the threshold effect and is higher than the equilibrium value in the low field region because of the time required for fast electrons to slow down. Note once again the effect of changing the boundary condition at the anode.

The three functions which will couple directly to the ion kinetics and the field equations in the self-consistent model of the cathode region are the ionization coefficient and the electron current and number densities versus position. The product of the first two of these, αj_e , gives the ionization source density which appears in the positive ion continuity equation. The electron number density appears in the Poisson equation. The numerical formulation of these equations and the method of solution were given in Section 4.2.

The numerical routines for solving Equations (49)-(52) have been incorporated into program SHEATH, and a fully self-consistent solution was obtained for the parameters given in Figure 13. The electron and ion number densities and drift velocities are shown as functions of y . (The assumption that $n_+ \sim \text{const}$ is seen to be justified and $mv_+^2 \gg kT$ over most

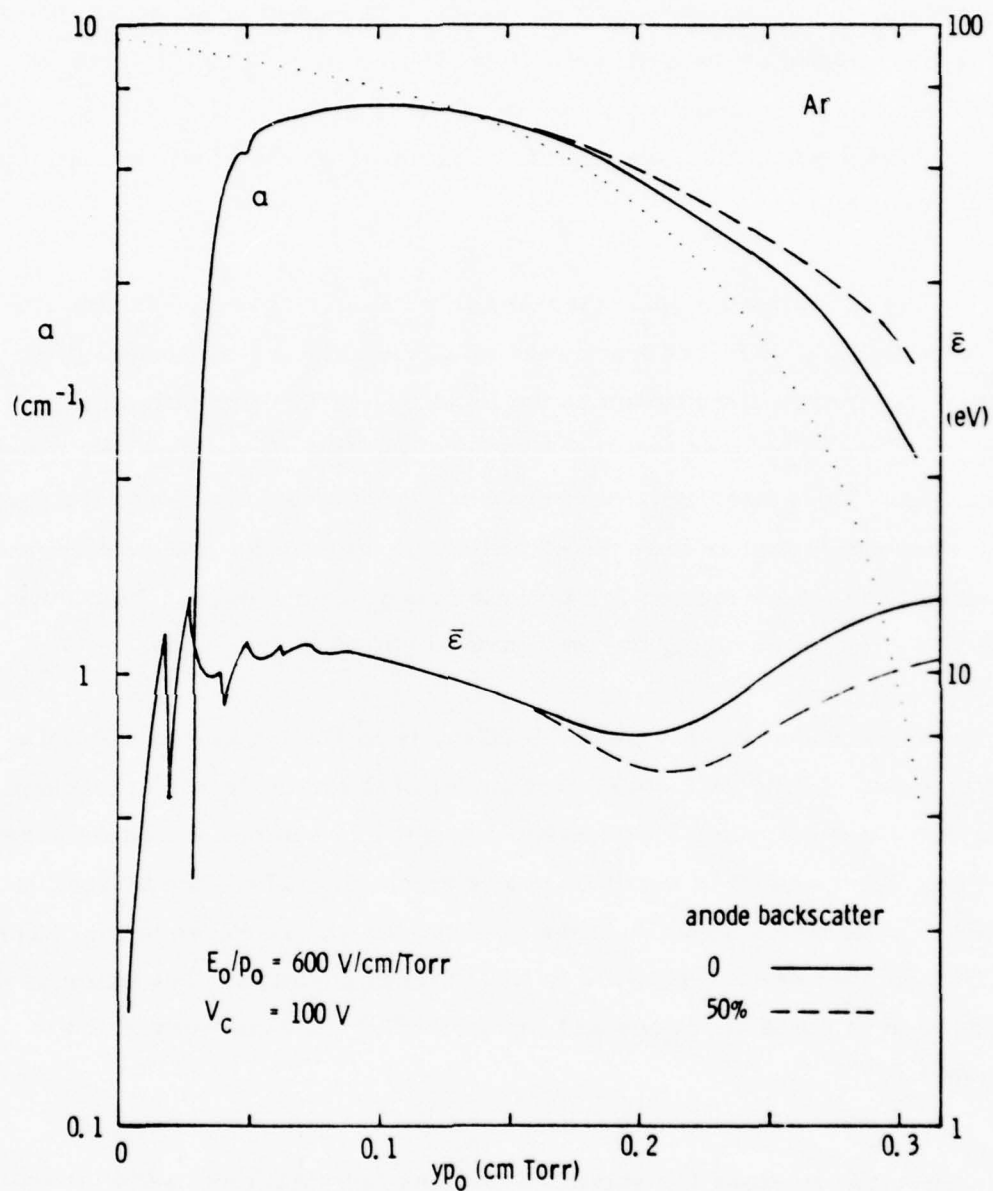


Figure 12 Townsend Ionization Coefficient and Mean Energy

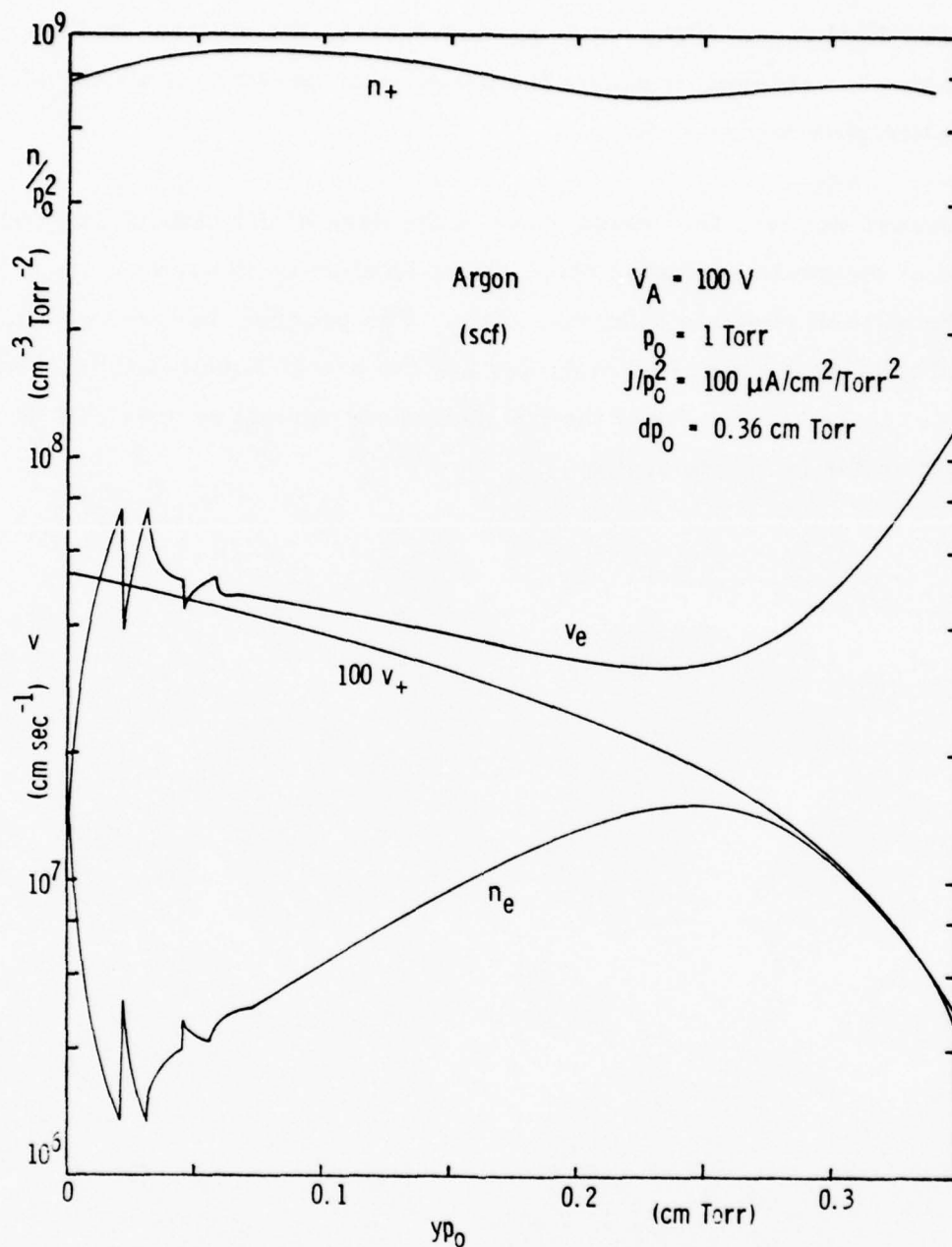


Figure 13 Self-Consistent Solution of the Cathode Fall

of the discharge.) The fact that $n_e \ll n_+$ everywhere indicates that the anode is located within the cathode fall. The situation is indicative of an obstructed discharge. If the anode is moved back, the electron density can continue to rise until it equals the positive ion density, at which point the negative glow begins to form.

As mentioned earlier, the region between the edge of the cathode fall and the head of the positive column could not be handled by the code in its original form, because of possible field reversals. The program has since been modified to allow a change of variables and the use of Equation (55). This has greatly increased the utility of the code and some typical results will be described in the following section.

6.2 The Cathode Fall and Negative Glow

In modeling the negative glow, the code was extended to incorporate a zero field, drift region. Electron loss mechanisms, such as attachment and recombination, were added. They do not significantly affect electron kinetics in the high field region of the cathode fall but are crucial in the negative glow and the transition into the positive column. Likewise, low energy cross sections, such as vibrational and rotational excitation in N_2 , have little impact on electrons within the cathode fall itself and only come into play at low mean energies.

One difficulty which came up in the modeling concerned the presence of field reversal at the edge of the cathode fall. The electric field falls sharply away from the cathode surface due to a layer of nearly constant positive space charge. The electron current density rises exponentially in this region until the electrons carry nearly all the current in the negative glow. At the edge of the cathode fall, the electron density is rising much faster than the current density, since the drift velocity is dropping with the field. Physically speaking, the secondary electrons produced by the propagating primary beam cannot be convected out of the low field region fast enough because of their reduced drift velocity so they pile up.

The difference between positive ion and electron densities determines the slope of the electric field through Poisson's equation. In the cathode fall region, the positive ion density is nearly constant and the electron density is negligible, so the field varies linearly with distance. At the edge of the cathode fall the electron density rises sharply to values which are comparable with the positive ion density. This causes the slope of the electric field to soften and perhaps to go through zero and turn positive. The rate at which electrons pile up at the boundary between the cathode fall and negative glow then determines the way in which the electric field stops falling and joins with the low field present in the negative glow. In particular the field might easily go through zero and remain negative for a while before the electron density comes up to turn it around.

Since current continuity must always be satisfied, any region of field reversal must have only a limited extent. The low energy electrons and positive ions will follow the field closely, except in cases of very rapid change. The high energy electrons, then, are the only thing available to carry the current through a field reversal. However, the current density of high energy electrons is falling monotonically away from the cathode. The balance is made up by an increase in secondary electron current. If the field reverses, the secondary electron drift velocity will follow it very closely resulting in a sharp rise in electron density until it exceeds the ion density. Then the slope of the electric field goes through zero and the field begins to increase. This reverses the whole process and the electron density turns over and approaches the ion density from above, eventually establishing a uniform field in the positive column.

The existence of field reversal in the negative glow presents serious computational difficulties in modelling the cathode region. In the first place, the localized potential well at the edge of the cathode fall results in trapped orbitals for low energy electrons. Thus, the characteristics no longer terminate on the electrodes where boundary conditions are established but form closed loops. These orbitals are populated continuously by ionization which must be balanced by recombination or some other loss mechanism, since no electrons can escape by convection. But the recombination rate depends on the positive ion density, which is not known until the next step in the iteration procedure. In addition, the presence of a large number of low energy electrons requires a much finer partitioning of the energy coordinate in this region.

In order to obtain additional understanding of the electron kinetics in the cathode region before addressing these computational questions, it was decided to run some typical cases using a field distribution which did not go through zero. This distribution consisted of two parts: a linearly falling electric field representing the cathode fall and a zero field region, or drift region, representing

the negative glow. In the drift region, we changed from an energy to a position coordinate since the characteristics are now constant energy surfaces. The stepsize is chosen as one-fourth of the minimum electron mean free path. The cross sections are as defined previously, except that we introduce anisotropic scattering. The degree of elastic backscattering was chosen to decrease exponentially with increasing energy.

The cross section for dissociative recombination of electrons with Ar_2^+ was derived from experimental measurements of the recombination rate as a function of electron temperature.⁴⁹ The following energy dependence was inferred,

$$\sigma_r = 8 \times 10^{-16} \text{ eV-cm}^2/\epsilon$$

The ionization and recombination rate constants in argon are shown in Figure 14 for an electric field which falls from 900 V/cm/Torr at the cathode to zero at 0.33 cm Torr and remains zero out to the anode at 0.83 cm Torr. The ionization rate constant shows the expected behavior, starting from zero when the electrons reach the ionization potential, then rising to a maximum and falling with the electric field.

The recombination rate constant drops initially as the primary group accelerates away from the cathode. As they undergo repeated inelastic collisions, the mean energy begins to decrease and consequently k_r increases. Just before the field goes to zero, ionization virtually disappears and the large group of electrons near zero energy is accelerated by the remaining electric field. As the mean energy of this group increases, the recombination rate drops. In the drift region, the electrons can only lose energy and recombination once again begins to rise. This behavior is clearly demonstrated in the evolution of the energy distribution function to be presented in the following.

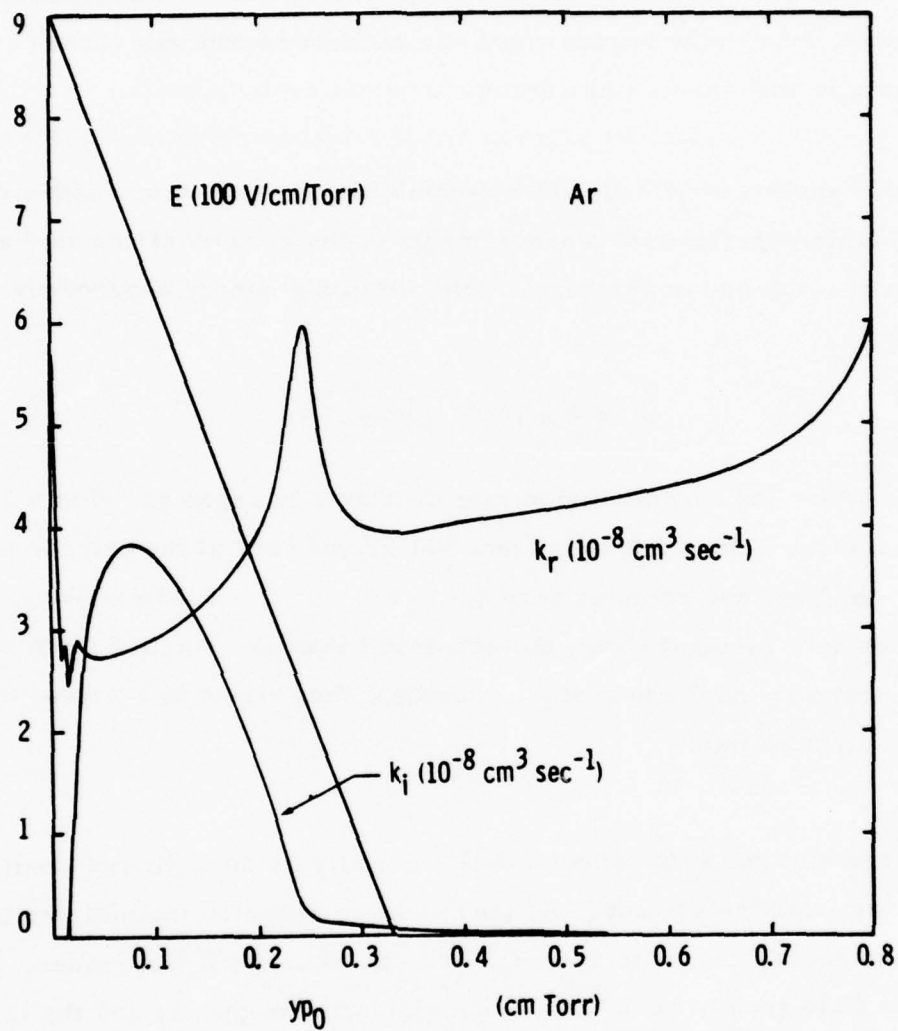


Figure 14 Ionization and Recombination Rate Constants

The Townsend ionization coefficient and mean electron energy are shown in Figure 15 for the same conditions as above. The parameter α here is actually the net ionization coefficient with recombination subtracted out (fractional ionization assumed to be $n_+/N = 10^{-7}$). Note that recombination becomes dominant in the negative glow or drift region. The dashed curve represents the equilibrium ionization coefficient, which is found by letting the electrons reach equilibrium at the local electric field strength. It has a maximum at the cathode surface and goes to zero when the field goes to zero. The actual ionization coefficient has a tail which extends well into the negative glow, a direct indication of the nonequilibrium character of the electron distribution function. The mean energy, $\bar{\epsilon}$, has the same features as the recombination rate but in the inverse sense.

The evolution of the electron energy distribution in the cathode fall and drift region is shown in Figure 16. Note the attenuation of the primary group as it gains energy in the electric field. Just below the primary group is a secondary group which consists of electrons having undergone one inelastic collision. Then comes a long tail of intermediate energy secondaries and finally a low energy group. The low energy secondaries are constantly being produced by the intermediate group until about $\varphi = 140$ eV when this group virtually disappears. At this point the mean energy is relatively low and there are very few electrons above ionization threshold, but there remains about a ten volt potential drop to the edge of the cathode fall. Thus, the mean energy once again begins to rise until the field goes away altogether. This is seen in Figure 16 as the low energy peak moves out to the inelastic threshold. Those electrons which cross the threshold and suffer inelastic collisions begin to form a second peak behind the principal one. This process continues throughout the drift region.

The electron current and number density are shown in Figure 17. As before, the current density rises exponentially in the cathode fall and levels off in the drift region. The current actually falls slightly at the end of the drift

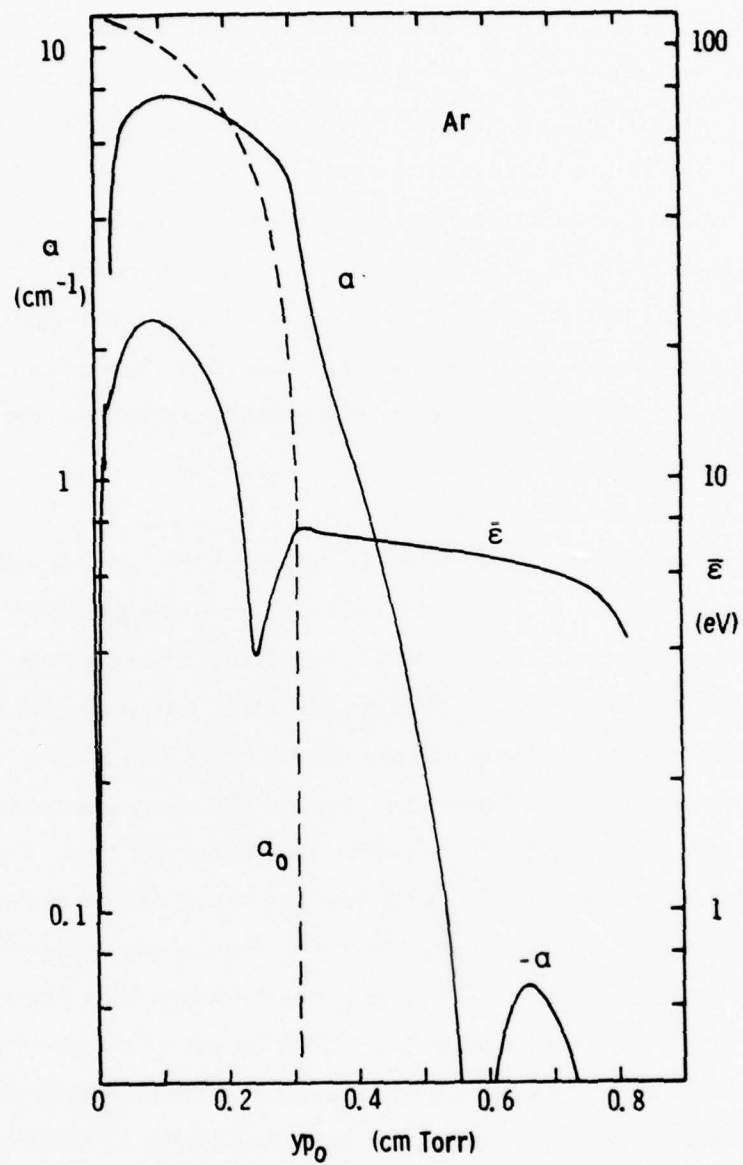


Figure 15 Townsend Coefficients and Mean Energy

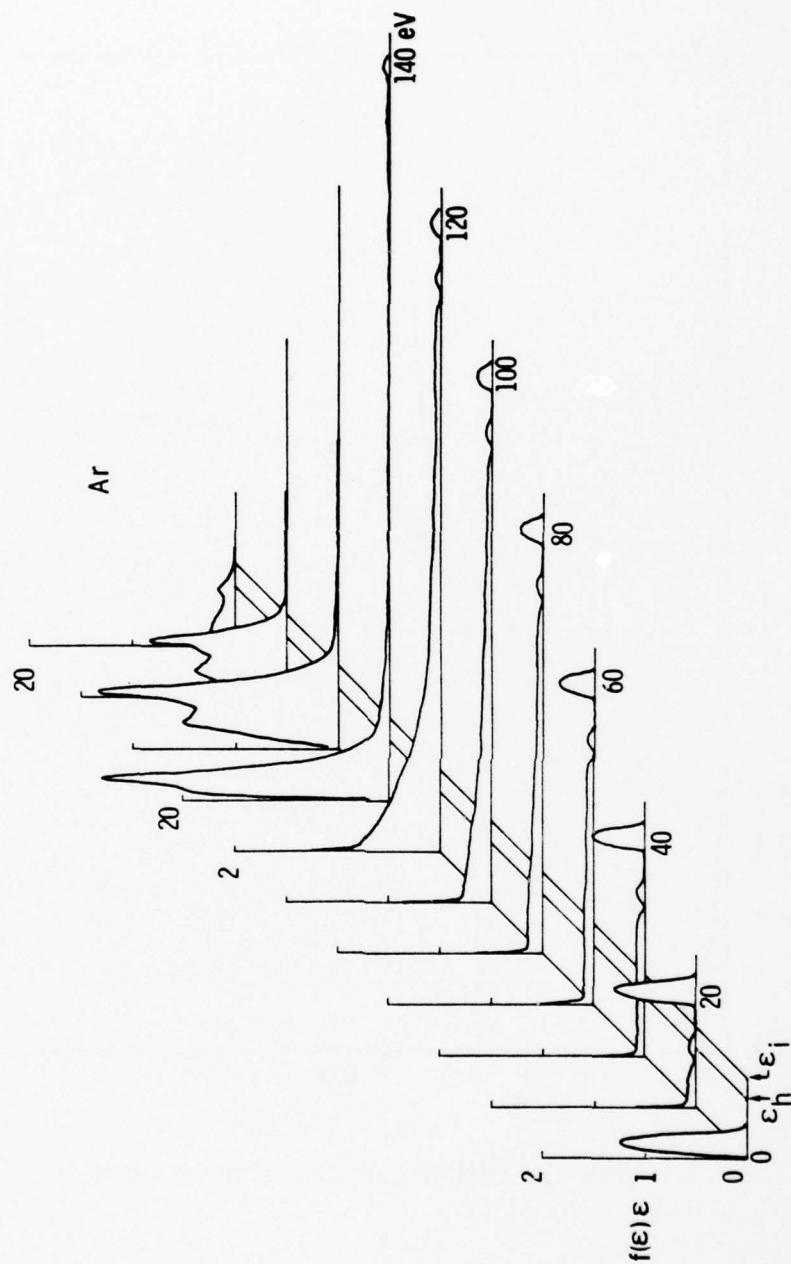


Figure 16 Electron Energy Distributions In the Cathode Fall and Negative Glow

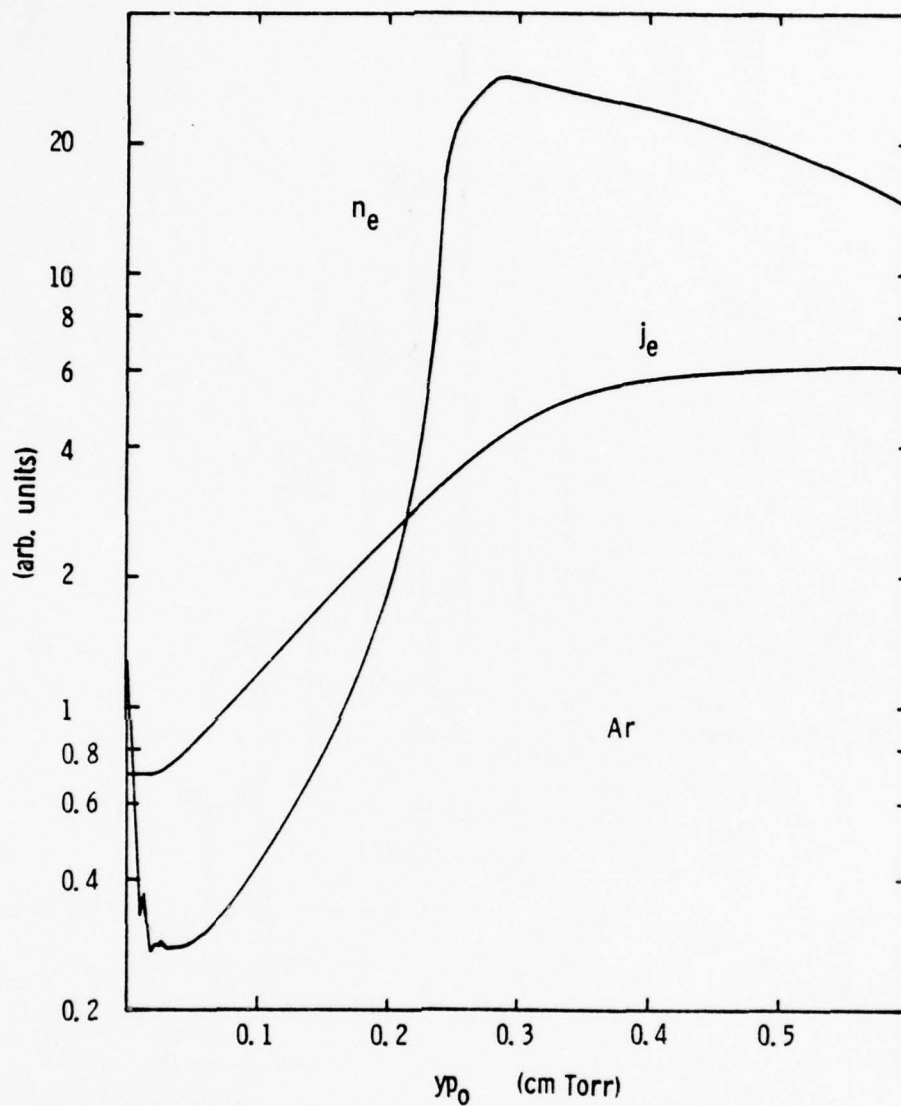


Figure 17 Electron Current and Number Density

region due to recombination. The electron density rises more rapidly than the current density because the drift velocity is falling with the field. In the zero field region the drift velocity begins rising again because of the presence of an absorbing anode. If the anode were removed the drift velocity would go to zero exponentially and, but for the presence of recombination, the electron density would go to infinity. In reality this would cause the electric field to increase which would reaccelerate the electrons, bringing their number density back down to the ion density and bringing the field to a constant value in the positive column.

A similar case was run in helium with the electric field falling from 225 V/cm/Torr at the cathode to zero at 1.33 cm Torr and the anode at 2.83 cm Torr. This corresponds to the same cathode fall potential of 150 V. The evolution of the electron energy distribution is shown in Figure 18. The energy distribution leaving the cathode was taken from the measurements of Hagstrom⁵⁰ and is somewhat broader than that for argon. The qualitative features of the distribution are the same. The curve in the lower right hand corner of Figure 18 shows the experimental distribution of Gill and Webb⁵¹ taken near the edge of the cathode fall. The potential in their case was about 260 V but the general shape of the distribution is very similar to that calculated here.

With a complete knowledge of the energy distribution as a function of position many observable features of the cathode region can be derived; for example, the visible sidelight emission. It is assumed that this emission comes from electronic levels of the atom which are excited by resonant transitions from the ground state. Using a general resonant type cross section, the excitation rate, and hence visible intensity in an optically thin medium, was calculated as a function of position. This is shown in Figure 19 for helium. All the visible features in the cathode region of a normal glow are evident, including the thin cathode dark space, cathode glow, and Crooks dark space. Note the sharp leading edge and diffuse trailing edge of the negative glow in agreement with experimental observation.

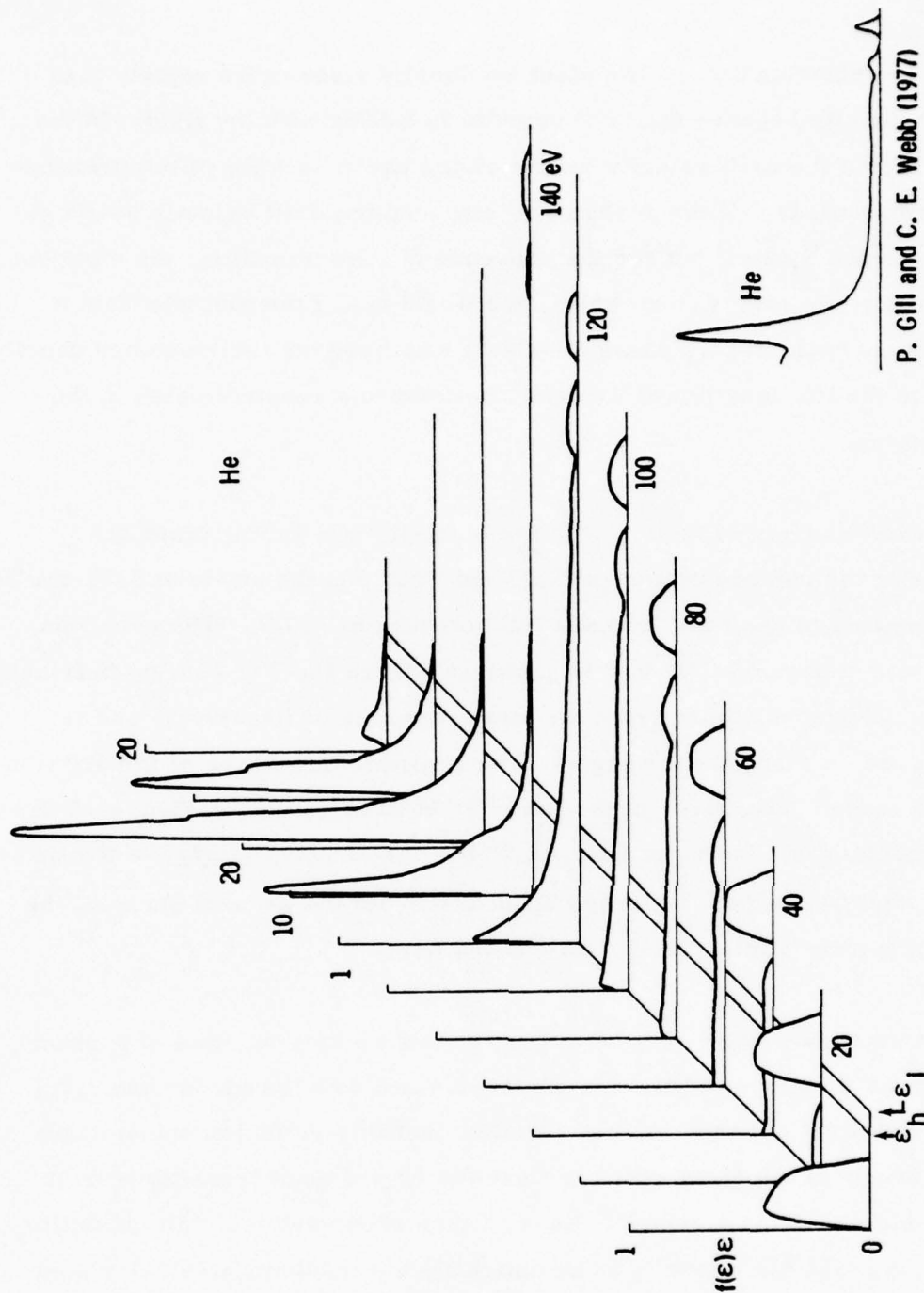


Figure 18 Electron Energy Distributions in the Cathode Fall and Negative Glow

P. Gill and C. E. Webb (1977)

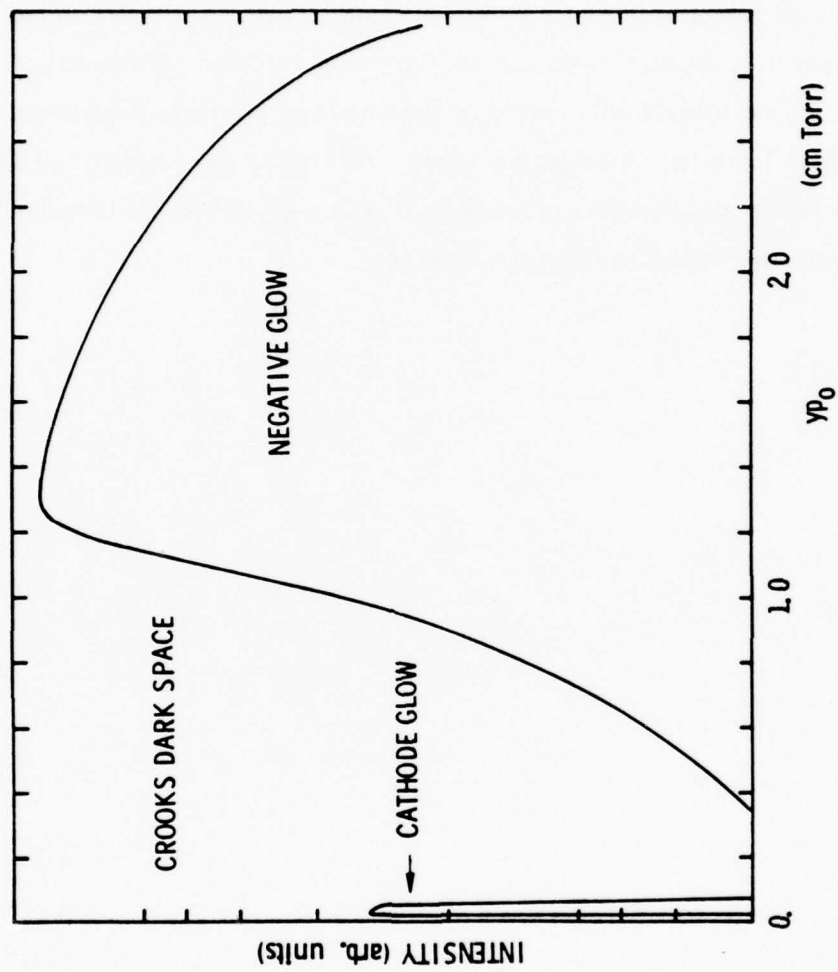


Figure 19 The Cathode Region In Helium

The usual pressure scaling in the cathode fall is preserved by the nonequilibrium formulation presented here. That is, the electric field strength is proportional to pressure, p , the current density scales as p^2 and distances vary inversely with p . Thus, all the characteristics of the cathode fall presented in Figures 14 to 19 are as valid at 1 atm as at 1 Torr. The inclusion of attachment as an electron loss mechanism does not destroy this scaling. However, recombination, which introduces a term quadratic in the charged particle densities, does alter the similarity laws in the negative glow. At higher pressures, where recombination is more significant, the length of the negative glow is expected to be reduced from the usual scaling prediction.

7.0 SHEATH CHARACTERISTICS

An investigation of the voltage-current characteristics of the cathode sheath using the computer program SHEATH has shown that there is a range of parameters where the gross electrical features are approximated by the Townsend model of ionization with a linearly varying electric field. Deviations occur at very high and very low values of the cathode fall potential, V_c . As V_c increases for a given cathode fall distance, d_c , the electrons are accelerated quickly to energies above the peak of the ionization cross section and current multiplication in the sheath is reduced. This behavior is seen in the numerical solution but not in the equilibrium model. At low values of V_c , on the order of several times the ionization potential, the free-fall region near the cathode, where no ionization takes place, becomes important. This region is not considered in most equilibrium models.

At intermediate values of V_c , near the normal operating conditions, a simple equilibrium model with linearly varying field has been used to estimate gas heating in the cathode sheath. Temperature profiles are calculated and it is found that thermal conduction to the cathode is more important than convective cooling for moderate Mach number flows.

7.1 Linear Field Approximation

It has been observed experimentally and confirmed in numerical simulations of the cathode fall region that the electric field, and consequently the discharge power density, vary linearly with distance from the cathode. This is true for both equilibrium³⁰ and nonequilibrium models with constant gas density as well as for a model incorporating the full gas dynamic equations of a compressible boundary layer.¹ Using this empirical observation as a starting point, it is possible to construct a very simple yet accurate picture of the cathode fall including gas flow.

First we will derive closed-form expressions for the cathode fall distance and potential drop as a function of the current and gas pressure. Then, the power density will be calculated to determine the temperature rise in the thermal boundary layer under steady-state conditions. This temperature rise corresponds to a gas density defect at the entrance to the positive column which can lead to thermal instabilities in the plasma.⁴⁴

The electron current density in the cathode fall satisfies the following continuity equation,

$$\frac{\partial j_e}{\partial y} = -\alpha j_e \quad (71)$$

where α is Townsend's first ionization coefficient and y is the distance from the cathode. The processes of electron loss, such as attachment and recombination, are negligible compared to ionization in the cathode fall. The solution of Equation (71) is

$$j_e = j_{e0} \exp\left[\int_0^y \alpha(y) dy\right] \quad (72)$$

where j_{e0} is the electron current density leaving the cathode.

In Townsend's original experiments, electrons produced by illumination of the cathode were allowed to drift in a uniform electric field and the current growth was measured as a function of distance. If the electrode separation is not too small, the electrons spend most of their time in equilibrium between the field, E , and the gas density, N , and α depends only on the ratio E/N . This dependence has the form

$$\alpha\left(\frac{E}{p_0}\right) = A p_0 \exp(-B p_0 / E) \quad (73)$$

where p_0 is the pressure reduced to 0°C and is proportional to N . A and B are constants.

In the cathode fall region, the electric field and gas density are changing so rapidly with position that the electrons never reach equilibrium, and it is not possible to relate α to any local variable. (It has been suggested⁴⁵ that the mean energy, ϵ , and through it α , may be expressed as functions of the average field, $V(y)/y$. This approach was later modified³⁹ to account for the free-flight region near the cathode.) However, the coefficient α appears in Equation (72) under an integral over position. In the present study, it has been found that the use of Equation (73) in (72) with a linear field dependence gives an accurate prediction of the electron current growth in the cathode fall. In other words, the expression for $\alpha(E/p_0)$ may not apply locally, but in an integral sense, over the whole region, it has some validity.

If the electric field is given by the expression,

$$E(y) = E_0 \left(1 - \frac{y}{d_c} \right) \quad (74)$$

where E_0 is the electric field at the cathode and d_c is defined as the cathode fall distance, then

$$\ln \frac{j_e(d_c)}{j_{eo}} = \int_0^{d_c} \alpha(y) dy = \bar{A} d_c \left[e^{-\bar{B}/E_0} - \frac{\bar{B}}{E_0} E_1 \left(\frac{\bar{B}}{E_0} \right) \right] \quad (75)$$

where E_1 is the exponential integral function, $\bar{A} = A \bar{p}_0$ and $\bar{B} = B \bar{p}_0$.

The electron and positive ion current densities at the cathode are related by

$$j_{eo} = \gamma j_{+o} \quad (76)$$

where γ is the secondary electron emission coefficient. At the edge of the cathode fall, the positive ion current density is negligible so

$$j_e(d_c) \approx j \quad (77)$$

and $\ln [j_e(d_c)/j_{eo}] = \ln(1 + 1/\gamma)$. The cathode fall distance can therefore be written from Equation (75) as

$$d_c = \frac{\ln(1 + 1/\gamma)}{\bar{A} \left[e^{-\bar{B}/E_o} - \frac{\bar{B}}{E_o} E_1 \left(\frac{\bar{B}}{E_o} \right) \right]} \quad (78)$$

The current density can be found from Poisson's equation,

$$\frac{\partial E}{\partial y} = \frac{e}{\epsilon_o} (n_e - n_+) \quad (79)$$

evaluated at the cathode surface

$$\left(\frac{\partial E}{\partial y} \right)_o \approx -\frac{e}{\epsilon_o} n_+ = -\frac{1}{\epsilon_o} \frac{1}{1 + \gamma} \frac{j}{v_{+o}} \quad (80)$$

where v_{+} is the positive ion drift velocity.

In the cathode fall region, the positive ion mobility is limited by charge exchange. If the cross section for this process is nearly constant then⁴³

$$v_{+} = k_{+} \left(\frac{E}{p_o} \right)^{\frac{1}{2}} \quad (81)$$

If we now define

$$d_c = \frac{E_o}{\left(\frac{\partial E}{\partial y} \right)_o} \quad (82)$$

then from Equation (80)

$$\frac{j}{p_o^2} = \epsilon_o k_{+} \frac{(1 + \gamma)}{p_o d_c} \left(\frac{E_o}{p_o} \right)^{3/2} \quad (83)$$

This expression is valid for any field dependence, not just the linear dependence of Equation (74). Equation (83) agrees very well with experimental observations in helium at 1 Torr and with numerical predictions.³⁰

We now have the current density and cathode fall distance expressed in terms of the physical constants, A , B , and γ , and the parameter, E_o . With the cathode fall potential given by $V_c = 1/2 E_o d_c$, we can plot $p_o d_c$ and V_c as functions of j/p_o^2 (Figure 20). The minimum in the cathode fall potential is defined as the normal operating condition, with the properties

$$\frac{j_n}{p_o^2} = 0.57 AB^{3/2} \epsilon_o k_+ \frac{1 + \gamma}{\ln(1 + 1/\gamma)} \quad (84)$$

$$V_n = 3 \frac{B}{A} \ln(1 + 1/\gamma) \quad (85)$$

$$p_o d_n = \frac{3.7}{A} \ln(1 + 1/\gamma) \quad (86)$$

These results for constant temperature are presented in many standard texts on gaseous electronics.

For a discharge in argon with an iron cathode, $\gamma = 0.04$, $A = 14 \text{ cm}^{-1} \text{ Torr}^{-1}$, $B = 180 \text{ V cm}^{-1} \text{ Torr}^{-1}$, and $k_+ = 8.25 \times 10^3 \text{ cm}^{3/2} \text{ Torr}^{1/2} \text{ V}^{-1/2} \text{ s}^{-1}$.

In this case

$$\frac{j_n}{p_o^2} = 4.5 \times 10^{-6} \text{ A cm}^{-2} \text{ Torr}^{-2}$$

$$V_n = 126 \text{ V}$$

$$p_o d_n = 0.86 \text{ cm Torr}$$

These values are in close agreement with the numerical calculations of Ward³⁰ even though he used a different expression for $\alpha(E/p_o)$. However, the normal current density is considerably low and the distance somewhat high in comparison with experiments. (The experimental values can be obtained with a different choice of physical constants.)

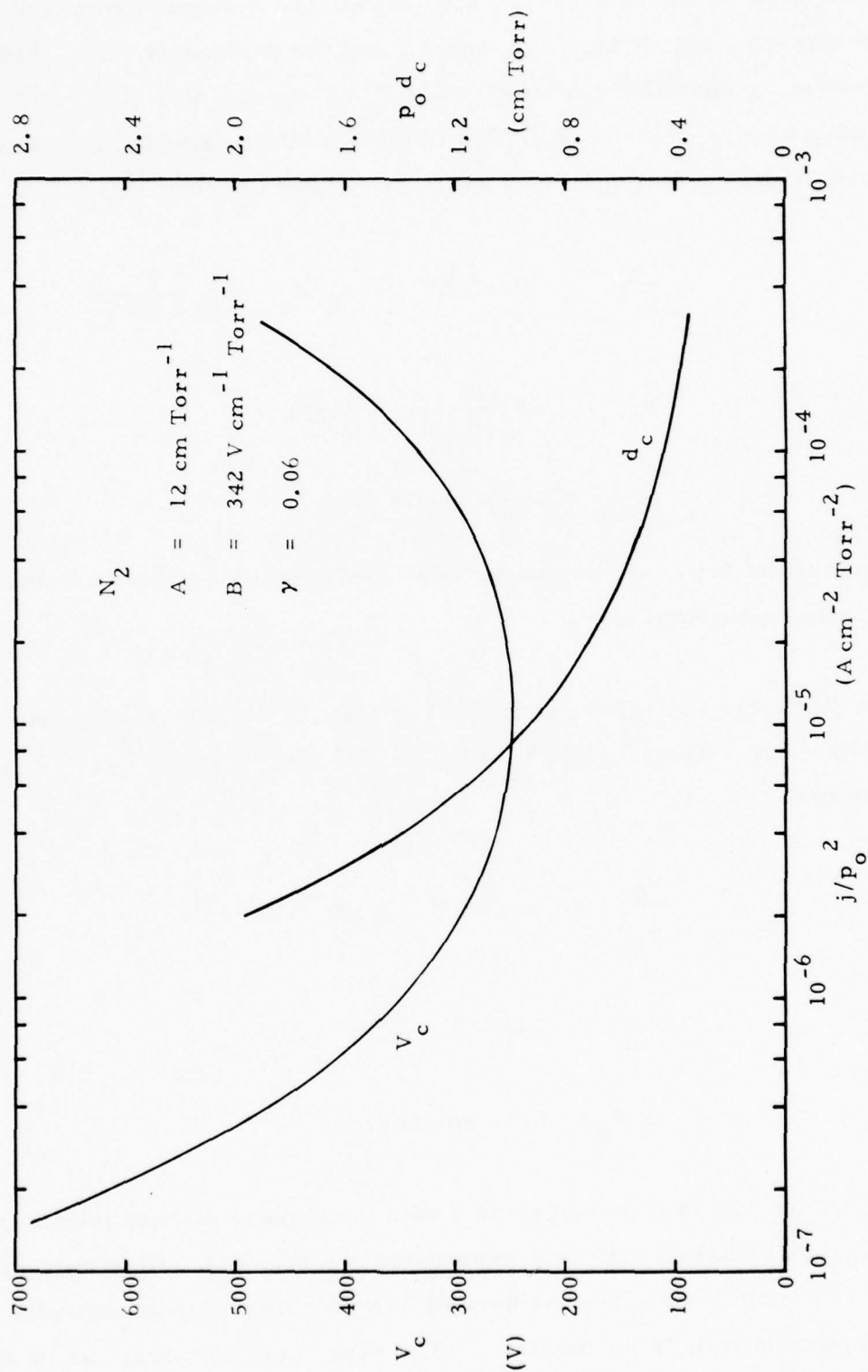


Figure 20 Voltage-Current Characteristic and Cathode Fall Distance in N_2

7.2 Gas Heating in the Cathode Sheath

The reduced pressure appearing in Equation (83) is measured at the cathode surface. Because of gas heating in the cathode fall region, p_o may be considerably different from the pressure in the positive column. The temperature rise in the cathode fall can be determined from a knowledge of the power distribution and the thermal conductivity of the gas. Since the current density is independent of position, the discharge power density, is given by

$$P_d = P_o \left(1 - \frac{y}{d_c} \right) \quad (87)$$

where $P_o = jE_o$. Essentially all of the power dissipated in the cathode fall goes into heating the positive ions which in turn heat the gas through charge transfer collisions. Thus, Equation (87) can be considered as the rate of heat addition to the gas.

In a discharge channel with flow parallel to the cathode surface, a boundary layer is established due to the finite viscosity of the medium. The gas velocity in the boundary layer goes from zero at the cathode to a maximum value in the free stream. For gas flows near standard density, ρ_s , the thickness of this layer, δ^* , is much greater than the normal cathode fall distance, and increases in the downstream direction. For example, in the case described in Reference (1) with a free stream density, $\rho_e = 0.3\rho_s$, the boundary layer displacement thickness was 0.2 cm at a distance 10 cm downstream of the nozzle. The cathode fall thickness was found to be 0.007 cm. Thus, the cathode fall is well within the laminar sublayer, and for subsonic flows at least, the effects of convective heat transfer in this region may be neglected.

We now define the heat conduction problem by considering a solid cathode of thickness t interfacing the gas at $y = 0$. The temperature of the back face of the cathode has the constant value T_o at $y = -t$. Heat addition to

the gas is defined by Equation (87) and the heat flux into the stream at $y = d_c$ is represented by q_c . The thermal conductivity of the gas is assumed to have a power law dependence on temperature, i. e.

$$\kappa_g = \kappa_o \left(\frac{T}{T_o} \right)^a \quad (88)$$

where T_o is some reference temperature, here taken to be the temperature at $y = -t$. The gas temperature in the cathode fall satisfies the equation,

$$\frac{\partial}{\partial y} \left(\kappa_g(T) \frac{\partial T}{\partial y} \right) + \dot{Q}(y) = 0 \quad (89)$$

where $\dot{Q}(y) = P_d(y)$. In the cathode itself

$$\kappa_c \frac{\partial^2 T}{\partial y^2} = 0 \quad (90)$$

where κ_c , the thermal conductivity of the cathode material, is assumed constant. The temperature distribution is then,

$$\kappa_c (T - T_o) = \left(\frac{1}{2} \dot{Q}_o d_c - q_c \right) (y + t) \quad (91)$$

for $-t < y < 0$ and

$$\frac{\kappa_o T_o}{1+a} \left[\left(\frac{T}{T_o} \right)^{1+a} - \left(\frac{T_w}{T_o} \right)^{1+a} \right] = \dot{Q}_o \left(\frac{y^3}{6 d_c} - \frac{y^2}{2} \right) + \left(\frac{1}{2} \dot{Q}_o d_c - q_c \right) y \quad (92)$$

for $0 < y < d_c$, where

$$\kappa_c (T_w - T_o) = \left(\frac{1}{2} \dot{Q}_o d_c - q_c \right) t \quad (93)$$

The temperature at the edge of the cathode fall, T_c , is specified by Equation (92) with $y = d_c$. The heat flux into the free stream is given by the usual expressions for local heat flux in laminar or turbulent flows over heated flat plates,⁴⁶ i. e.

$$\text{Laminar: } q_c(x) = 0.332 k P^{1/3} R_x^{1/2} (T_c - T_a) \frac{1}{x} \quad (94a)$$

$$\text{Turbulent: } q_c(x) = 0.0288 k R_x^{4/5} (T_c - T_a) \frac{1}{x} \quad (94b)$$

Here the thermal conductivity, k , was assumed constant, P is the dimensionless Prandtl number, R_x the Reynold's number (Ux/ν), and $T_a = T_\infty + \sqrt{P} \frac{U^2}{2c_p}$ is the adiabatic wall temperature. In both cases, the heat flux increases with T_c and decreases with x , the distance measured from the leading edge. However, for laminar flow ($R_x < 5 \times 10^5$) $q_c(x) \sim x^{-1/2}$, while for turbulent flow ($R_x > 5 \times 10^5$) $q_c(x) \sim x^{-1/5}$.

An estimate will now be made of the relative importance of q_c in determining the temperature distribution in the cathode fall. For a turbulent flow with $a = 1$ and $T_a = T_o$, the temperature at $y = d_c$ is found from Equation (22) to be,

$$\kappa_o (T_c - T_o) \left(1 + 0.0058 R_x^{4/5} \frac{d_c}{x} \right) = \frac{1}{6} \dot{Q}_o d_c^2 \quad (95)$$

The temperature without flow is obtained by setting $R_x = 0$. Thus convective cooling can be neglected when $U \ll U_* = \frac{625 \nu}{d_c} \left(\frac{x}{d_c} \right)^{1/4}$. When $U = U_*$, the temperature at the edge of the cathode fall is reduced by a factor of two. The critical Mach number, M_* , is given by

$$M_* \left(1 + \frac{\gamma-1}{2} M_*^2 \right) = \frac{625 \mu}{c_\infty \rho_w d_c} \left(\frac{x}{d_c} \right)^{1/4} \quad (96)$$

where μ and c_∞ are the free stream viscosity and sound speed, respectively, and $\rho_w = \rho_s (p_o/760 \text{ Torr})$ is the gas density at the wall.

For nitrogen at $T_{\infty} = 300^{\circ}\text{K}$ this condition becomes

$$M_* \left(1 + \frac{\gamma-1}{2} M_*^2 \right)^{5/4} = 34.5 (\rho_{\infty} x)^{1/4} \quad (97)$$

with ρ_{∞} in amagat and x in cm. The critical Mach number at $x = 10$ cm in N_2 at standard density is $M_* = 5.6$.

The temperature distribution defined by Equation (92) agrees very well with the numerical results of Reference (1). When convective cooling is ignored the temperature rise in the cathode fall region is from Equation (92).

$$\frac{\kappa_o T_o}{1+a} \left[\left(\frac{T}{T_o} \right)^{1+a} - \left(\frac{T_w}{T_o} \right)^{1+a} \right] = \frac{1}{6} \dot{Q}_o d_c^2 \quad (98)$$

Here we see the importance of cooling the cathode in order to minimize the density defect caused by gas heating. However, cooling the cathode to a temperature much below T_{∞} can have only a limited effect if $\Delta T \gg T_{\infty}$.

The boundary layer on a flat plate makes a transition from laminar to turbulent flow at a Reynold's number,⁴⁶

$$R_x = \frac{U_{\infty} x}{\nu} \sim 3 \times 10^5 \quad (99)$$

where U_{∞} is the free-stream velocity, x is the distance from the leading edge of the plate and ν is the kinematic viscosity. In nitrogen at STP $\nu = 0.133 \text{ cm}^2/\text{sec}$, and the transition occurs at about

$$x_{\text{crit}} = \frac{1.2 \text{ cm}}{M} \quad (100)$$

where $M = U_{\infty}/c_{\infty}$ is the free-stream Mach number. For $x > x_{\text{crit}}$, momentum and heat transfer in the boundary layer are dominated by turbulent mixing. The thickness of the layer is⁴⁶

$$\delta = 0.37 x R_x^{-0.2} \quad (101)$$

corresponding to the point at which the longitudinal velocity reaches 99 per-cent of its free-stream value. For a given velocity, δ grows as $x^{0.8}$ until the entire flow channel is turbulent.

The normal thickness of the cathode dark space in a glow discharge is typically⁵²

$$d_n p_o = 0.3 - 1.3 \text{ cm Torr} \quad (102)$$

where p_o is the reduced pressure at the cathode surface, i.e.,

$$p_o = p \frac{273 \text{ K}}{T_o} \quad (103)$$

In a nitrogen discharge at STP with an iron cathode⁵²

$$d_n p_o = 0.42 \text{ cm Torr} \quad (104)$$

and

$$d_n = 5.5 \times 10^{-4} \text{ cm.}$$

On the other hand, we see from Equation (101) that $\delta > 0.036 \text{ cm/M}$ in the turbulent regime. Thus, under normal conditions at atmospheric pressure, the cathode sheath is embedded well within the turbulent boundary layer.

For a given temperature the kinematic viscosity is inversely proportional to pressure, so δ varies as $p^{-0.2}$. On the other hand, d_n varies as p^{-1} . Thus, at low pressure, the ratio of d_n to δ is small only at very large x , but in this case the transition to turbulence also occurs at larger values of x .

Written in terms of X_{crit} we have

$$\frac{d_n}{\delta} = 0.015 \left(\frac{x_{\text{crit}}}{x} \right)^{0.8} M \quad (105)$$

where the constant is independent of pressure.

In the region very close to the wall, the velocities are so small that viscous forces continue to dominate over inertia forces. This is known as the laminar sublayer. The thickness of this layer on a flat plate is⁴⁶

$$\delta_l = 29.5 \times R_x^{-0.9} \quad (106)$$

For a given velocity, δ_l grows as $x^{0.1}$, or much more slowly than δ . Using Equation (100) in Equation (106) we see that $\delta_l \gtrsim 4.2 \times 10^{-4}$ cm/M in nitrogen. Thus, for subsonic flows, the normal cathode dark space and laminar sublayer have roughly the same extent. The pressure scaling of δ_l is as $p^{-0.9}$, similar to d_n . Written in terms of x_{crit} for nitrogen at 0°C, we have

$$\frac{d_n}{\delta_l} = 1.3 \left(\frac{x_{crit}}{x} \right)^{0.1} M \quad (107)$$

where once again the constant is independent of pressure. For argon at 0°C, it becomes 1.2, while for helium at the same temperature, it is 0.5.

In the laminar region, the transport of heat normal to the flow takes place by conduction. This can be seen by introducing the dimensionless form of the energy equation with constant fluid properties

$$u \frac{\partial h^0}{\partial x} + v \frac{\partial h^0}{\partial y} = \frac{1}{PR_x} \left(\frac{\partial^2 T}{\partial x^2} + \frac{\partial^2 T}{\partial y^2} \right) + \frac{E}{R_x} \Phi + Q \quad (108)$$

where $\Phi \approx \frac{\partial u}{\partial y}^2$ is the viscous dissipation function, $P = \rho \frac{\nu c}{\kappa}$ is the Prandtl number, and $E = \frac{U_\infty^2}{c_p (\Delta T)_0}$ is the Eckert number.

In the definitions above, c_p is the heat capacity per unit mass, κ is the thermal conductivity, and $(\Delta T)_0$ is the difference between the wall temperature and the maximum temperature in the boundary layer. The lengths in Equation (108) are normalized to x and the velocities to U_∞ . The rate of heat addition is

normalized as follows:

$$\dot{Q} = \frac{\dot{Q} x}{\rho c_p U_\infty (\Delta T)_0} \quad (109)$$

The orders of magnitude of the normalized velocities in Equation (108) are found from the solution of the laminar boundary layer equations to be

$$u \sim 1$$

and

$$v \sim \frac{\delta_\ell}{x}$$

The derivatives of h^0 and T with respect to x are of order 1. The derivatives with respect to y are estimated as follows: Since the heat addition takes place within a sheath of thickness, d , the temperature (and h^0) will reach a maximum value at y_{\max} , such that $0 < y_{\max} < d$. Thus, in the region $0 < y < y_{\max}$

$$\frac{\partial}{\partial y} \sim \frac{x}{d}$$

and

$$\frac{\partial^2}{\partial y^2} \sim \frac{x^2}{d^2}$$

Later we will see that $y_{\max} \sim d$ and these approximations are valid throughout the sheath.

Now, replacing the terms in Equation (108) with their orders of magnitude, we have

$$1 + \frac{\delta_\ell}{d} = \frac{1}{PR_x} \left(1 + \frac{x^2}{d^2} \right) + \frac{E}{R_x} \frac{x^2}{\delta_\ell^2} + \dot{Q} \quad (110)$$

The terms on the left in Equation (110) are both of order unity for the normal cathode sheath. The first term on the right is small compared to the second, i.e., there is little or no heat flux along the surface. Using Equations (101) and (105), the second term becomes

$$\frac{17}{PM^2} \left(\frac{x}{x_{\text{crit}}} \right)$$

where $P \sim 1$ for gases. So for subsonic flow and $x > x_{\text{crit}}$, the convective

terms on the left of Equation (108) are negligible compared to the conductive term on the right. The ratio of viscous heating to thermal conduction is of the order E , which is small when

$$(\Delta T)_0 \gg \frac{U_\infty^2}{c_p} \quad (111)$$

Equating the remaining two terms in Equation (110) we find, for $P = 1$,

$$(\Delta T)_0 \sim \frac{Qd^2}{\kappa} \quad (112)$$

In the cathode sheath, the principal heat addition is by collisions with positive ions, which account for most of the current in a cold cathode sheath.

Thus,

$$\dot{Q} \sim jE \quad (113)$$

where j is the current density and E the electric field. Still dealing in orders of magnitude, we can rewrite Equation (112) as

$$(\Delta T)_0 \sim j \frac{Vd}{\kappa} \quad (114)$$

where $V = Ed$ is the drop in potential across the sheath. Typical values of $(\Delta T)_0$ for various gases on an iron cathode are shown in Table I at 1 Torr and 300°K.

Table I

	He	H ₂	Ar	N ₂	
$(\Delta T)_0$	0.26	8.7	18.5	139.	(°K)

These were obtained by using normal values of current density, potential and sheath thickness.

Now that we have an equation describing heat dissipation in the sheath, we can construct a model which couples the field, the plasma, and the gas in a self-consistent manner. In order to examine the effects of gas density

variations within the sheath on the sheath characteristics, we begin with a simple model which treats the electrons as being in equilibrium with the field. It has been shown in Section 6 that this is not a good approximation in treating the fine details of sheath structure such as electron density oscillations near the cathode. However, for determining the electric field variation with position and the rate of heat addition to the gas, it is quite an adequate approximation in the vicinity of the normal operating point.

The equations to be solved for the steady state are simply

$$\frac{\partial j_e}{\partial y} = S + \alpha j_e - r_e n_e n_+ \quad (115)$$

$$j_e = e n_e v_e$$

$$j_+ = j - j_e = e n_+ v_+$$

$$\frac{\partial E}{\partial y} = \frac{e}{\epsilon_0} (n_+ - n_e) \quad (116)$$

$$v_e = \mu_e p_0 \left(\frac{E}{p_0} \right)$$

$$v_+ = k_+ \left(\frac{E}{p_0} \right)^{1/2}$$

$$\frac{\partial}{\partial y} \left(\kappa(T) \frac{\partial T}{\partial y} \right) + j_+ E = 0 \quad (117)$$

The Townsend ionization coefficient α is represented by

$$\alpha = A p_0 \exp (- B p_0 / E)$$

The various constants for nitrogen are

$$\begin{aligned}
 A &= 12 \text{ cm}^{-1} \text{ Torr}^{-1} \\
 B &= 342 \text{ V cm}^{-1} \text{ Torr}^{-1} \\
 \mu_e p_0 &= 2.8 \times 10^5 \text{ cm}^2 \text{ Torr V}^{-1} \text{ sec}^{-1} \\
 k_+ &= 8 \times 10^3 \text{ cm}^{3/2} \text{ Torr}^{1/2} \text{ V}^{-1/2} \text{ sec}^{-1} \\
 (T) &= 2.6 \times 10^{-4} \left(\frac{T}{300^\circ \text{K}} \right)^{0.77} \text{ W cm}^{-1} \text{ }^\circ \text{K}^{-1} \\
 r_e &= 8 \times 10^{-7} \text{ cm}^3 \text{ sec}^{-1}
 \end{aligned}$$

The numerical integration is started at the edge of the sheath, where $n_e \approx n_+$ and proceeds until the boundary conditions $j_+ = \gamma j_e$ and $T = T_0$ are satisfied at the cathode surface. Since the two conditions must be satisfied simultaneously, a "shooting" technique is employed, where the initial temperature is varied until convergence is achieved.

With regard to pressure scaling, we make the following observations. In the absence of recombination and gas heating, the similarity variables (i.e., variables which make the system of equations independent of pressure) are S/p^3 , j/p^2 , E/p , and yp . Using these variables, the recombination term in Equation (115) and the heat addition term in Equation (117) are directly proportional to pressure. Recombination is only significant in the negative glow and positive column and does not affect the sheath characteristics appreciably. However, as pointed out in the last section, gas heating is very important even at low pressures. Thus, the usual pressure scaling no longer holds.

If κ were constant, then temperature changes in the cathode sheath would scale directly with pressure. Since κ increases with T , the actual scaling should be less than linear with pressure. However, the heating term is modified by the variation of p_0 in the sheath and it will be shown below that the effects of variable κ and variable p_0 tend to offset one another, such

that ΔT still increases directly with pressure. This fact represents the major stumbling block to operating cold cathode discharges at high pressure.

The electric field in the sheath is plotted in Figure 21 as a function of position for three different pressures. Scaling variables are used so that, if p_0 were constant, all three curves would coincide. The deviations are minor for pressures up to 300 Torr. Note in particular that E/p at the cathode surface is practically constant. The cathode fall potential is only slightly higher at 300 Torr than at 10 Torr, but increases significantly at 1 atm.

The temperature distribution in the sheath is shown in Figure 22. The flow velocity is assumed to be small so that

$$\left. \frac{\partial T}{\partial y} \right|_{y=d} \approx 0 \quad (118)$$

This is also true under static conditions if the electrode spacing is large compared to the sheath dimension. Notice that the width of the thermal boundary layer is less than the cathode fall distance and that the temperature reaches its maximum value well within the sheath. At 300 Torr, the temperature at the plasma-sheath boundary is 950°K and the gas density is only one third of its free stream value. In an e-beam sustained device where the electric field is determined by the applied voltage, the E/p_0 or E/N at the edge of the sheath will be three times as high as in the core flow. Thus, if E/N must be maintained below a critical value where volume ionization begins to compete with the e-beam source, the temperature in the boundary layer presents a severe limitation on the applied voltage, and hence the power density, which can be achieved before instabilities occur.

In the transient case, where a voltage pulse is applied at $t = 0$, the temperature distributions of Figure 22 will take some time to develop. There are two time scales of importance here: The time required to heat the gas in

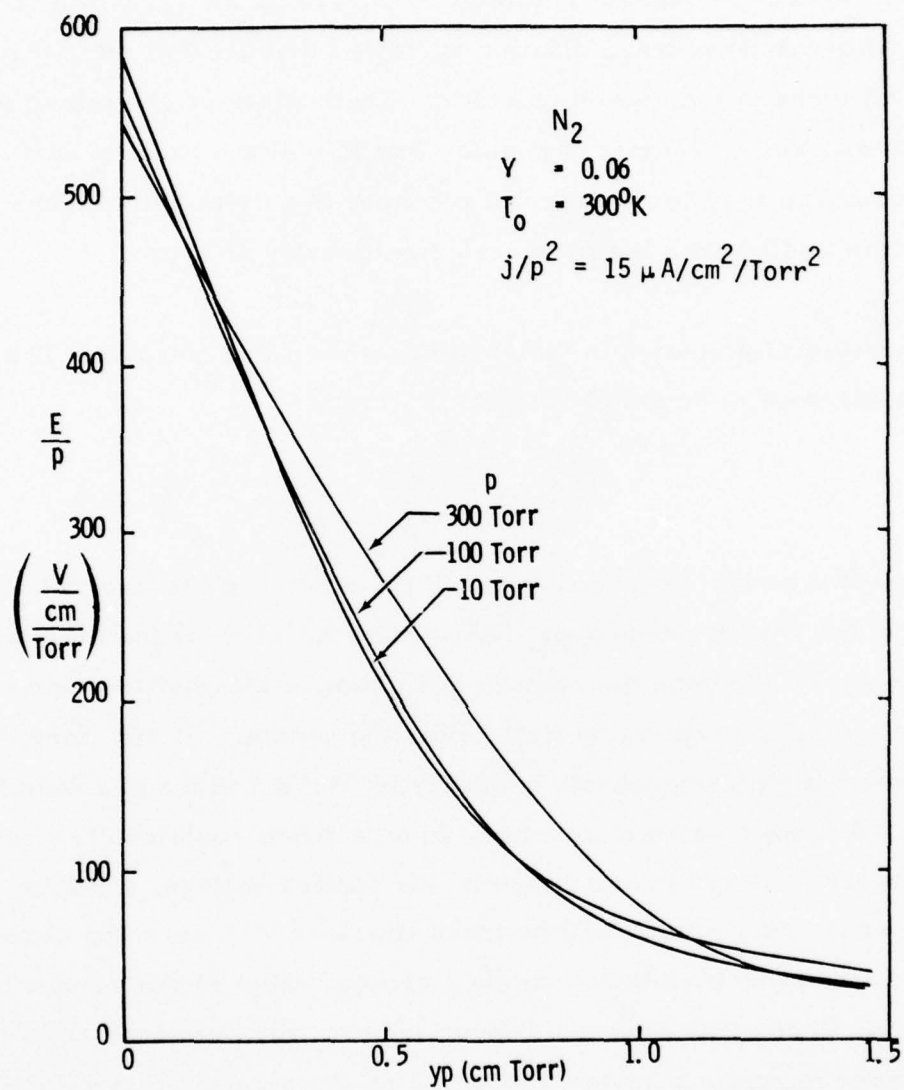


Figure 21 Electric Field in Cathode Sheath with Gas Heating

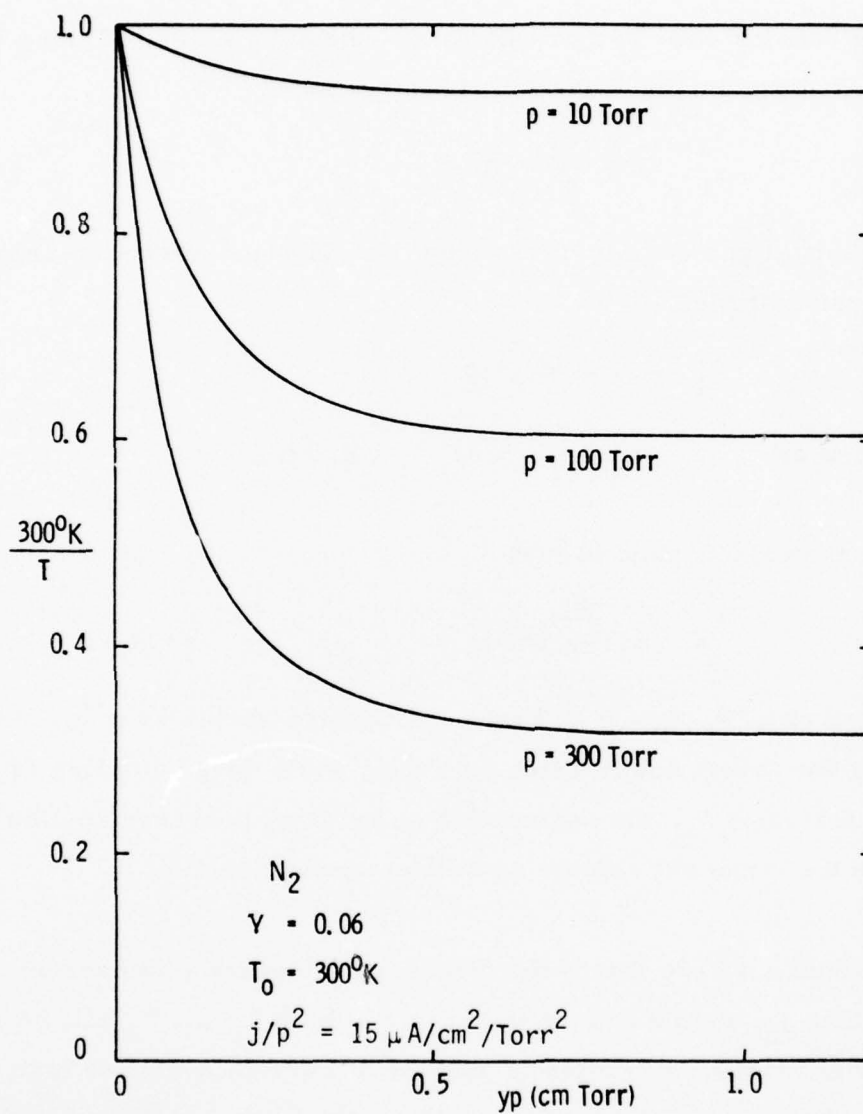


Figure 22 Temperature Variation in the Cathode Sheath

the sheath, τ_1 , and the time it takes a pressure disturbance to propagate across the sheath, τ_2 . The first characteristic time is approximately

$$\tau_1 \sim \frac{\rho c_v}{jE} (\Delta T)_0 \quad (119)$$

where c_v is the specific heat per unit mass at constant volume. Taking for nitrogen $\rho c_v = 3 Nk$ and using Equation (114), we have

$$\tau_1 \sim \frac{3 Nk}{2} d^2 \quad (120)$$

where N is the initial gas density. In nitrogen at STP and normal current density on an iron cathode,

$$\tau_1 \sim 0.65 \mu\text{sec}$$

This value scales as p^{-1} , so that a 1 Torr $\tau_1 \sim 0.5 \text{ msec}$.

The second characteristic time is just

$$\tau_2 = \frac{d}{c_\infty} \quad (121)$$

Again in nitrogen at STP, $\tau_2 \sim 0.017 \mu\text{sec}$. This also scales as p^{-1} . Since the pressure in the sheath equilibrates on a time scale corresponding to τ_2 , which is much less than τ_1 , the assumption of constant pressure applies to some degree in the transient regime as well as in steady state.

It should be pointed out here that if the discharge is operated at current densities greater than j_n , then d is less than d_n , and both τ_1 and τ_2 will be smaller than their normal values. Attempts to operate at current densities less than j_n will result in bunching of the current at the cathode such that the local $j = j_n$. This is a two-dimensional effect which has not been treated under the present contract due to time limitations.

The temperature rise across the sheath is plotted in Figure 23 as a function of pressure. Note the nearly linear dependence as suggested earlier. The

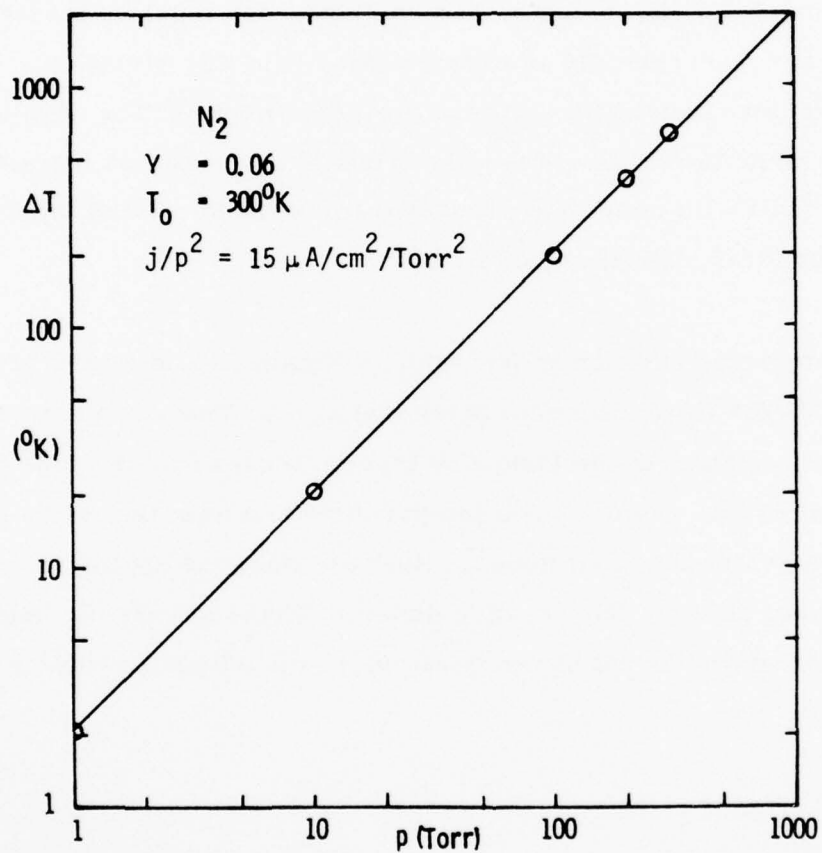


Figure 23 Temperature Rise in the Cathode Sheath

appearance of these temperature increments and associated density defects at the edge of the cathode sheath on time scales as defined above must have serious consequences for the stability of discharge devices at high pressure. Although the adiabatic propagation of density disturbances at the local sound speed is too slow to account for many of the observed instabilities in TEA discharges and e-beam sustained devices, these disturbances may be driven by locally enhanced ionization and gas heating at much greater velocities. Therefore, the coupled field, plasma, and gas equations must be treated self-consistently and time-dependently in order to deal with this situation. In addition to longitudinal instabilities, there are other instabilities resulting from transverse nonuniformities in the electric field or external ionization which cannot be dealt with under the present framework but which must be considered in a general stability analysis.

The full temperature distribution in the cathode sheath and boundary layer is shown in Figure 24 for three different Mach numbers. The sheath dimension has been expanded relative to the boundary layer thickness in order not to obscure the detail in this region. The temperature and heat flux at the sheath-boundary layer interface are continuous. Note the minimal cooling provided by low Mach number flows. The relative density change across the boundary is actually greater at higher Mach numbers due to the adiabatic cooling of the core flow.

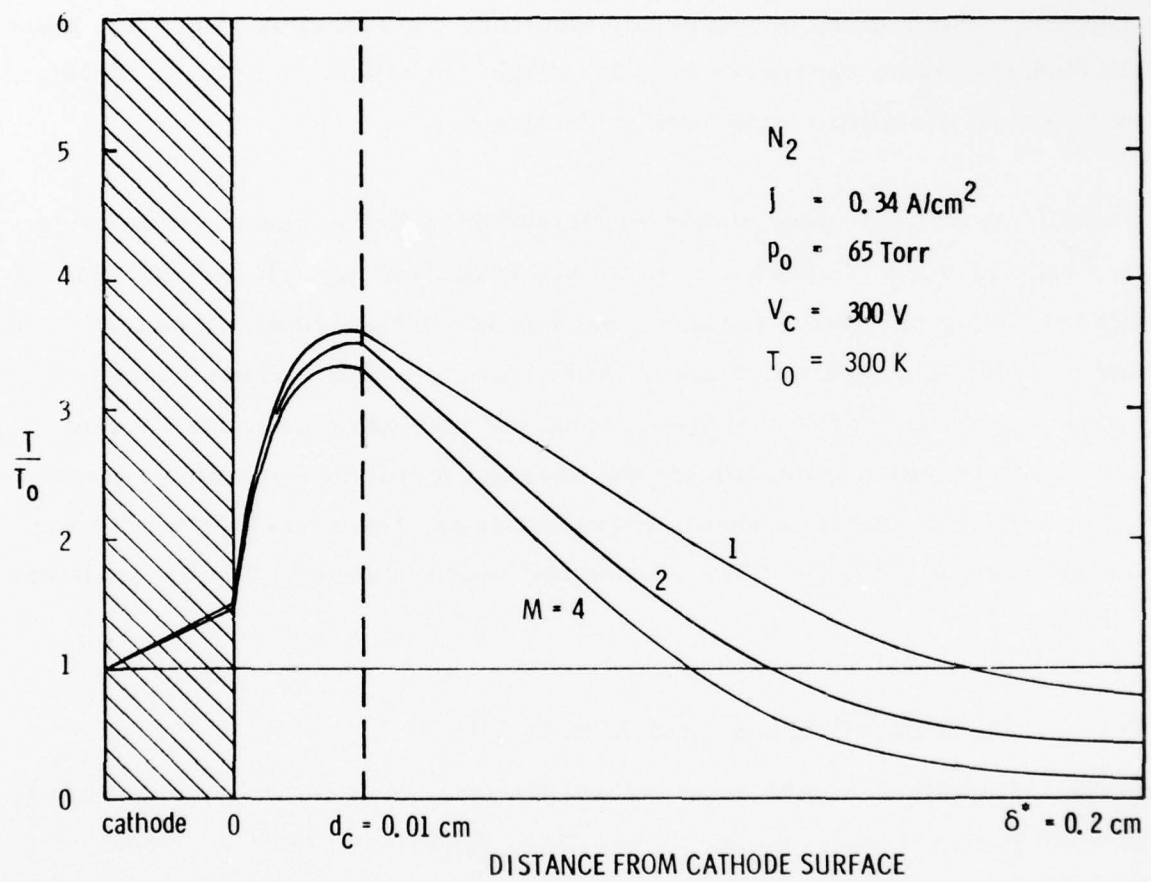


Figure 24 Temperature Distribution in the Cathode Sheath-Boundary Layer

AD-A070 819

NORTHROP RESEARCH AND TECHNOLOGY CENTER PALOS VERDES --ETC F/6 20/9
PLASMA SHEATH PROCESSES. (U)

APR 79 W H LONG
NRTC78-46R

F33615-77-C-2048
NL

UNCLASSIFIED

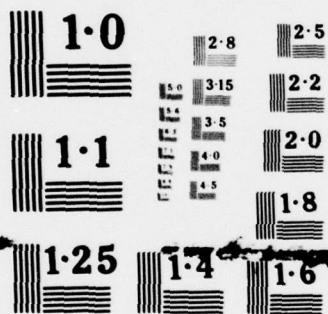
AFAPL-TR-79-2038

2 OF 2
AD
A070819



END
DATE
FILMED

8-79
DDC



NATIONAL BUREAU OF STANDARDS
MICROCOPY RESOLUTION TEST CHART

8.0 STABILITY ANALYSIS

The temperature and electric field at the cathode surface are critical in determining the stability of the discharge. If thermally enhanced electron emission becomes significant, the uniform glow collapses into an arc. This occurrence can be forestalled by proper cooling and conditioning of the cathode. For a given pressure and electrode configuration, however, there exists a maximum current density for stable operation. Electrode cooling and thermal stability are covered in Section 8.1.

The effects of field tailoring and auxiliary ionization on sheath characteristics and discharge stability are examined in Section 8.2. It is found that field tailoring in e-beam sustained devices is effective in countering thermal and chemical changes which occur in the flow direction. These changes occur principally in the positive column, but they can modify the current density distribution which affects the sheath. Auxiliary ionization typically has a negligible effect on sheath characteristics, but it can lead to thermal instabilities at the edge of the cathode fall which propagate into the positive column.

8.1 Electrode Cooling and Thermal Stability

In the last section, it was assumed that the cathode surface was maintained at a temperature $T_o = 300^\circ\text{K}$. In practice, the cathode must be cooled on the side away from the discharge, for example, by passing a fluid with high heat capacity over the surface. The temperature at the cathode-gas interface then depends upon the thermal flux incident from the discharge. The effect of raising the temperature at the cathode surface is to decrease the density of adjacent gas and, if the current density is held constant, to increase the thermal flux. This process leads to an instability in which the cathode temperature and electric field at the surface increase without bound.

The combination of increasing temperature and electric field eventually changes the electron emission process from one which is independent of T to one which increases with T , e.g., thermionic field emission. When the emission of electrons is an increasing function of T , the slope of the voltage-current characteristic for the sheath goes negative and the discharge collapses into an arc. In the following paragraphs we will show that this process is inevitable once the local current density is raised above a critical value which depends on pressure.

At low temperature, the principal mechanisms for emission of electrons from the cathode are ion impact and photoemission. Under ion impact, the electron current at the cathode is related to the ion current by

$$j_{e,i} = \gamma_i j_+ \quad (122)$$

where γ_i is the electron yield per ion. The factor γ_i is a function of ion species and energy as well as surface material and condition. In the high field region of the cathode sheath the ion species is typically the singly ionized component of the parent gas with an average energy

$$\epsilon_i \sim E/NQ \quad (123)$$

where Q is the cross section for symmetric charge exchange. In argon with $E_o/p_o \sim 1000 \text{ V cm}^{-1} \text{ Torr}^{-1}$, $\epsilon_i \sim 5 \text{ eV}$ and in helium with $E_o/p_o \sim 230 \text{ V cm}^{-1} \text{ Torr}^{-1}$, $\epsilon_i \sim 2.5 \text{ eV}$. The yields for these ions on atomically clean tungsten are⁵³ $\gamma_i (\text{Ar}^+) = 0.10$ and $\gamma_i (\text{He}^+) = 0.29$. On tungsten covered with a monolayer of N_2 , $\gamma_i (\text{Ar}^+) = 0.035$ and $\gamma_i (\text{He}^+) = 0.17$. Thus the treatment of the surface is critical in determining accurate sheath characteristics.

In addition to ions incident on the cathode surface there may also be photons with sufficient energy to eject an electron. The threshold frequency for photoemission, ν_o is defined by

$$h\nu_o = \phi \quad (124)$$

where φ is the work function of the material. This ranges from 2 eV to 5 eV for most metals. An expression for the photoelectric current was derived by Fowler⁵⁴

$$j_{e, ph} = CT^2 \int_0^{\infty} I(\nu) \chi \left[\frac{h(\nu - \nu_0)}{kT} \right] d\nu \quad (125)$$

where C is a constant that depends on the properties of the solid, I is the incident radiation intensity, and χ is a universal function which Fowler expressed in series form.

The intensity, $I(\nu)$, is dependent on the gas and the operating conditions and geometry of the discharge. In general, we can write

$$I(\nu) = \eta(\nu, E) j_e \ell(\nu) \quad (126)$$

where η is the efficiency for producing photons of frequency ν in the discharge and ℓ is a characteristic length. If the radiation is not trapped by the gas, then ℓ is defined by the geometry of the discharge region. If there is significant trapping, then ℓ is related to the trapping distance.

For a given gas and applied electric field, the photoelectric current is directly proportional to j_e , i.e.,

$$j_{e, ph} = \gamma_{ph} j_e \quad (127)$$

where γ_{ph} is a function of E and various geometrical factors. Now we can relate the total electron current to the ion current at the cathode surface by

$$j_e = \frac{\gamma_i + \gamma_{ph}}{1 - \gamma_{ph}} j_+ \quad (128)$$

and define an effective γ

$$\gamma = \frac{\gamma_i + \gamma_{ph}}{1 - \gamma_{ph}}$$

which includes both ion and photon processes. In a gas where the uv emission comes principally from transitions between excited or ionic states, there is little trapping and γ may be much greater than γ_i .

The cathode fall potential at a given current density, and hence the heat loading in the sheath, is a sensitive function of γ . In particular, the normal current density increases with γ . Therefore the choice of gas and cathode material and the treatment of the cathode surface can have a significant effect on the operating characteristics of the discharge.

The heat flux to the surface of the cathode is just

$$\kappa \frac{\partial T}{\partial y} \bigg|_{y=0} = jV \quad (129)$$

For a given γ the cathode fall potential, V , is a function of $\xi_w = jT_w^2/p^2$, where T_w is the temperature at the cathode surface. If the cathode thickness is t and the back face is held to a temperature, T_o , then T_w is given by

$$\frac{\kappa_c}{t} (T_w - T_o) = jV(\xi_w) \quad (130)$$

where κ_c is the thermal conductivity of the cathode. Solving Equation (30) for j in terms of the similarity parameter ξ , we have

$$j^{3/2} = \frac{\kappa_c}{t} \left[\frac{\xi_w^{1/2} - \xi_o^{1/2}}{V(\xi_w)} \right] \quad (131)$$

The quantity in brackets has an absolute maximum as a function of ξ_w . Therefore, above a certain value of j there exists no steady-state ξ_w or T_w . At this critical current density, the temperature and electric field at the cathode continue to increase until arcing occurs.

From the form of Equation (131) it is clear that arcing may be forestalled by effective cooling. In particular, the ratio κ_c/t should be maximized by using thin, highly conductive cathodes. It is also desirable to use gases with low normal current densities so that the heat loading in the sheath is minimized. By using very clean, water-cooled, metal electrodes, a normal

glow can be maintained in pure hydrogen at pressures as high as 13 atm and currents as high as 14 amps.⁵⁵

The cathode fall potential as a function of reduced current density in nitrogen is shown in Figure 25 for a number of pressures. The cathode is 1 cm thick aluminum, cooled on the back face to 300°K. The curves are shifted to the left at high pressures because of the reduced gas density at the cathode surface. At the critical current density for each pressure, the slope of the curves goes to infinity. The circles indicate the points where the wall temperature reaches the melting point for aluminum. Obviously the emission process will become thermionic before then and the discharge will collapse into an arc. At pressures above one atmosphere, this transition occurs below the normal current density and the discharge always arcs.

8.2 Field Tailoring and Auxiliary Ionization

In an electric discharge with transverse gas flow, significant heating and chemical reaction may occur during transit through the device. The change in gas density and chemical composition will alter the ratio between external and volume ionization and may cause instabilities to occur. One technique for counteracting this effect would be to vary the electric field in the flow direction by segmenting the electrodes. This approach would also allow individual ballasting or current control of each segment which would tend to maintain a uniform current distribution.

The changes which take place as the gas flows through the discharge occur principally in the positive column. Since the velocity in the sheath region is small, there is little communication between upstream and downstream segments. However, the gas heating which occurs in the sheath causes the thermal boundary layer to grow at a more rapid rate.¹ The expansion of this hot, turbulent gas into the positive column together with the normal bulk heating of the core flow leads to a severe reduction of the local gas

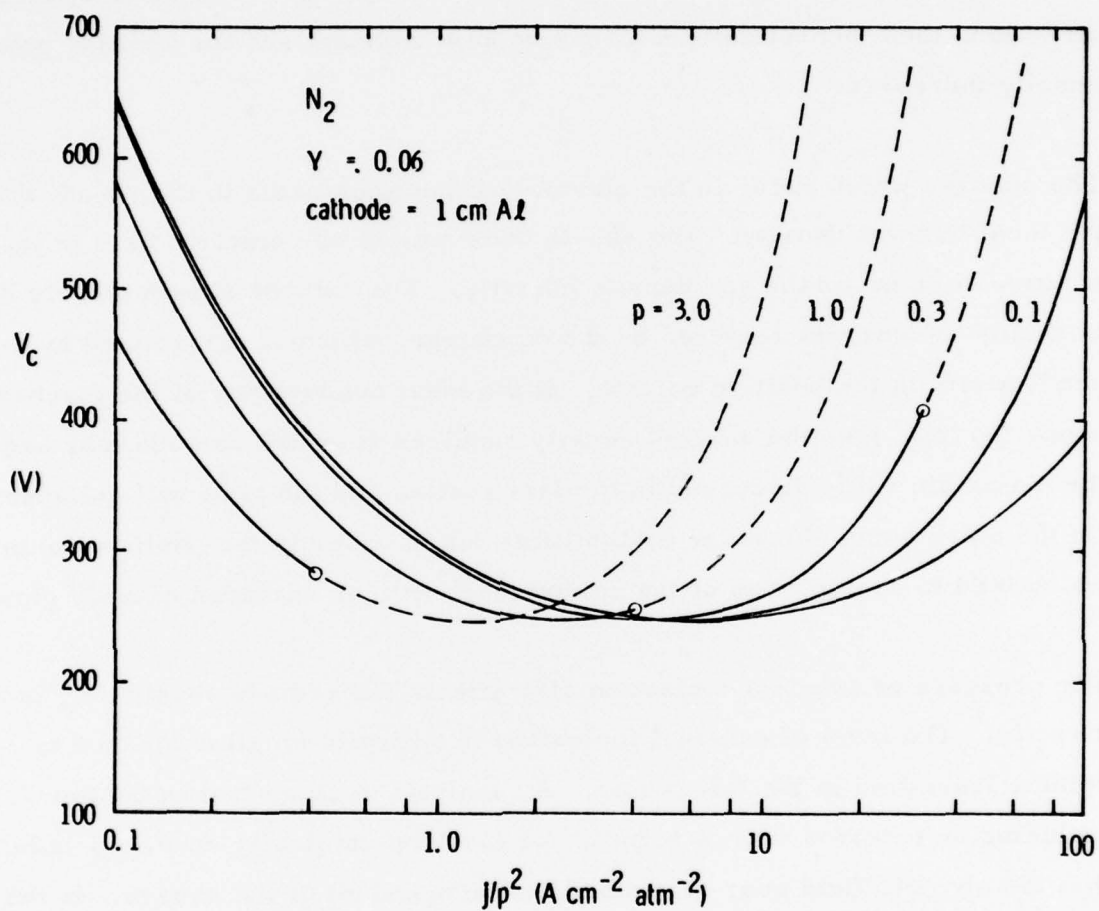


Figure 25 Voltage-Current Characteristics with Gas Heating
(pressures are given in atmospheres)

density and, for constant field, a corresponding increase in E/N . Most e-beam sustained discharges are operated at E/N s limited by some form of ionization or thermal instability. An E/N which is allowed to increase in the flow direction, then, restricts the power density which can be achieved in these devices. If the electric field is gradually reduced in the downstream direction, then theoretically E/N can be kept constant and the limiting power density increased.

The changes which occur in the plasma are communicated to the sheath through the local current density. The sheath does not see the electric field in the positive column or the gas density directly. The cathode sheath merely has to supply the current required by the discharge, which is determined by the conductivity in the positive column. If the local conductivity of the discharge drops too low, then the current density required from the cathode may exceed the maximum value discussed in the last section and the glow will collapse. On the other hand, there are instabilities which occur in the positive column which lead to constriction of the column even with an extended cathode glow.

The presence of external ionization also affects the cathode sheath only indirectly. The level of external ionization is typically small compared to volume ionization in the fall region. An analysis such as that in Section 7.2, including an external source term in the electron continuity equation, indicates that the electric field near the cathode is independent of the source. In the transition to the positive column, however, the electric field is higher than with no external ionization. This high field in a region where the gas density is reduced by heating does strengthen the possibility of thermal instabilities.

9.0 CONCLUSIONS

The research under this contract has answered many questions relating to basic processes in the plasma sheath. In particular, the effects of nonequilibrium energy distributions and gas heating on sheath characteristics and stability have been addressed. However, the present findings do not close the book on the study of interactions between sheath and plasma in high pressure discharges and ionized gas flows.

Two particular aspects of the sheath problem require further study. One is the treatment of the cathode surface. The potential drop across the cathode sheath, and hence the heat loading in this region, can be reduced by increasing the effective electron yield. This can be accomplished by the use of oxides as dielectric layers or the use of helium as a gas layer above the surface. Furthermore, the tendency of the positive column to constrict and eventually collapse at high pressures may be averted by employing restrictive or semiconducting cathode materials to provide localized ballasting. The resistive cathode would also allow tailoring the field without alternating metallic and dielectric strips which result in strong transverse fields at the surface.

The other area needing more study is the sheath-plasma interface. Under the present contract it was not possible to obtain a smooth, self-consistent field transition in this region using the nonequilibrium code and the equilibrium model is questionable in the operating regime where stability becomes a factor. The problem can be solved by modifying the iteration scheme used to obtain a self-consistent field. This would allow the calculations to be extended to the positive column where the field is uniform and boundary conditions can be established without the presence of an anode.

10.0 REFERENCES

1. C. G. Parazzoli, "Turbulent Boundary Layer Over the Cathode of a High Current Density Discharge: Numerical Calculation and Experimental Results," AIAA 15th Aerospace Sciences Meeting, Los Angeles, California, paper 77-64 (24 January 1977).

Non-Equilibrium Electron Kinetics

2. W. P. Allis, "Review of the Cathode Region of a Glow Discharge," Proceedings of U.S. -Japan Joint Seminar on the Glow Discharge and Its Fundamental Processes, Boulder, Colorado, (12 July 1977).
3. J.H. Ingold, "A Model for the Normal Cathode Fall," Proceedings of U.S. -Japan Joint Seminar on the Glow Discharge and Its Fundamental Processes, Boulder, Colorado, (12 July 1977).
4. H. Tagashira, Y. Sakai, and S. Sakamoto, "The Development of Electron Avalanches in Argon at High E/N Values: II. Boltzmann Equation Analysis," J. Phys. D:Appl. Phys., Vol. 10, p. 1051 (1977).
5. Y. Sakai, H. Tagashira, and S. Sakamoto, "The Development of Electron Avalanches in Argon at High E/N Values: I. Monte Carlo Simulation," J. Phys. D: Appl. Phys., Vol. 10, p. 1035 (1977).
6. G. Fournier, and D. Pigache, "Calculation of the Cathode Region of a Glow Discharge," Bull. Am. Phys. Soc., 21, p.174 (1976).
7. W.P. Allis, "Étude d'une Décharge a Haute Pression Ionisée par un Faisceau d'Électrons a Haute Énergie," Rev. de Phys. Appliquée, Tome 10, No. 3, p.97 (May 1975).
8. J. Lucas, and H.T. Saelee, "A Comparison of a Monte Carlo Simulation and the Boltzmann Solution for Electron Swarm motion in Gases," J. Phys. D:Appl. Phys., Vol. 8, p.640 (1975).

9. L. Friedland, "Electron Multiplication in a Gas Discharge at High Values of E/p ," J. Phys. D: Appl. Phys., Vol. 7, p. 2246 (1974).
10. A. Tran. Ngoc, E. Marode, and P. C. Johnson, "A Monte Carlo Study of the Electron Distribution in the Cathode Fall Region of a Glow Discharge in Helium," Proceedings of IEE Conference on Gas Discharges, London, p. 370 (1974).
11. A. M. Aleskovskii, "Kinetic Theory of the Negative Glow," Sov. Phys. - Tech. Phys., Vol. 17, No. 9, p. 1458 (March 1973).
12. Y. Sakai, H. Tagashira, and S. Sakamoto, "The Variation of Steady State Electron Mean Energy Between Parallel Plates in Argon," J. Phys. B: Atom. Molec. Phys., Vol. 5, p. 1010 (May 1972).
13. L. E. Kline, and J. G. Siambis, "Computer Simulation of Electrical Breakdown in Gases; Avalanche and Streamer Formation," Phys. Rev. A, Vol. 5, No. 2, p. 794 (February 1972).
14. E. C. Whipple, Jr., and L. W. Parker, "Numerical Solution of the Krook-Model Boltzmann Equation for a Plasma Diode," Phys. Fluids, Vol. 14, No. 11, p. 2368 (November 1971).
15. A. B. Parker, and P. C. Johnson, "The Dielectric Breakdown of Low Density Gases: I. Theoretical," Proc. R. Soc. Lond. A, Vol. 325, p. 511 (1971).
16. J. H. Parker, Jr., and J. J. Lowke, "Theory of Electron Diffusion Parallel to Electric Fields: I. Theory," Phys. Rev., Vol. 181, p. 290 (1969).
17. R. W. L. Thomas and W. R. L. Thomas, "Monte Carlo Simulation of Electrical Discharges in Gases," J. Phys. B: Atom. Molec. Phys., Vol. 2, p. 562 (1969).

Collision-Dominated Sheaths

18. R.C. Dolson and O. Biblarz, "Analysis of the Voltage Drop Arising From a Collision-Dominated Sheath," J. Appl. Phys., Vol. 47, No. 12, p. 5280 (December 1976).
19. J. Koppitz and K. Stuhm, "Experiments on Plane Overvolted Discharges in N_2 , and Comparison with Calculations," Appl. Phys., Vol. 12, p. 23 (1977).
20. W.T. Leland, J.T. Ganley, and M.J. Kircher, "Calculation of Cathode Fall in Electron Beam Sustained Discharges," 1976 IEEE Conf. on Plasma Science, Austin, Texas, LASL Report LA-UR76-1160.
21. W.H. Long, Jr., and A. Garscadden, "Two-Dimensional, Time Development of Plasma Instabilities," Bull. Am. Phys. Soc., Vol. 21, No. 2, p. 174 (February 1976).
22. L.E. Kline and L.J. Denes, "Investigations of Glow Discharge Formation with Volume Pre-ionization," J. Appl. Phys., Vol. 46, No. 4, p. 1567 (April 1975).
23. G.L. Rogoff, "Initial Development of Glow-to-arc Transition Due to Electric Field Distortion," Bull. Am. Phys. Soc., 20, p. 234 (1975).
24. O.B. Evdokimov, V.V. Kremnev, G.A. Mesyats, and V.B. Ponomarev, "Field Distribution in a Gas Discharge Excited by Fast Electrons," Sov. Phys. -Tech. Phys., Vol. 18, No. 11, p. 1478 (May 1974).
25. L.E. Kline, "Calculations of Discharge Initiation in Over-Volted Parallel-Plane Gaps," J. Appl. Phys., Vol. 45, No. 5, p. 2046 (May 1974).
26. R. Rosa, "Properties of the Collisional Plasma Sheath with Ionizations," J. Phys. A:Math., Nucl. Gen., Vol. 7, No. 4, p. 541 (1974).
27. E.P. Velikhov, S.A. Golubev, Yu. K. Zemlsov, A.F. Pal', I.G. Persiantsev, V.D. Pis'mennyi, and A.T. Rakhimov, "Non-Self-Sustaining Stationary Gas Discharge Induced by Electron-Beam

Ionization in N_2 - CO_2 Mixtures at Atmospheric Pressure, " Sov. Phys.-JETP, Vol.38, No.2, p.267 (February 1974).

28. H.W. Friedman, "Nonlinear Analysis of the Positive Column," Phys. Fluids, Vol.10, No.9, p.2053 (September 1967).
29. A.L. Ward, "Approximate Calculations of Cathode-Fall Characteristics," IEEE Trans. on Electron Devices, p.255 (1963).
30. A.L. Ward, "Calculation of Cathode-Fall Characteristics," J. Appl. Phys., Vol.33, No.9, p.2789 (September 1962).

Other Boltzmann Studies

31. W.H. Long, Jr., W.F. Bailey, and A. Garscadden, "Electron Drift Velocities in Molecular-gas-Rare-gas Mixtures," Phys. Rev. A., Vol. 13, No. 1, p. 471 (January 1976).
32. W.H. Long, Jr. and W.F. Bailey, "Anisotropic Electron Distributions in Molecular Gas Discharges," Bull. Am. Phys. Soc., Vol. 19, No. 2, p. 151 (February 1974).
33. J. Fletcher and D.S. Burch, "Theoretical Electron Distribution Functions for Townsend Discharges in Argon," Phys. Rev. A, Vol. 7, No. 4, p. 1341 (April 1973).
34. B. Sherman, J. Math. Anal. Appl., Vol. 1, p. 342 (1960).
35. T. Holstein, "Energy Distribution of Electrons in High Frequency Gas Discharges," Phys. Rev., Vol. 70, p. 367 (September 1946).
36. W.H. Long, Jr., "Electron Transport in Argon," Bull. Am. Phys. Soc., Vol.22, No.2, p.204 (February 1977).

Other References

37. L. J. Kieffer and G. H. Dunn, *Rev. Mod. Phys.* 38, 1 (1966)
38. K. B. Persson, *J. Appl. Phys.* 36, 3086 (1965).
39. A. Tran Ngoc, E. Marode, and P. C. Johnson, *J. Phys. D: Appl. Phys.* 10, 2317 (1977).
40. M. Schaper and H. Scheibner, *Beit. Plasma Phys.* 9, 45 (1969).
41. F. E. Spencer, Jr. and A. V. Phelps, *Proc. 15th Symp. on Eng. Aspects of MHD*, Philadelphia, Pennsylvania, Paper IX 9.1 (1976).
42. D. Rapp and P. Englander-Golden, *J. Chem. Phys.* 43, 1464 (1965).
43. Iu. M. Kagan and V. I. Perel', *Sov. Phys. Dok.* 1, 289 (1956).
44. W. H. Long, Jr. and A. Garscadden, *Bull. Am. Phys. Soc.* 22, 195 (1977).
45. J. M. S. Schofield, *Proc. 12th Int. Conf. Phenomena in Ionized Gases, Part I* (Amsterdam, North Holland), p. 73 (1975).
46. H. Schlichting, *Boundary Layer Theory*, (Pergamon Press 1955), p. 269.
47. H. J. Herring and G. L. Mellor, NASA CR-2068, June 1972.
48. J. O. Hirschfelder, C. F. Curtiss, and R. B. Bird, *Molecular Theory of Gases and Liquids*, (John Wiley & Sons, Inc., New York, March 1964), pp. 528-539.
49. Y-J Shiu and M. A. Biondi, *Phys. Rev. A* 17, 868 (1978).
50. H. D. Hagstrom, *Phys. Rev.* 104, 672 (1956).
51. P. Gill and C. E. Webb, *J. Phys. D: Appl. Phys.* 10, 299 (1977).
52. A. von Engel, *Ionized Gases*, (Clarendon Press, Oxford, 1955).

- 53. H. D. Hagstrom, Phys. Rev. 104, 1516 (1956).
- 54. K. H. Fowler, Phys. Rev. 38, 45 (1931).
- 55. H. Y. Fan, Phys. Rev. 55, 769 (1939).

APPENDIX

Asymptotic Solutions

The collisional Boltzmann equation for electrons suffering elastic and inelastic collisions is not amenable to exact, closed-form solution except in the case of constant collision frequency. In the general case, numerical methods are employed using tabulated experimental cross sections. In order to make the solution tractable, it has usually been necessary to make some approximation in the angular dependence of the velocity distribution function. The most common technique is to expand this function in a series of Legendre polynomials, which is then truncated after two terms. This approximation, which has been labelled P1, is very accurate at moderate electric field strengths in cases where the inelastic cross sections are not too large and the elastic cross section is isotropic. In the present work, we have used an approximation where electrons moving with the field are placed in one group and electrons moving against the field in another. This technique, which will be called G2, is most accurate at high field strengths where high energy electrons are scattered predominantly in the forward or backward directions.

In order to examine quantitatively the accuracy of these and other angular approximations, we now consider a situation where the Boltzmann equation has a closed form solution in the limit of high electron energy. The cross sections are assumed to be constant and isotropic. The total inelastic cross section is denoted by Q_h and the total elastic cross section by Q_e . The Boltzmann equation can then be written,

$$e \frac{E}{N} \cos \theta \left(\frac{\partial f}{\partial \varphi} + \frac{\partial f}{\partial \xi} \right) = -Qf + f_o Q_e + \frac{\epsilon + \epsilon_h}{\epsilon} f_o (\epsilon + \epsilon_h) Q_h (\epsilon + \epsilon_h) \quad (1)$$

where $Q = Q_e + Q_h$ and the other symbols are defined as in Section 4.1. Along the characteristic, where $\varphi + \xi$ is equal to the maximum energy of electrons emitted by the cathode, there are no in-scattered electrons and the last term in Eq. (1) vanishes. (This term is also negligible in the homogeneous case when E/N is small or Q is large.) Considering f as an explicit function of ξ alone, we can write Eq. (1) as,

$$e \frac{E}{N} \cos \theta \frac{\partial f}{\partial \xi} = -Qf + f_0 Q_e \quad (2)$$

The partial derivative in (2) can be expressed in the coordinate system (ϵ, x) where $\epsilon = \xi / \cos^2 \theta$ is the total energy and $x = \cos \theta$, i. e.

$$\cos \theta \frac{\partial f}{\partial \xi} = x \frac{\partial f}{\partial \epsilon} + \frac{1-x^2}{2\epsilon} \frac{\partial f}{\partial x} \quad (3)$$

At high energies the second term on the right is negligible compared to the first except in a small angular range around $x = 0$. Therefore, we can write Eq. (2) in the asymptotic limit as,

$$x \frac{\partial f}{\partial u} = -f + \frac{Q_e}{2Q} \int_{-1}^1 f dx \quad (4)$$

where $u = NQ\epsilon/eE$.

The solution of this equation has the form

$$f(u, x) = g(u) h(x)$$

where the functions g and h satisfy

$$\frac{1}{g} \frac{\partial g}{\partial u} = -\alpha \quad (5a)$$

and

$$\frac{Q_e}{2Q} \int_{-1}^1 h dx = (1 - \alpha x)h \quad (5b)$$

The constant α must be positive to meet the boundary condition, $f \rightarrow 0$, at infinity.

The solution of Eq. (5) is

$$g(u) = e^{-\alpha u}$$

and

$$h(x) = \frac{Q_e/Q}{1 - \alpha x}$$

with the condition that $\frac{1}{2} \int_{-1}^1 h dx = 1$. This last equality fixes α so that there is a single, well-defined function describing the electron energy distribution,

$$f(u, x) = \frac{Q_e/Q}{1 - \alpha x} e^{-\alpha u} \quad (6)$$

with α given by $\alpha = \frac{Q_e}{2Q} \ln \left(\frac{1 + \alpha}{1 - \alpha} \right)$. Thus, in the asymptotic limit, the distribution approaches a Maxwellian form with temperature $T_e = \frac{eE/N}{\alpha Q}$.

The angular dependence exhibits a peak in the forward direction which becomes sharper as $\alpha \rightarrow 1$. The dependence of α on Q_h/Q_e is given in Table I.

Table I

Q_h/Q_e	0.1	0.3	1.0	10.	∞
α	0.5030	0.7521	0.958	0.999	1
f_1/f_0	0.542	0.921	1.566	2.727	3
f_2/f_0	0.195	0.561	1.586	4.318	5
f_3/f_0	0.060	0.305	1.427	5.834	7
f_4/f_0		0.156	1.211	7.295	9
f_5/f_0		0.073	0.987	8.717	11

Another method of solving Eq. (4) would be to multiply by successive Legendre polynomials and integrate over x to obtain the following series of equations,

$$\frac{1}{3} \frac{\partial f_1}{\partial u} + f_0 = \frac{Q_e}{Q} f_0 \quad (7a)$$

$$\frac{2}{5} \frac{\partial f_2}{\partial u} + \frac{\partial f_0}{\partial u} + f_1 = 0 \quad (7b)$$

$$\frac{3}{7} \frac{\partial f_3}{\partial u} + \frac{2}{3} \frac{\partial f_1}{\partial u} + f_2 = 0 \dots \quad (7c)$$

where the functions f_0, f_1, f_2, \dots are defined by the expansion $f(u, x) = \sum_{\ell=0}^{\infty} f_{\ell}(u) P_{\ell}(x)$. If the series is approximated by the first two terms, i. e., $f_{\ell} = 0$ for $\ell \geq 2$. Then the solution of (7) is given by,

$$f_0 = e^{-\alpha_1 u} \text{ and } f_1 = \alpha_1 e^{-\alpha_1 u}$$

where $\alpha_1 = \sqrt{3 Q_h / Q}$.

This is the P1 approximation commonly used to solve the Boltzmann equation in the general case of nonconstant cross sections. Once again the solution is Maxwellian with temperature $T_e = \frac{eE/N}{\alpha_1 Q}$ the value of α_1 approaches the exact result, α , at small values of Q_h / Q_e . In the limit of large inelastic cross section, α_1 goes to $\sqrt{3}$ while α goes to 1. Thus, the temperature in the tail of the distribution may be off by as much as a factor of $\sqrt{3}$.

If three terms are retained in the angular expansion of f , the solution of (7) is given by

$$f_0 = e^{-\alpha_2^2 u} \quad f_1 = \frac{\alpha_2^2}{1 - \frac{4}{15} \alpha_2^2} e^{-\alpha_2^2 u}$$

$$f_2 = \frac{2}{3} \frac{\alpha_2^2}{1 - \frac{4}{15} \alpha_2^2} e^{-\alpha_2^2 u}$$

where $\alpha_2 = \sqrt{\frac{3 Q_h/Q}{1 + \frac{4}{5} Q_h/Q}}$. This is the P2 approximation.

Note that α_2 approaches $\sqrt{5/3}$ for large Q_h/Q_e .

In order to see how well these approximations represent the exact distribution, we have expanded the function in Eq. (6) in a Legendre series. The coefficients of this series are given in Table I for a number of values of Q_h/Q_e . The coefficients of the truncated expansions are given in Table II along with the appropriate α values. As the inelastic cross section increases relative to Q_e , more terms are required in the angular expansion to adequately represent the distribution function. This is because the distribution is becoming more and more peaked in the forward direction. In the limit as $Q_h \rightarrow \infty$, the angular distribution approaches a delta function which has the Legendre coefficients 1, 3, 5, . . . , $2\ell + 1$, . . .

Table II

Q_h/Q_e	0.1		0.3		1.0	
	P1	P2	P1	P2	P1	P2
$\alpha_{1,2}$	0.522	0.516	0.832	0.764	1.224	1.035
f_1/f_0	0.522	0.541	0.832	0.905	1.224	1.449
f_2/f_0		0.182		0.461		1.000

Before leaving the angular expansion technique, it is interesting to compare the infinite series solution with the exact solution obtained by separation of variables. By a process of successive substitution, it can be shown that the equations (7) are satisfied by functions f_ℓ which have a common exponential factor $\exp(-\alpha_\infty u)$, where α_∞ is given by the continued fraction,

$$\frac{Q_e}{Q} = 1 - \frac{1}{3} \alpha_\infty \left(\frac{\alpha_\infty}{1 - \frac{2}{5} \alpha_\infty \left(\frac{2/3 \alpha_\infty}{1 - \frac{3}{7} \alpha_\infty \left(\frac{3/5 \alpha_\infty}{1 - \frac{4}{9} \alpha_\infty \left(\frac{4/7 \alpha_\infty}{1 - \dots} \right)} \right)} \right)} \right)} \right)$$

In this expression the two series are

$$\frac{1}{3}, \frac{2}{5}, \frac{3}{7}, \frac{4}{9}, \dots, \frac{n}{2n+1}, \dots$$

and $1, \frac{2}{3}, \frac{3}{5}, \frac{4}{7}, \dots, \frac{n}{2n-1}, \dots$

The value of α_∞ found in this way is equal to the exact value, α , given previously. Therefore, the solution using the Legendre expansion approaches the exact asymptotic solution as more and more terms are included.

Another very simplified approach in dealing with angular velocity distributions is to divide the electrons into two groups. One moving with the electric field and the other moving against it. This type of a distribution is most nearly realized in the cold cathode region of a glow discharge where the scattering of high energy electrons is predominantly forward or backward and the inelastic cross sections are comparable to the elastic. This is also precisely the regime in which the Legendre expansion has the most trouble converging. In this case, the Boltzmann equation is written as follows,

$$\frac{eE}{N} \frac{\partial f_+}{\partial \epsilon} = -(Q_e^- + Q_h) f_+ + Q_e^- f_- \quad (8a)$$

$$\frac{eE}{N} \frac{\partial f_-}{\partial \epsilon} = -Q_e^- f_+ + (Q_e^- + Q_h) f_- \quad (8b)$$

where Q_e^- is the cross section for elastic backscattering. For equal forward and backward scattering, $Q_e^- = Q_e/2$. Notice that the cross section for forward scattering does not appear at all in the equations. Only the backscattering and inelastic collisions are significant in shaping the distribution function. The solution to Eqs. (8) in the asymptotic limit is

$$f_+ + f_- = e^{-\beta u}$$

$$f_+ - f_- = \sqrt{\frac{Q_h}{2Q_e^- + Q_h}} e^{-\beta u}$$

where $\beta = \sqrt{Q_h(2Q_e^- + Q_h)}/Q$ and $u = NQ\epsilon/eE$ as before. Once again the distribution approaches a Maxwellian at high energy. This time the coefficient of u in the exponent goes to 1 as Q_h/Q_e^- increases just as in the exact asymptotic solution. However, for small values of Q_h/Q_e^- , the approximation is not as good as P1. This is because of the conflicting assumptions of isotropic scattering in the one case and forward-backward scattering in the other. For real gases at energies above 10 eV, the cross sections are more nearly described by the latter assumption.

It would be useful to establish a criterion for terminating the angular expansion which would result in a good approximation to the distribution function. If we require that the term which is dropped in the series of Eqs. (7) be less than 10% of those remaining, then the criterion for using the P_n approximation is

$$\frac{f_{n+1}}{f_{n-1}} < 0.1 \frac{n(2n+3)}{(n+1)(2n-1)}$$

Using Table I, we see that P1 is a good approximation for $Q_h/Q_e \leq 0.1$ while at least seven terms must be retained for $Q_h/Q_e = 0.3$. With larger inelastic cross sections the criterion is never satisfied.

An alternative condition is to require that f_1/f_0 in the truncated expansion be within 5% of the exact asymptotic value. This criterion is satisfied for P1 at $Q_h/Q_e = 0.1$, for P2 at 0.3, and for P3 at 1. The error in α , which goes as one over the electron temperature, is about equal to the error in f_1/f_0 , which is proportional to the drift velocity of the high energy electrons. Thus, the electron transport coefficients are much more accurately predicted by the expansion method than are the angular distributions themselves.

GLOSSARY

a	Subscript denoting attachment
a	Attachment Rate
\vec{a}	Electron acceleration vector
A_ℓ	Coefficients for Legendre expansion
\vec{B}	Magnetic field vector
\vec{c}, c	Electron velocity vector and magnitude
c_p	Heat capacity per unit mass
c_y	y-component of electron velocity
\vec{C}, C	Molecular velocity vector and magnitude
d	Detachment rate
d	Anode-cathode separation
d_c	Cathode fall thickness
d_n	Normal cathode fall thickness
e	Absolute value of electronic charge
$\vec{E}, E(y)$	Electric field vector and magnitude
E_o	Electric field at cathode surface
f	Electron distribution function
f_+, f_-	Distribution of electrons moving with and against the electric field
f_A	Current distribution at anode: $f_A = f(\epsilon, y = d) \epsilon$
f_o	Isotropic distribution function
F_A	Probability distribution at anode: $F_A = f(\epsilon, y = d) \epsilon^{1/2}$
g	Magnitude of relative velocity

h	Subscript denoting inelastic collisions
h^o	Stagnation enthalpy
i	Subscript denoting ionization
I	Radiation intensity at cathode
j	Total current density
j_e, j_+	Electron and ion current density
j_n	Normal current density
k	Boltzmann's constant
K	In-scattering operator
K_e	In-scattering operator for elastic collisions
m	Electron mass
m_+, m_-	Ion masses
M	Mach number
M	Molecular mass
n_e, n_+, n_-	Electron and ion number densities
N	Neutral number density
N^*	Neutral excited state density
p	Pressure
p_o	Reduced pressure
P_d	Discharge power density
P_l	Legendre polynomials
q	Heat flux
q_c	Heat flux at edge of cathode

Q	Total collision cross section
Q	Rate of heat addition
Q_a	Total attachment cross section
Q_e	Total elastic cross section
Q_h	Total inelastic cross section
Q_i	Total ionization cross section
Q_r	Total recombination cross section
r	Subscript denoting recombination
\vec{r}	Position vector
r_e	Electron-ion recombination coefficient
r_i	Ion-ion recombination coefficient
s	Subscript denoting superelastic collisions
S	External ionization source term
t	Time
t	Thickness of cathode
T	Gas temperature
T_a	Adiabatic wall temperature
T_o	Temperature of back face of cathode
T_w	Temperature of front face of cathode
T_∞	Free stream temperature
u, v	Flow velocities in x, y directions
U	Free stream velocity

\vec{v}_+, \vec{v}_-	Ion drift velocities
v_e	Electron drift velocity
V_c	Cathode fall potential
V_n	Normal cathode fall potential
W	Electron drift velocity
x	Position coordinate in flow direction
y	Position coordinate parallel to electric field
Y_ℓ^m	Spherical harmonics
z	Ionization rate
α	Townsend ionization coefficient
γ	Polar scattering angle
γ, γ_i	Secondary electron emission coefficient
γ_{ph}	Photoelectric efficiency
δ	Boundary layer thickness
δ^*	Boundary layer displacement thickness
δ_ℓ	Thickness of laminar sublayer
ϵ	Total kinetic energy
$\bar{\epsilon}$	Electron mean energy
ϵ_h	Energy lost in inelastic collision
ϵ_i	Energy lost in ionizing collision
ϵ_0	Permittivity of free space
θ	Angle between electron velocity and $-\vec{E}$

κ_c	Thermal conductivity of cathode
κ_g	Thermal conductivity of gas
μ	Coefficient of viscosity
μ_e	Electron mobility
ν	Kinematic viscosity
ν_+, ν_-	Ion collision frequency
$\bar{\epsilon}$	Kinetic energy in field direction
ρ	Gas Density
ρ_∞, ρ_e	Free stream gas density
σ_e	Differential elastic cross section
σ_h	Differential inelastic cross section
σ_r	Recombination cross section
τ	Shear stress
τ_1, τ_2	Characteristic times for gas heating in the cathode sheath
φ	Electron potential energy or field potential
φ_w	Work function of cathode material
ϕ	Azimuthal angle for electron velocity
Φ	Viscous dissipation function
ψ	Azimuthal scattering angle
ω	Solid angle for scattering